Copy No. 113

UNCLASSIFIED

[redacted]

RM No. L6L10b

CLASSIFICATION CHANGED TO [redacted]

Section Copy

PERSONAL COPY

RESEARCH MEMORANDUM

INVESTIGATION AT HIGH SPEEDS OF A HORIZONTAL-TAIL MODEL IN THE LANGLEY 8-FOOT HIGH-SPEED TUNNEL

By

Ralph P. Bielat

Langley Memorial Aeronautical Laboratory
Langley Field, Va.

CLASSIFICATION CANCELLED

AUTHORITY H.L.DRYDEN 6- 5 53

[redacted] CHANGE# 1411 W.H.L.

This document contains classified information affecting the National Defense of the United States within the meaning of the Espionage Act, USC 50:31 and 32. Its transmission or the revelation of its contents in any manner to an unauthorized person is prohibited by law. Information so classified may be imparted only to persons in the military and naval services of the United States, appropriate civilian officers and employees of the Federal Government who have a legitimate interest therein, and to United States citizens of known loyalty and discretion who of necessity must be informed thereof.

CANCELLED

NATIONAL ADVISORY COMMITTEE FOR AERONAUTICS

WASHINGTON

January 31, 1947

CLASSIFICATION CHANGED TO [redacted]

UNCLASSIFIED

UNCLASSIFIED

NASA Technical Library
3 1176 01437 0226

 [redacted]

NATIONAL ADVISORY COMMITTEE FOR AERONAUTICS

RESEARCH MEMORANDUM

INVESTIGATION AT HIGH SPEEDS OF A HORIZONTAL-TAIL MODEL IN THE LANGLEY 8-FOOT HIGH-SPEED TUNNEL

By Ralph P. Bielat

SUMMARY

Pressure-distribution measurements and elevator hinge-moment measurements were made to determine the aerodynamic characteristics of a horizontal-tail model having an NACA 65-108 airfoil section equipped with a 30-percent-chord sealed unbalanced elevator and a 10-percent-chord plain trim tab The tests were made for various angles of attack and control-surface deflections at Mach numbers ranging from 0.40 to 0.90. Data are presented for tests made with the surfaces of the model smooth and also with boundary-layer transition fixed at the 0.10-chord station by a row of carborundum grains on each surface.

The results of the investigation indicated that for small elevator deflections and for Mach numbers up to 0.85 no adverse changes in the lift-curve slopes, control-surface effectiveness, and hinge-moment parameters occurred. At Mach numbers in the range from 0.85 to 0.90 the values of the lift-curve slopes showed an abrupt decrease, the elevator effectiveness decreased rapidly, and the negative value of rate of change of elevator hinge-moment coefficient with elevator deflection C_{h_δ} increased abruptly. The tab effectiveness, however, remained almost constant throughout the Mach number range. Fixing transition at the 10-percent-chord station on both surfaces reduced the values of the lift-curve slopes and the elevator effectiveness. The value of the hinge-moment parameter C_{h_δ} was also reduced throughout the Mach number range.

INTRODUCTION

Recent developments in aircraft propulsive units have led to the design of airplanes that operate at speeds in excess of 500 miles

UNCLASSIFIED [redacted]

per hour. Up to the present time, however, aerodynamic data on the component parts of an airplane designed to operate at these high speeds have been lacking. Hence, a comprehensive research program has been undertaken by the National Advisory Committee for Aeronautics in order to supply this information. References 1 to 4 describe the general aerodynamic characteristics for a wing of high aspect ratio.

The tests reported herein describe the characteristics of a horizontal-tail model having an NACA 65-108 airfoil section and a 30 percent-chord sealed unbalanced elevator equipped with a 10 percent-chord plain trim tab. The tests consisted of measurements of the pressures at four spanwise stations and elevator hinge moments at Mach numbers ranging from 0.40 to 0.90. The results include the pressure distributions, lift, span loadings, pitching moments, elevator hinge moments, and tab characteristics. Some data are also presented which show the effects of fixed transition at the 10-percent-chord station on both the upper and lower surfaces of the model.

SYMBOLS

a	speed of sound in undisturbed stream
b	span of model, feet (2)
b_e	span of one elevator, feet (0.989)
c	section chord of model, feet
$\bar{c}$	root-mean-square chord of elevator measured behind hinge axis, feet (0.136)
c'	mean aerodynamic chord of model, feet (0.519)
H	elevator hinge moment
M	Mach number in undisturbed stream (V/a)
p	static pressure in undisturbed stream
p_l	local static pressure at point on model
P	pressure coefficient $\left(\frac{p_l - p}{q}\right)$

P_{cr} pressure coefficient corresponding to attainment of local speed of sound at some point on model

q dynamic pressure in undisturbed stream $\left(\frac{1}{2}\rho V^2\right)$

S gross area of model, square feet (0.998)

V velocity of undisturbed stream

x distance along chord from leading edge of airfoil section

y distance along semispan from center line

α angle of attack

δ control surface deflection with respect to chord line; positive when trailing edge is down

ρ mass density of undisturbed stream

C_h elevator hinge-moment coefficient $\left(\frac{H}{q b_e \bar{c}^2}\right)$

ΔP resultant pressure coefficient across elevator seal $\left(P_{\text{below seal}} - P_{\text{above seal}}\right)$

c_n section normal-force coefficient $\left(\frac{1}{c}\int_0^c \left(P_L - P_U\right) dx\right)$

c_m section pitching-moment coefficient about 25-percent-chord station $\left(\frac{1}{c^2}\int_0^c \left(P_U - P_L\right)\left(x - \frac{c}{4}\right) dx\right)$

C_N normal-force coefficient $\left(\frac{2}{S}\int_0^{b/2} c_n c \, dy\right)$

$C_{m_{c/4}}$ pitching-moment coefficient about 25-percent-chord station

$$\left(\frac{2}{Sc'}\int_0^{b/2} c_m c^2 \, dy\right)$$

[redacted]

$$C_{h_\alpha} = \left(\frac{\partial C_h}{\partial \alpha}\right)_{\delta,\delta_t}$$

$$C_{h_\delta} = \left(\frac{\partial C_h}{\partial \delta}\right)_{\alpha,\delta_t}$$

$$C_{h_{\delta_t}} = \left(\frac{\partial C_h}{\partial \delta_t}\right)_{\alpha,\delta}$$

$$\delta_{\delta_t} = \left(\frac{\partial \delta}{\partial \delta_t}\right)_{C_h=0}$$

$$C_{N_\alpha} = \left(\frac{\partial C_N}{\partial \alpha}\right)_{\delta,\delta_t}$$

$$C_{N_\delta} = \left(\frac{\partial C_N}{\partial \delta}\right)_{\alpha,\delta_t}$$

$$\alpha_\delta = \left(\frac{\partial \alpha}{\partial \delta}\right)_{C_N,\delta_t}$$

The subscripts outside the parentheses indicate the factors held constant during the measurement of the parameters.

Subscripts:

L lower surface of airfoil section

t tab

U upper surface of airfoil section

APPARATUS AND MODEL

The Langley 8-foot high-speed tunnel, in which the tests were conducted, is of the single-return circular-cross-section, closed-throat type. The air-stream turbulence in the tunnel is small but is slightly higher than in free air. For these tests the airspeed was continuously controllable to a choking Mach number of 0.950 (uncorrected for tunnel-wall interference).

The horizontal-tail model tested had an NACA 65-108 airfoil section, an aspect ratio of 4.01, a taper ratio of 2.01:1.00, and no dihedral. The model was equipped with a 0.30c sealed, unbalanced elevator and a 0.10c plain trim tab which had a span equal to 50 percent of the elevator span. The nose radius of the elevator was approximately one-half the airfoil thickness at the hinge axis. The model was constructed of medium hard brass except for the right elevator which was constructed of duralumin. Other pertinent data for the model are given in figure 1 and in tables I and II. The ordinates for the NACA 65-108 airfoil section are given in table III. From the 70-percent-chord station to the trailing edge the NACA 65-108 airfoil section was modified to make the sides of the elevator and trim tab straight. The model was designed to operate with the camber surface on the bottom. Thus the "lower surface" ordinates specified in table III are for the camber side of the airfoil. The size of the model was kept small to insure the attainment of a Mach number of 0.90 without choking the tunnel.

The right elevator, on which the elevator hinge moments were measured, was attached to the stabilizer by needle-bearing hinges of negligible friction. Details of the sealed gap between the stabilizer and the right elevator are shown in figure 1. The electrical strain gage used to measure the elevator hinge moments was fastened to a special friction clamp which also permitted adjustment of the elevator angle. Static calibration tests were made of the right elevator to permit correction for elevator deflection under load; these corrections have been applied to the hinge-moment data.

The left elevator, on which pressures were measured, was attached to the stabilizer by means of friction hinges. The gap between the stabilizer and left elevator was sealed with shellac. Twenty static-pressure orifices were placed at each of four stations along the span on the left half of the horizontal tail model. The spanwise locations of the stations in percent of the semispan are 15, 40, 70, and 90. The approximate chordwise locations of these orifices at each station are shown in figures presenting pressure-

distribution data. Trim tabs at fixed angles of deflection of 0° and $\pm 10^{\circ}$ could be fitted into the trailing edge of the elevators as shown in figure 1. This type of construction simulates hinged trim tabs with the gap sealed.

The model was supported in the tunnel by means of a vertical support plate which is described completely in reference 1.

TESTS

All lift and pitching-moment data were obtained from pressure-distribution measurements, and all elevator hinge-moment data were obtained by use of the electrical strain gage. The measurements were made for angles of attack from -6° to 5° for an elevator deflection of 0°, and for angles of attack from -2° to 5° for elevator deflections of $\pm 2.5^{\circ}$, $\pm 5^{\circ}$, -10°, and -15°. Some of the tests were repeated with trim tabs set at deflections of $\pm 10^{\circ}$ on the elevator. The Mach number range extended from 0.40 to 0.90 (corrected values). Data are also shown for an uncorrected Mach number of 0.925. The Reynolds number based on the mean aerodynamic chord of the model (0.519 ft) varied from 1.25×10^{6} at a Mach number of 0.40 to 1.92×10^{6} at a Mach number of 0.90. Tests were made with a $\frac{3}{16}$-inch-wide strip of No. 60 carborundum grains glued to both the upper and lower surfaces at the 10-percent-chord station of the model in order to determine the effects of fixing transition.

REDUCTION OF DATA

The test data presented herein have been corrected for tunnel-wall interference. A complete description of the corrections is given in reference 1. The corrections have been applied to all data obtained at Mach numbers up to and including 0.90. The magnitude of the corrections was found to be very small, the maximum correction to the Mach number being approximately 1 percent. The maximum correction to the dynamic pressure was only about 2 percent.

The tunnel choked at the model at a Mach number of 0.95. Numerous tests have indicated that the data obtained in a wind tunnel when it is choked at the model are not applicable to the prediction of the aerodynamic characteristics for free air (for example, see reference 5) and therefore no data are presented for the choked condition. There was also a perceptible tendency towards choke at a

Mach number of 0.925. The results obtained at this Mach number, even if completely corrected for the usual effects of wind-tunnel wall interference, may not, therefore, indicate the flight characteristics. The data which have been included herein for a Mach number of 0.925 are therefore considered to be of uncertain value.

RESULTS AND DISCUSSION

Pressure-Distribution Measurements

Pressure distributions for the 40-percent-semispan station for elevator deflections of 0°, $\pm 5^{\circ}$, and -15° and a tab deflection of 0° are presented in figures 2 to 5. Similar data for the 40-percent-semispan station and the 90-percent-semispan station for an elevator deflection of 0° and a tab deflection of -10° are shown in figures 6 and 7. The data shown are considered to be representative of the changes that occur in the pressure distributions for each spanwise station and, in general, for the chordwise changes in pressure distribution due to control surface deflections. The effect of control-surface deflection on the chordwise pressure-distribution diagrams is shown by comparing figures 3 to 6 with figure 2. The effect of tab deflection on the chordwise pressures at two spanwise stations can be seen by comparing figures 6 and 7.

Normal-Force Characteristics

The chordwise-pressure-distribution diagrams have been integrated to obtain section normal-force coefficients and pitching-moment coefficients. These coefficients have been used to determine the spanwise variations in section loadings and pitching moments. The spanwise variations in section loadings for elevator deflections of 0°, $\pm 5^{\circ}$, and -15° with the tab deflected 0° and for an elevator deflection of 0° with the tab deflected $\pm 10^{\circ}$ are presented in figures 8 to 13. Figure 14 illustrates the spanwise variation in span-loading ratio for elevator deflections of 0° and $\pm 5^{\circ}$. The theoretical curve for the span-loading ratio has been obtained by use of charts presented in reference 6. The effects of compressibility on the spanwise loading for various elevator deflections (figs. 9 to 11) are seen to be similar to the effects of the data shown for zero elevator deflection. (See fig. 8.) Of more significance, however, is the fact that for all the elevator deflections (fig. 14) no adverse spanwise shift in loading occurred up to an uncorrected Mach number of 0.925. The effect of tab deflection on the spanwise

loading can be seen by comparing figures 12 and 13 with figure 8. The tab extends from the root to the 50-percent semispan station, and this area is principally affected by the tab.

The spanwise load distributions have been integrated to determine the total normal forces. The variation of normal-force coefficient with Mach number for several angles of attack and control-surface deflections is presented in figure 15. The variation of normal-force coefficient with Mach number for a range of angle of attack and elevator deflection with the tab deflected 0° and with transition fixed on both surfaces is shown in figure 16. Large changes in the normal-force characteristics for elevator deflections in the range of $\pm 5^{\circ}$ generally occurred above a Mach number of about 0.85. The slope of the lift curve (fig. 17) also showed a decrease above a Mach number of 0.85. The decrease in lift-curve slope $C_{N_{\alpha}}$ was accompanied by a negative shift in the angle for zero lift. The high Mach numbers attained before these changes occur is due partly to the low aspect ratio (reference 7) and to the small thickness ratio of the horizontal-tail model.

Figure 17 also shows the effect of compressibility on the lift-curve slope $C_{N_{\delta}}$ produced by deflection of the elevator. For small elevator deflections, the slope $C_{N_{\delta}}$ increased up to a Mach number of 0.85 and then decreased rapidly. In general, the elevator was effective in producing changes in lift for all elevator deflections tested up to a Mach number of 0.85; however, for small elevator deflections ($\pm 5^{\circ}$) the effectiveness was reduced. (See fig. 15.) The control surfaces were effective in producing changes in the loading over the stabilizer only when the local velocities over the stabilizer remained subsonic. When the flow over the airfoil was largely supersonic, deflection of the control surface had relatively little effect on the supersonic flow ahead of it. (See reference 8.) This effect was particularly true for the small control-surface deflections ($\delta = \pm 5^{\circ}$). Although some control effectiveness was indicated for all elevator deflections at speeds considerably above the critical speed, a better degree of control effectiveness can be maintained by resorting to large elevator deflections. Figure 5 shows that for an elevator deflection of -15° for angles of attack of 0° and -2° and up to a Mach number of 0.909 the pressures on the upper surface were increased so that no supersonic velocities existed on that surface. For this condition, deflection of the elevator produced changes in loading over the stabilizer upper surface. As shown in figure 17, for a large elevator angle (-10°), the value of $C_{N_{\delta}}$ increases at Mach numbers above 0.85, whereas for small angles a loss of effectiveness is noted. The large angles, however, require the application of large hinge moments which may be beyond the physical capabilities of the pilot.

The elevator effectiveness factor α_δ, which is the ratio of C_{N_δ} to C_{N_α}, is shown in figure 18. For small elevator deflections the elevator effectiveness decreased from a value of 0.67 at a Mach number of 0.40 to 0.48 at a Mach number of 0.85 and to a value of 0.15 at an uncorrected Mach number of 0.925.

Transition was fixed at the 10-percent-chord station in order to determine the aerodynamic characteristics of the horizontal tail with a turbulent boundary layer such as might exist over a full-scale tail. The most notable effect of fixing the transition was the reduction in the lift-curve slopes C_{N_α} and C_{N_δ} (fig. 17) and in elevator effectiveness α_δ (fig. 18).

Pitching-Moment Characteristics

Pitching-moment coefficients, based on the mean aerodynamic chord, which indicate the twisting moments that may be encountered on the horizontal tail are presented in figure 19. The variation of pitching-moment coefficient with Mach number (below a Mach number of 0.85) for various angles of attack and for elevator deflections in the range of $\pm 5^\circ$ (fig. 19) is generally small. For angles of attack of 0° and -2° and for elevator deflections of -10° and -15° the pitching-moment coefficients showed a continuous positive increase throughout the Mach number range. The variation of pitching-moment coefficient with normal-force coefficient for $\delta = 0^\circ$ and $\delta_t = 0^\circ$ is shown in figure 20.

Elevator Hinge-Moment Characteristics

The variation of hinge-moment coefficient with elevator deflection is presented in figures 21 to 23. Figures 24 and 25, which were obtained from figures 21 to 23, show hinge-moment-coefficient variation with Mach number and hinge-moment-coefficient variation with angle of attack, respectively. The hinge-moment-coefficient variation with elevator deflection, Mach number, and angle of attack with transition fixed is shown in figures 26, 27, and 28, respectively.

No large changes in the elevator hinge-moment coefficients occurred for small elevator deflections up to a Mach number of 0.85. (See fig. 24.) At greater Mach numbers marked changes in the hinge-moment characteristics occurred for all elevator deflections.

The effect of compressibility on the usual hinge-moment parameters

$$\left(\frac{\partial C_h}{\partial \alpha}\right)_{\delta=0^\circ,\ \delta_t=0^\circ}$$

and

$$\left(\frac{\partial C_h}{\partial \delta}\right)_{\alpha=0^\circ,\ \delta_t=0^\circ}$$

with Mach number with and without transition fixed is shown in figure 29. These slopes are the average values for angles of attack from -1° to 1° and elevator deflections from -1° to 1°. In general, the hinge-moment parameters indicated little variation below a Mach number of 0.825. In the range of Mach number from 0.85 to 0.925 the hinge-moment parameters showed large and irregular variations. Fixing transition made the parameter C_{h_α} slightly more negative, the parameter C_{h_δ} less negative, and lessened the severity of the compressibility effects on both these parameters.

Visual readings of the strain-gage recording instrument were made in order to determine the magnitude of the hinge-moment fluctuations. Low-frequency hinge-moment fluctuations were observed which, at a Mach number of 0.90, amounted to approximately 10 percent of the value of hinge-moment fluctuation reported in reference 9.

Data on average resultant pressure coefficient ΔP across the elevator seal are shown in figure 30. The resultant pressure coefficient ΔP across the seal may be used in designing the balance of an internally sealed elevator. In general, the variation of the resultant pressure coefficient with elevator deflection is approximately linear for elevator deflections from -6° to 5° up to a Mach number of 0.878. For the larger elevator deflections, a decrease in resultant pressure coefficient per degree of elevator deflection occurs. At the higher Mach numbers, that is, 0.905 and 0.925, a decrease in resultant pressure coefficient generally occurs for elevator deflections from -8° to approximately 5° with an increase for the larger negative elevator deflections.

Tab Characteristics

The ability of the tab to produce changes in elevator hinge-moment coefficients is shown in figure 23. The tab effectiveness $C_{h_{\delta_t}}$

is presented in figure 31 which shows that the tab is effective throughout the Mach number range. Of particular interest, however, is the effectiveness of the tab when used as a control trimming or balancing device. The rate of change of elevator deflection with tab deflection to produce zero elevator hinge moment $\left(\frac{\partial\delta}{\partial\delta_t}\right)_{C_h=0}$ is shown in figure 32. In general, the tab was effective in trimming the elevator throughout the Mach number range. Because C_{h_δ} increased at a much faster rate than $C_{h_{\delta_t}}$ at Mach numbers greater than 0.85, however, it was found that approximately 30 percent more tab deflection was necessary to balance the elevator at a Mach number of 0.90 than was required at a Mach number of 0.40.

SUMMARY OF RESULTS

Tests of a horizontal-tail model with an unbalanced elevator indicated the following results:

1. For small elevator deflections and for Mach numbers up to 0.85 there were no adverse changes in the lift-curve slopes, control-surface effectiveness, and hinge-moment parameters.

2. At Mach numbers in the range of 0.85 to 0.90 the values of the lift-curve slopes and the elevator effectiveness decreased rapidly, and the negative value of the elevator hinge-moment parameter C_{h_δ} increased abruptly. The tab, however, retained its effectiveness in producing increments in elevator hinge-moment coefficients throughout the Mach number range of the tests.

3. Fixing transition at the 10-percent-chord station on the upper and lower surfaces reduced the values of the lift-curve slopes and the elevator effectiveness. The value of the hinge-moment parameter C_{h_δ} was also reduced throughout the Mach number range.

Langley Memorial Aeronautical Laboratory
National advisory Committee for Aeronautics
Langley Field, Va

REFERENCES

1. Whitcomb, Richard T.: Investigation of the Characteristics of a High-Aspect-Ratio Wing in the Langley 8-Foot High-Speed Tunnel. NACA RM No. L6H28a, 1946.

2. Ferri, Antonio: Preliminary Investigation of Downwash Fluctuations of a High-Aspect-Ratio Wing in the Langley 8-Foot High-Speed Tunnel. NACA RM No. L6H28b, 1946.

3. Mattson, Axel T.: Investigation of Dive Brakes and Dive-Recovery Flap on High-Aspect-Ratio Wing in the Langley 8-Foot High-Speed Tunnel. NACA RM No. L6H28c, 1946.

4. Luoma, Arvo A.: An Investigation of a High-Aspect-Ratio Wing Having 0.20-Chord Plain Ailerons in the Langley 8-Foot High-Speed Tunnel. NACA RM No. L6H28d, 1946.

5. Byrne, Robert W.: Experimental Constriction Effects in High-Speed Wind Tunnels. NACA ACR No. L4L07a, 1944.

6. Anon: Spanwise Air-Load Distribution. ANC-1(1), Army-Navy-Commerce Committee on Aircraft Requirements. U.S. Govt. Printing Office, April 1938.

7. Stack, John, and Lindsey, W. F.: Characteristics of Low-Aspect-Ratio Wings at Supercritical Mach Numbers. NACA ACR No. L5J16, 1945.

8. Lindsey, W. F.: Effect of Compressibility on the Pressures and Forces Acting on Modified NACA 65,3-019 Airfoil Having a 0.2-Chord Flap. NACA ACR No. L5G31a, 1946.

9. Luoma, Arvo A., and Liccini, Luke L.: An Investigation of the Hinge-Moment Fluctuations of a 0.20-Chord Plain Ailerons on a High-Aspect-Ratio Wing in the Langley 8-Foot High-Speed Tunnel. NACA RM No. L6L10a, 1947.

TABLE I

DIMENSIONS OF HORIZONTAL-TAIL MODEL

Horizontal tail:	
Airfoil section	NACA 65-108
Span, feet	2
Gross area, square feet	0.998
M. A. C., feet	0.519
Aspect ratio	4.01
Taper ratio	2.01:1.00
Elevator:	
Span, feet	1.979
Gross area of elevator behind hinge axis, square feet	0.297
Root-mean-square chord, feet	0.156
Ratio elevator chord to airfoil chord	0.300
Trailing-edge angle, degrees	9.75
Tab:	
Number of tabs	2
Span of each tab, feet	0.494
Total tab area, square feet	0.057
Mean chord, feet	0.059
Ratio tab chord to elevator chord	0.333
Ratio tab span to elevator span	0.50

NATIONAL ADVISORY
COMMITTEE FOR AERONAUTICS

TABLE II

DIMENSIONS OF TIP SHAPE OF HORIZONTAL-

TAIL MODEL IN INCHES

[Symbols defined in figure 1]

Plan-form contour of tip		
Distance from tip x	y_S	y_E
0	1.200	-1.200
.010	1.555	-.664
.020	1.697	-.407
.050	1.950	-.080
.080	2.110	.145
.100	2.193	.266
.200	2.493	.678
.300	2.674	.930
.400	2.791	1.083
.500	2.875	1.185
.600	2.932	1.244
.720	2.971	1.273
Elevation contour of tip		
Distance from tip x	y_U	y_L
0	0	0
.010	.031	.042
.020	.042	.058
.050	.065	.086
.080	.078	.105
.100	.085	.114
.200	.110	.145
.300	.125	.164
.400	.134	.176
500	.141	.184
.600	.145	.188
.720	.147	.192

NATIONAL ADVISORY
COMMITTEE FOR AERONAUTICS

TABLE III

ORDINATES FOR NACA 65-108 AIRFOIL (INVERTED)

[Stations and ordinates in percent of wing chord]

Upper surface		Lower surface	
Station	Ordinate	Station	Ordinate
0	0	0	0
.526	.601	.474	-.651
.779	.720	.721	-.790
1.283	.890	1.217	-.998
2.537	1.173	2.462	-1.359
5.041	1.587	4.959	-1.903
7.542	1.906	7.458	-2.330
10.042	2.174	9.958	-2.690
15.040	2.595	14.960	-3.267
20.037	2.914	19.963	-3.710
25.031	3.151	24.969	-4.047
30.026	3.319	29.974	-4.291
35.019	3.423	34.981	-4.453
40.013	3.462	39.987	-4.534
45.006	3.426	44.994	-4.522
50.000	3.305	50.000	-4.409
54.994	3.090	55.006	-4.186
59.989	2.801	60.011	-3.873
64.985	2.456	65.015	-3.486
70.000	2.063	70.000	-3.043
80.000	[a]1.378	80.000	[a]-2.031
90.000	[a].689	90.000	[a]-1.016
100.000	[a]0	100.000	[a]0

L.E. radius, 0.434.
Slope of radius through end of chord, 0.04212

[a]Ordinates derived for straight-side elevator and trim tab.

NATIONAL ADVISORY
COMMITTEE FOR AERONAUTICS

[redacted]

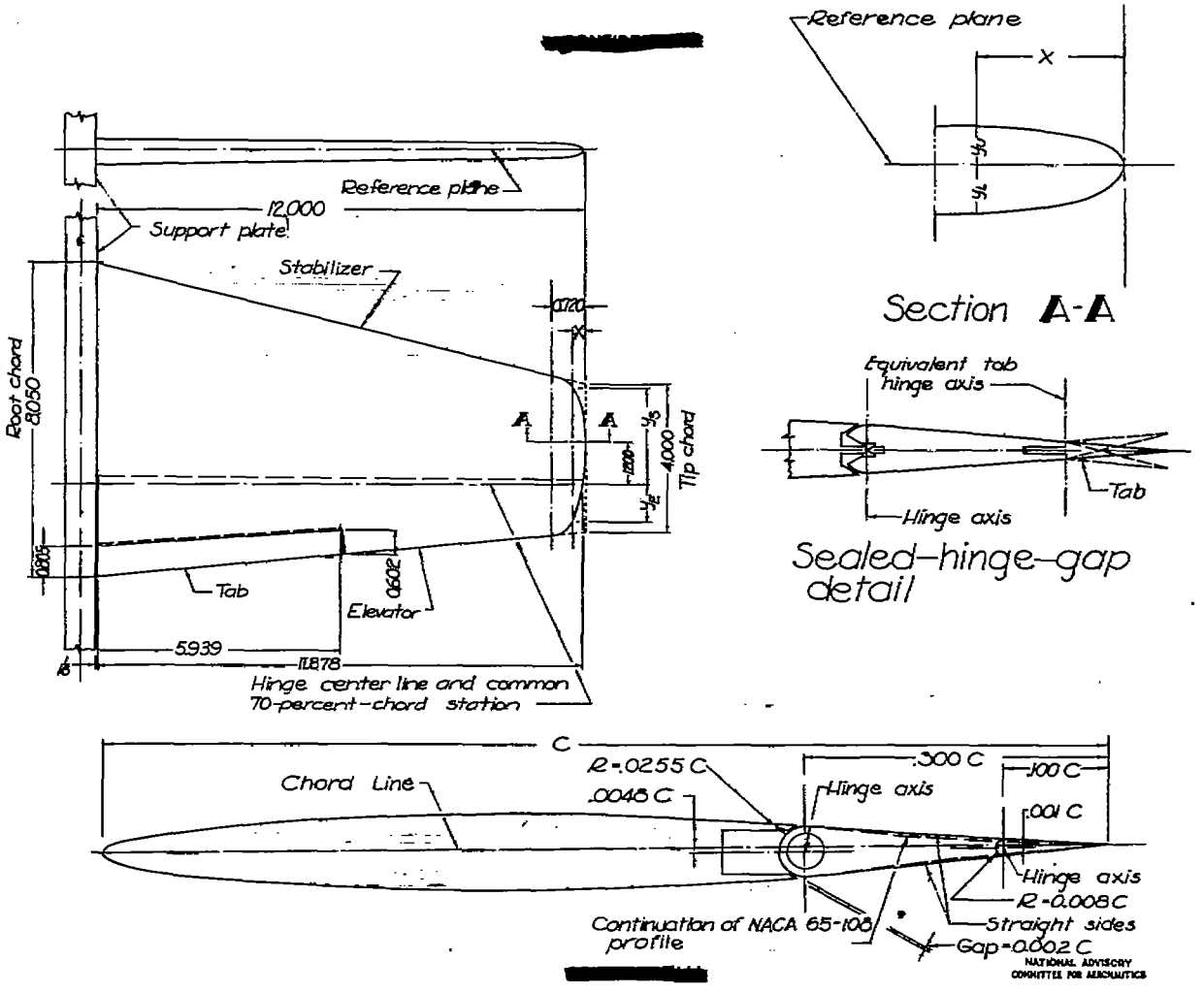

[redacted]

Figure 1.-Details of horizontal-tail model tested. (Dimensions in inches.)

[redacted]

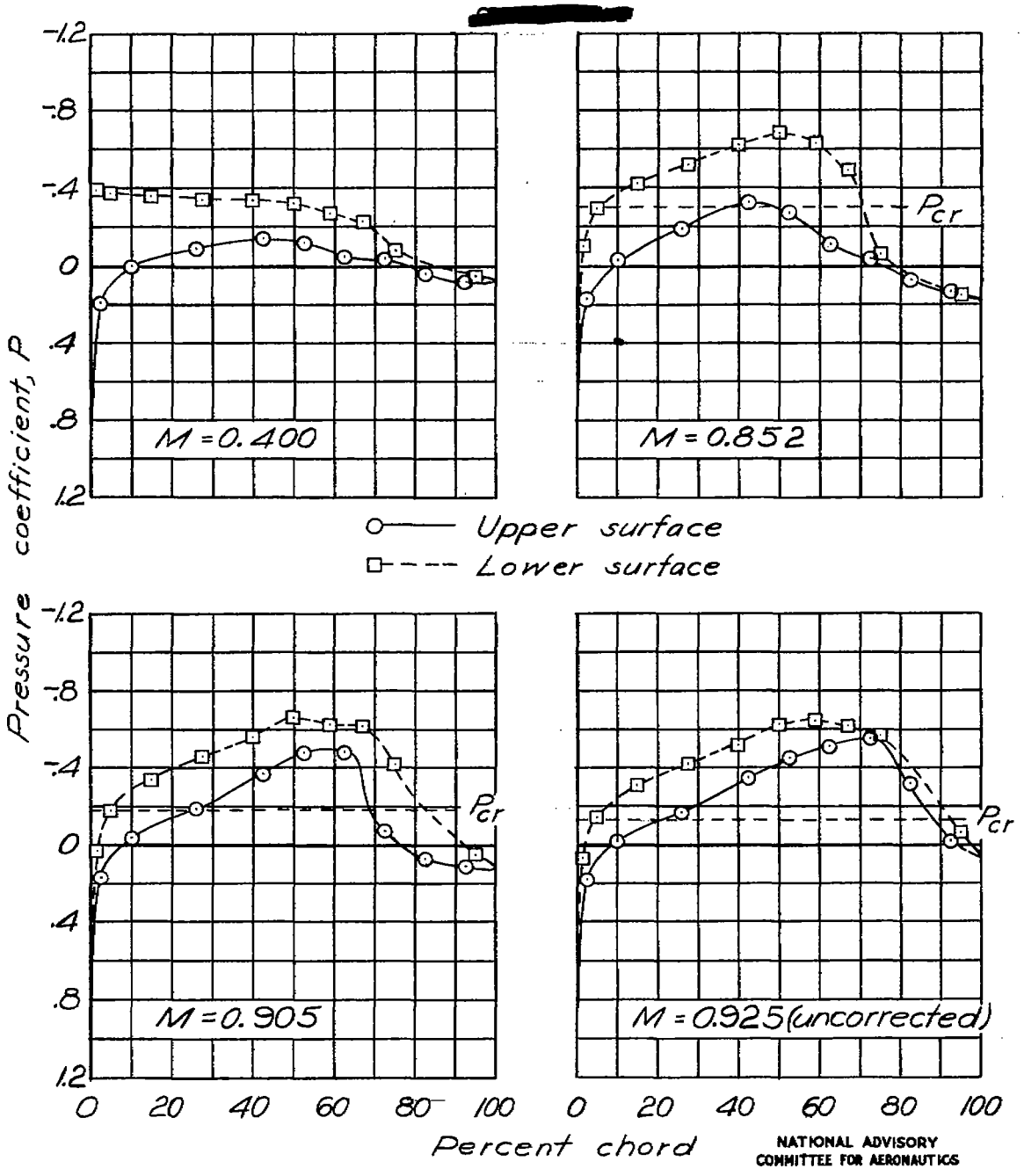

(a) $\alpha = -2°$.

[redacted]

Figure 2.- Pressure distribution about the horizontal tail at the 40-percent-semispan station. $\delta = 0°$; $\delta_f = 0°$.

[redacted]

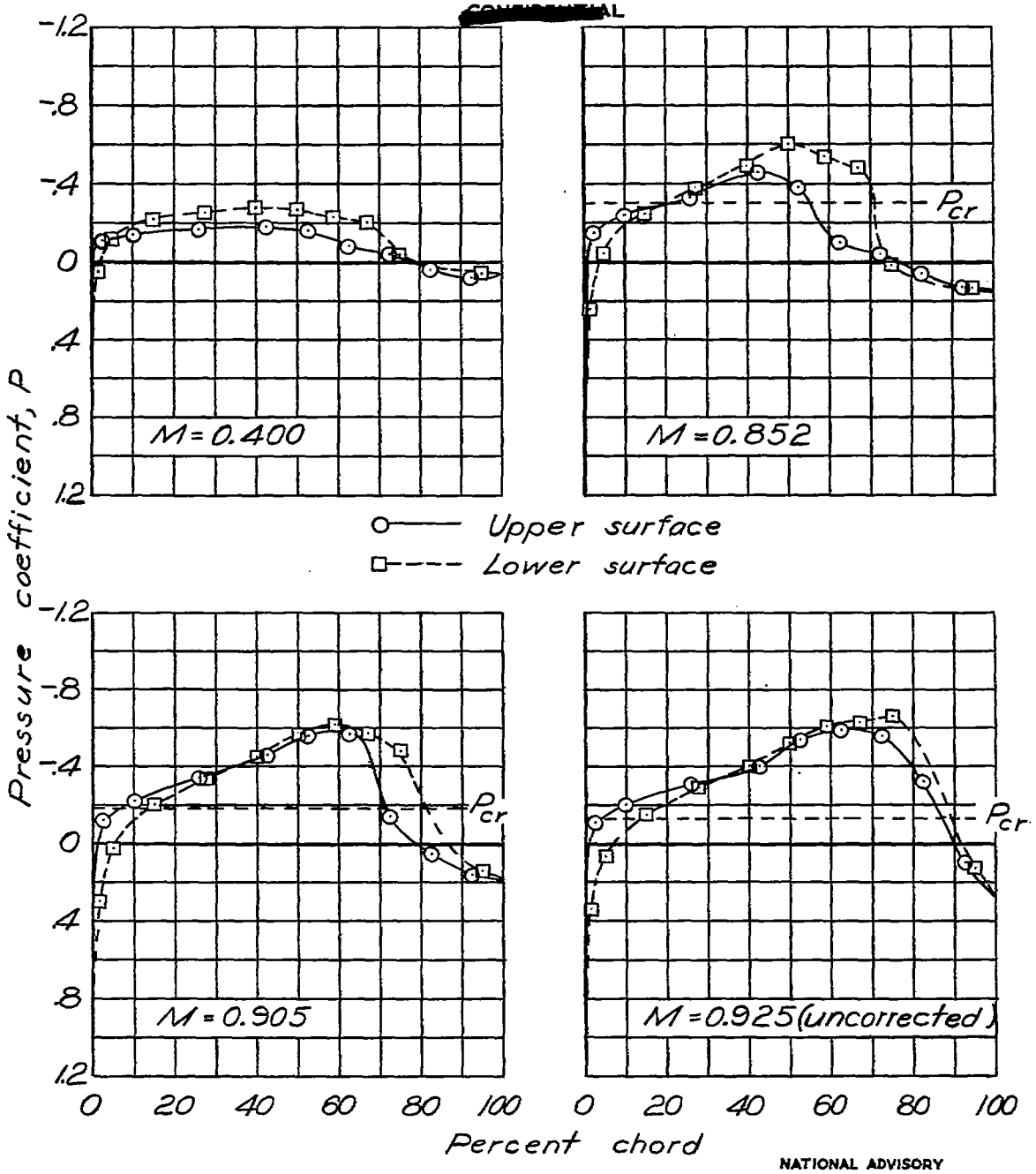

NATIONAL ADVISORY COMMITTEE FOR AERONAUTICS

(b) $\alpha = 0°$.

[redacted]

Figure 2.- Continued.

[redacted]

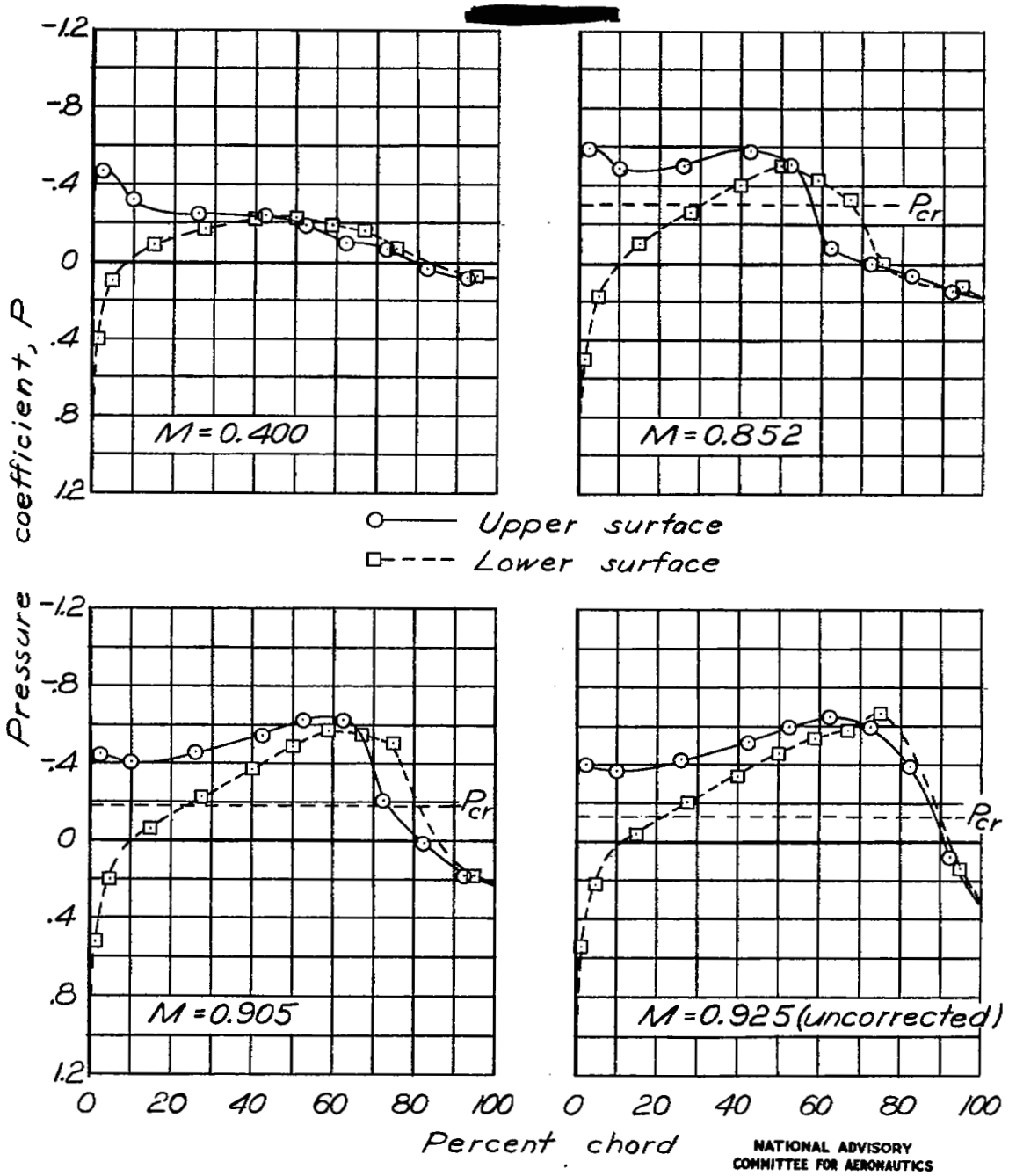

NATIONAL ADVISORY COMMITTEE FOR AERONAUTICS

(c) $\alpha = 2°$.

[redacted]

Figure 2.- Continued.

[redacted]

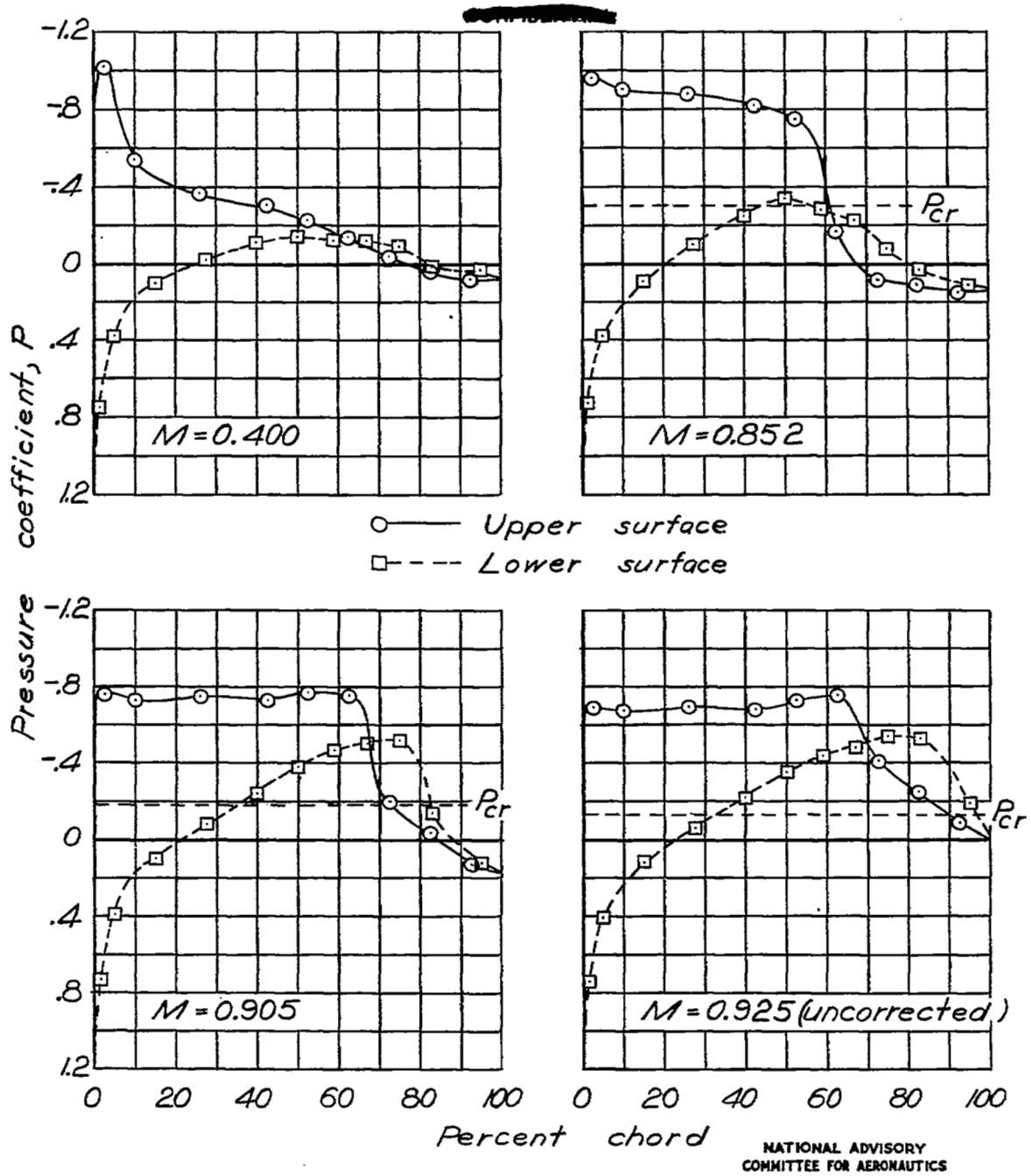

(d) $\alpha = 5°$.

[redacted]

Figure 2.– Concluded.

[redacted]

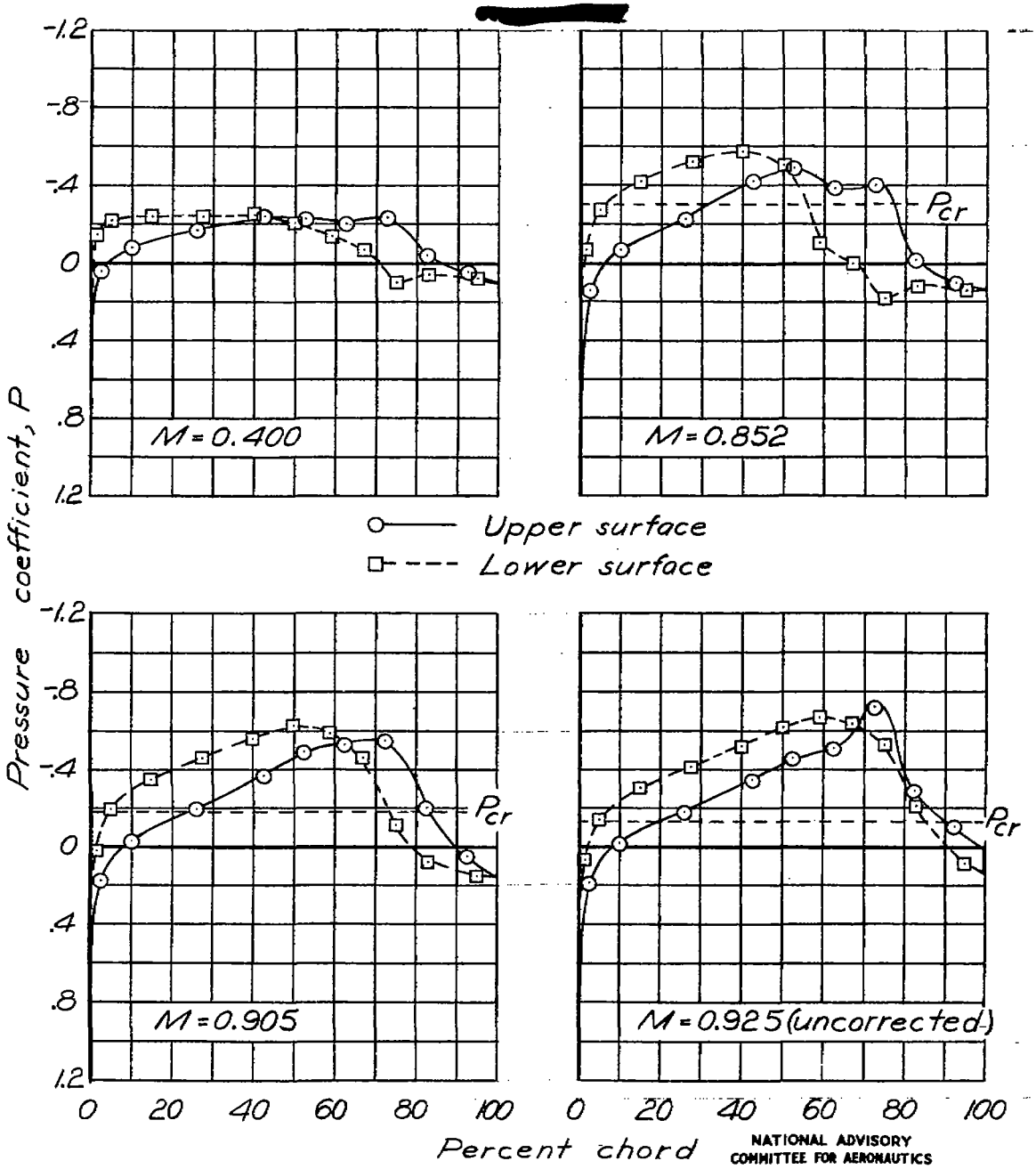

(a) $\alpha = -2°$.

[redacted]

Figure 3.– Pressure distribution about the horizontal tail at the 40-percent-semispan station. $\delta = 5°$; $\delta_t = 0°$.

[redacted]

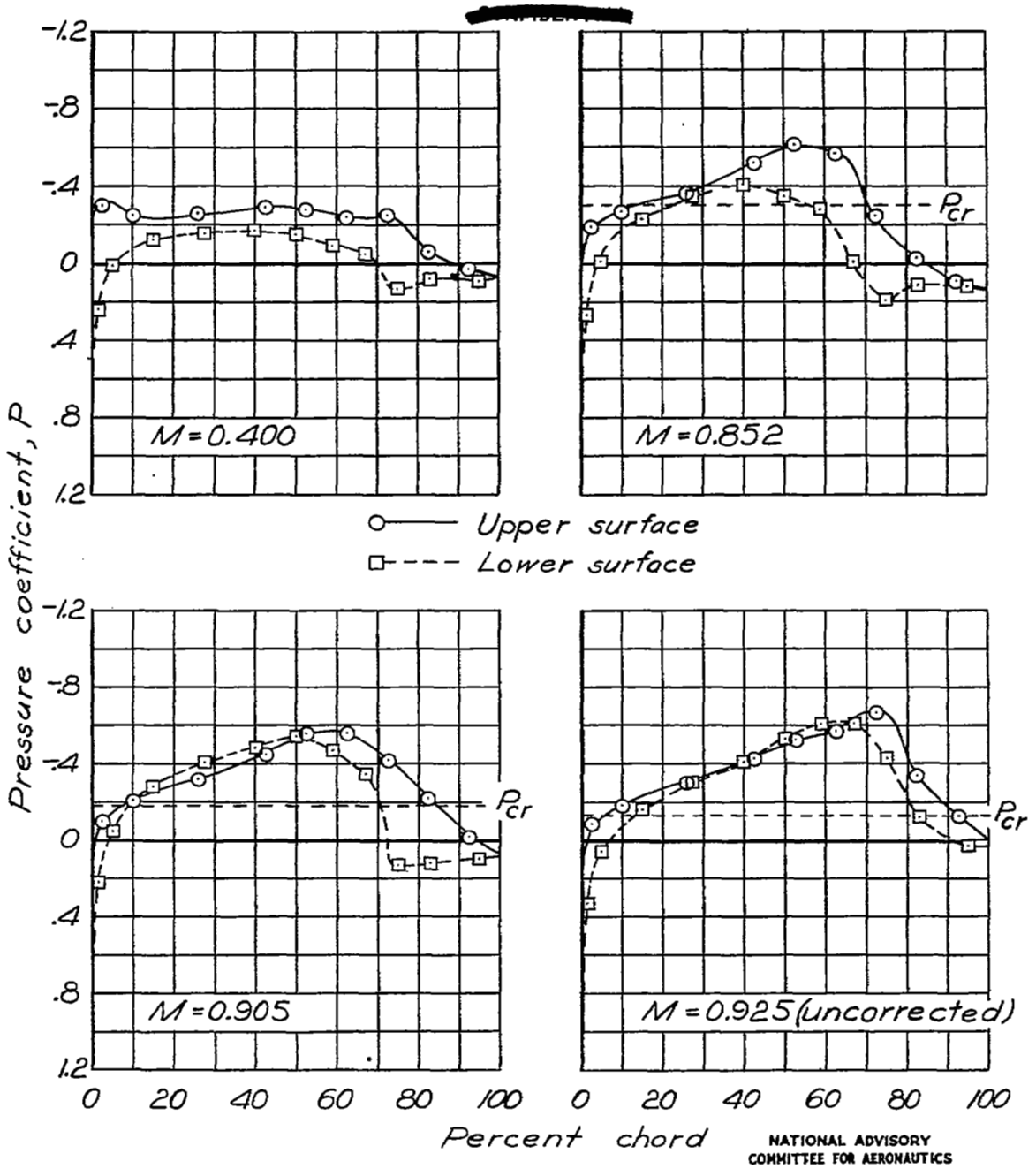

(b) $\alpha = 0°$.

[redacted]

Figure 3.– Continued.

[redacted]

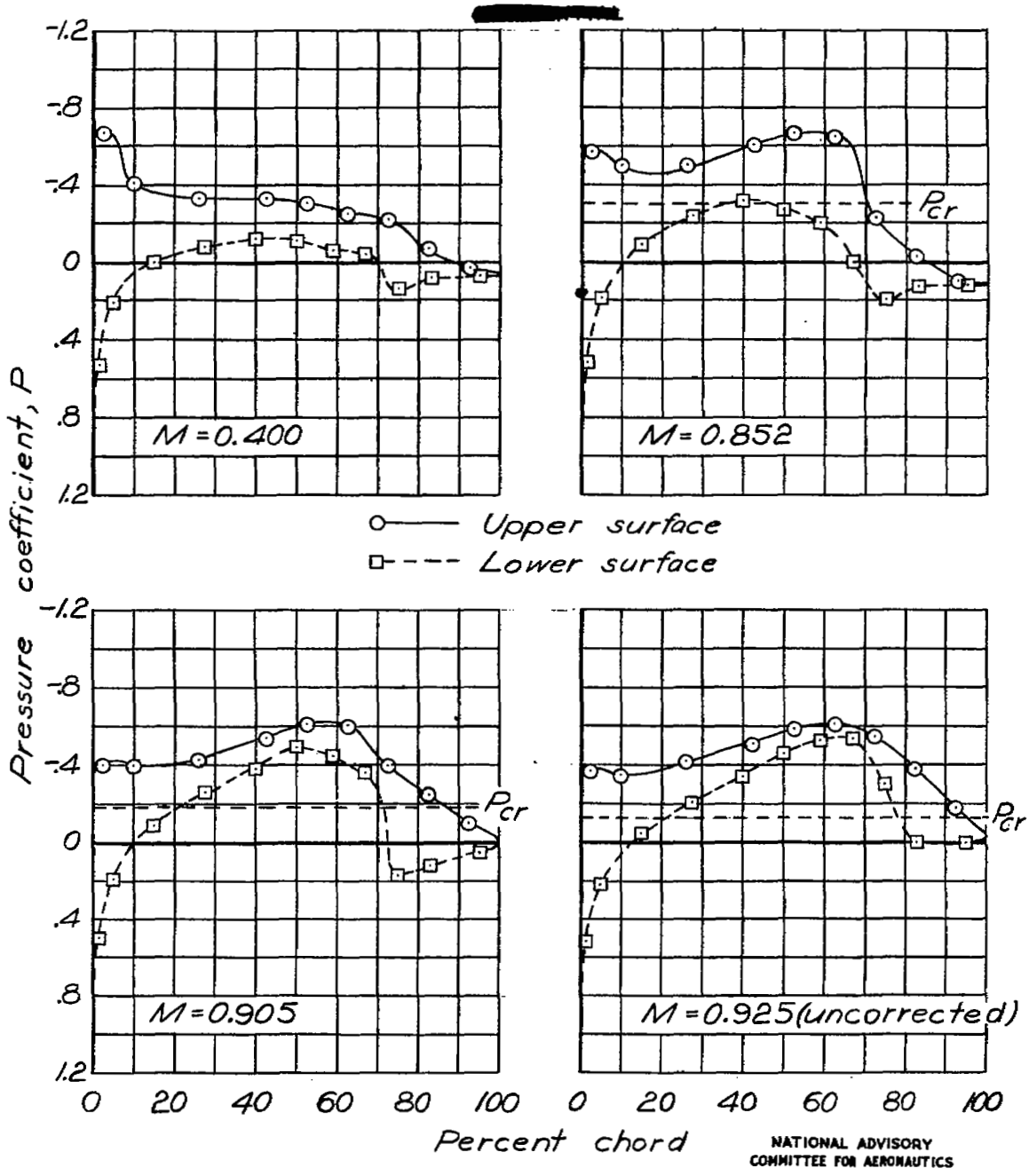

(c) $\alpha = 2°$.

[redacted]

Figure 3.- Continued.

[redacted]

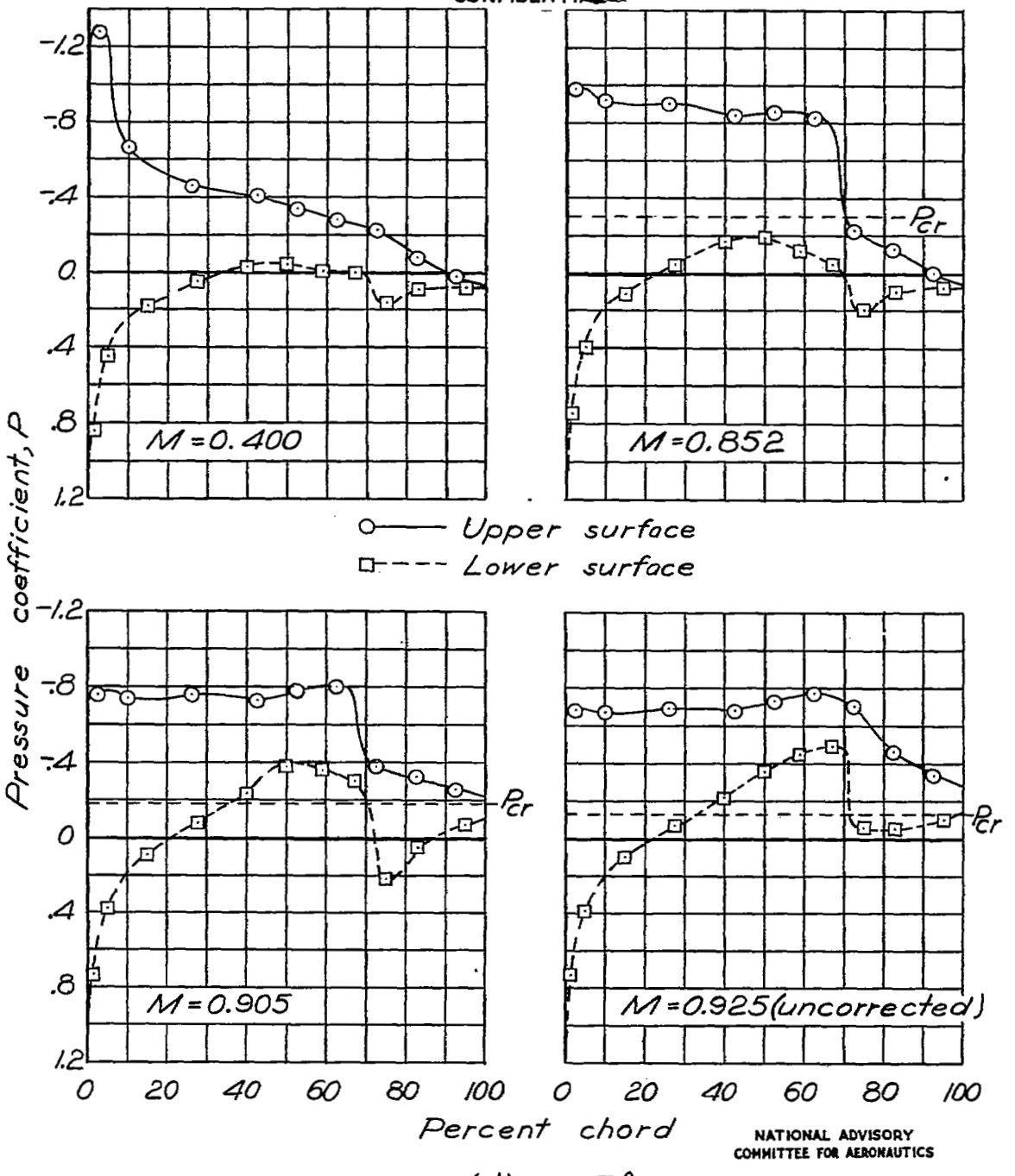

(d) $\alpha = 5°$.

[redacted]

Figure 3.- Concluded.

[redacted]

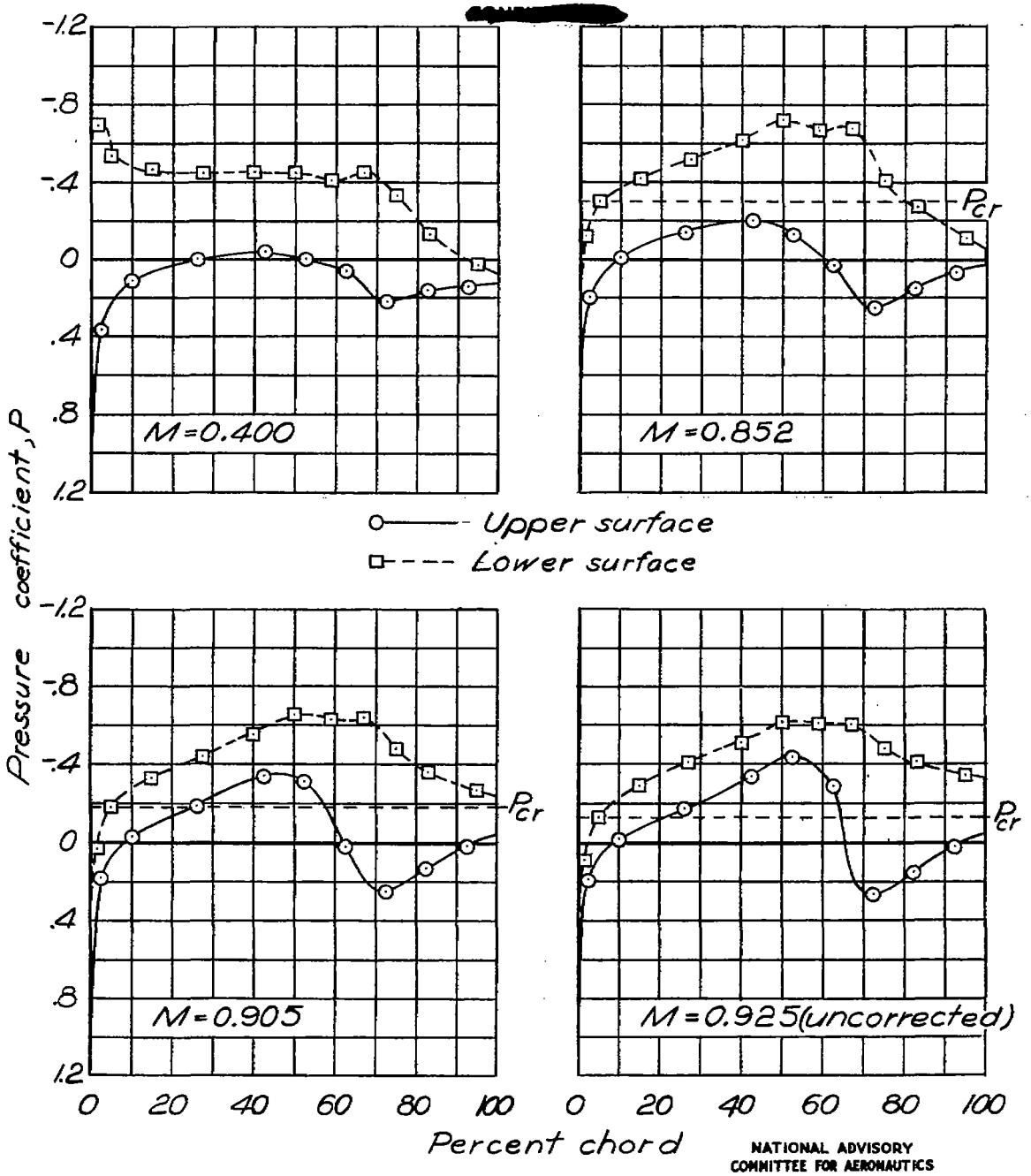

(a) $\alpha = -2°$

[redacted]

Figure 4.—Pressure distribution about the horizontal tail at the 40-percent-semispan station. $\delta = -5°$; $\delta_t = 0°$.

[redacted]

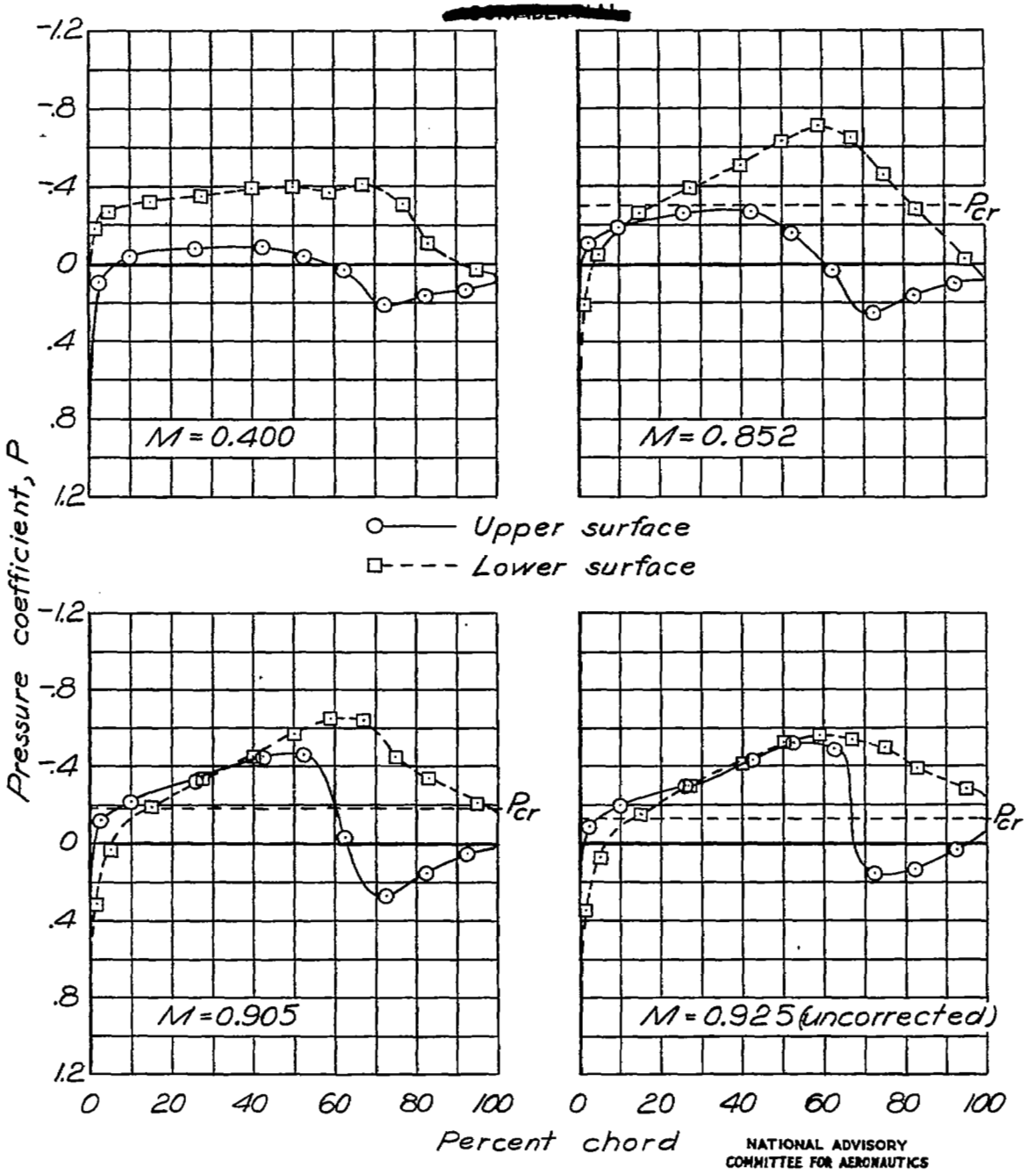

(b) $\alpha = 0°$.

[redacted]

Figure 4.– Continued.

[redacted]

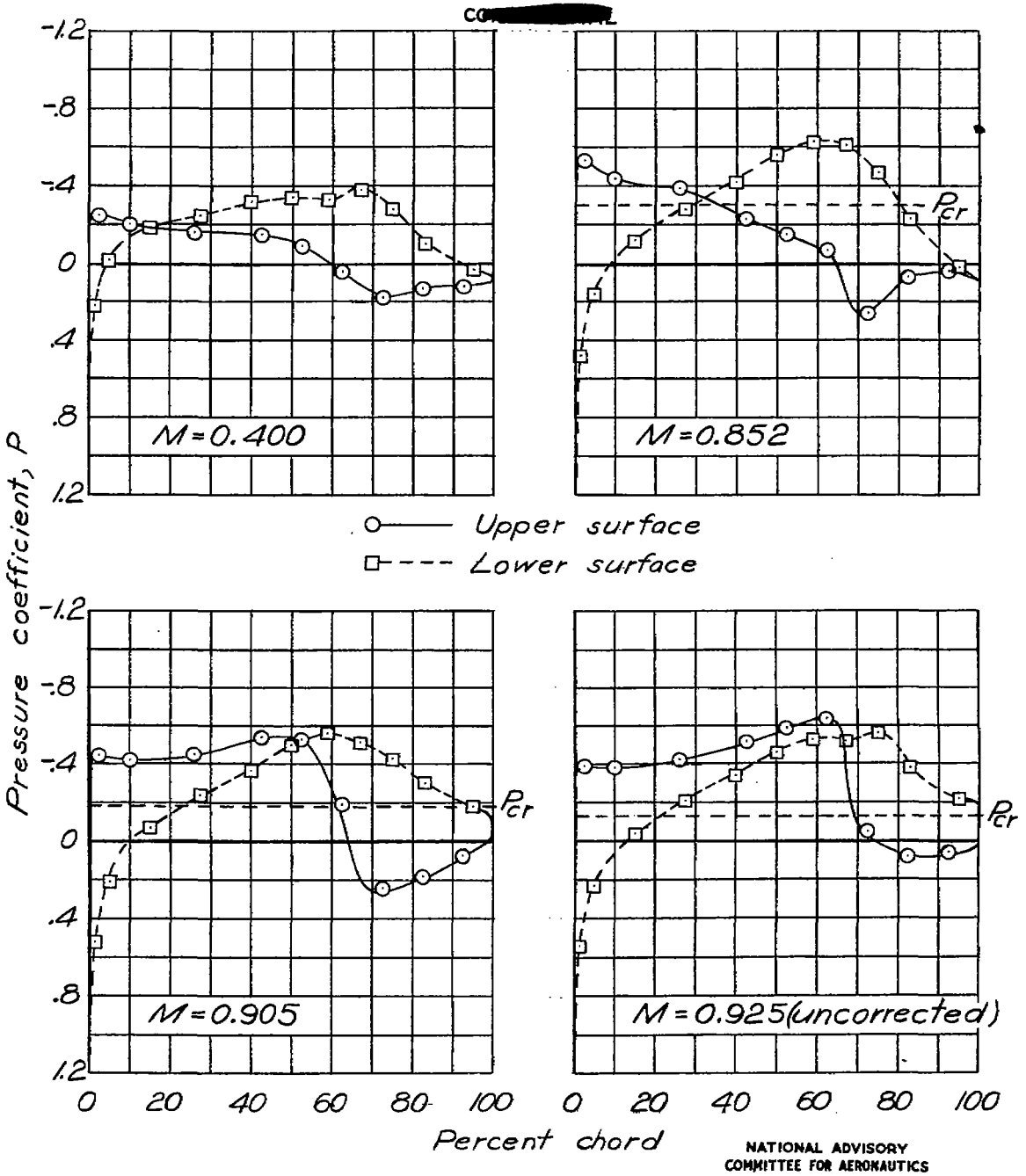

(c) $\alpha = 2°$.

[redacted]

Figure 4.- Continued.

[redacted]

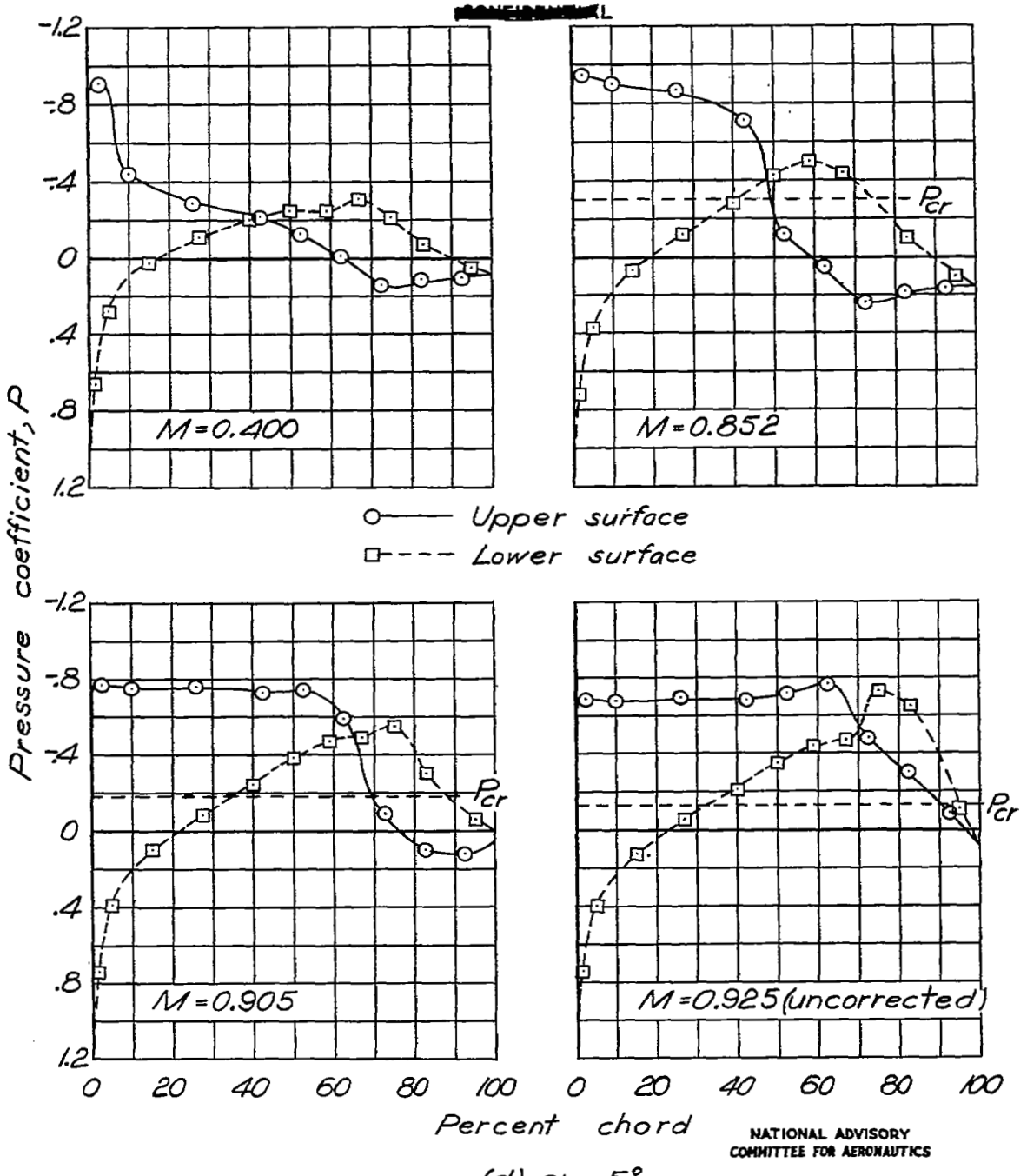

(d) $\alpha = 5°$.

[redacted]

Figure 4.– Concluded.

[redacted]

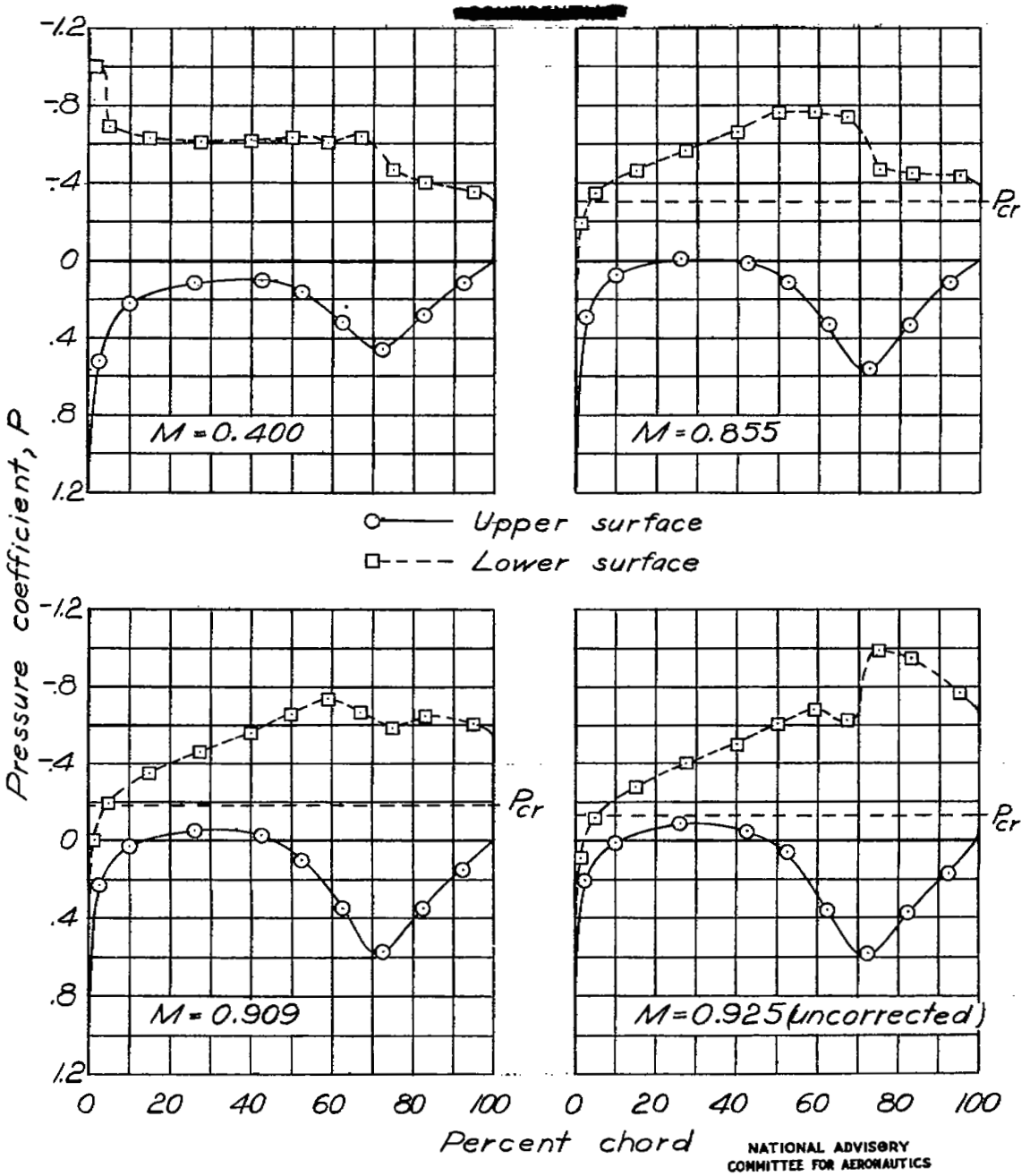

(a) $\alpha = -2°$.

[redacted]

Figure 5.– Pressure distribution about the horizontal tail at the 40-percent-semispan station. $\delta = -15°$; $\delta_f = 0°$.

[redacted]

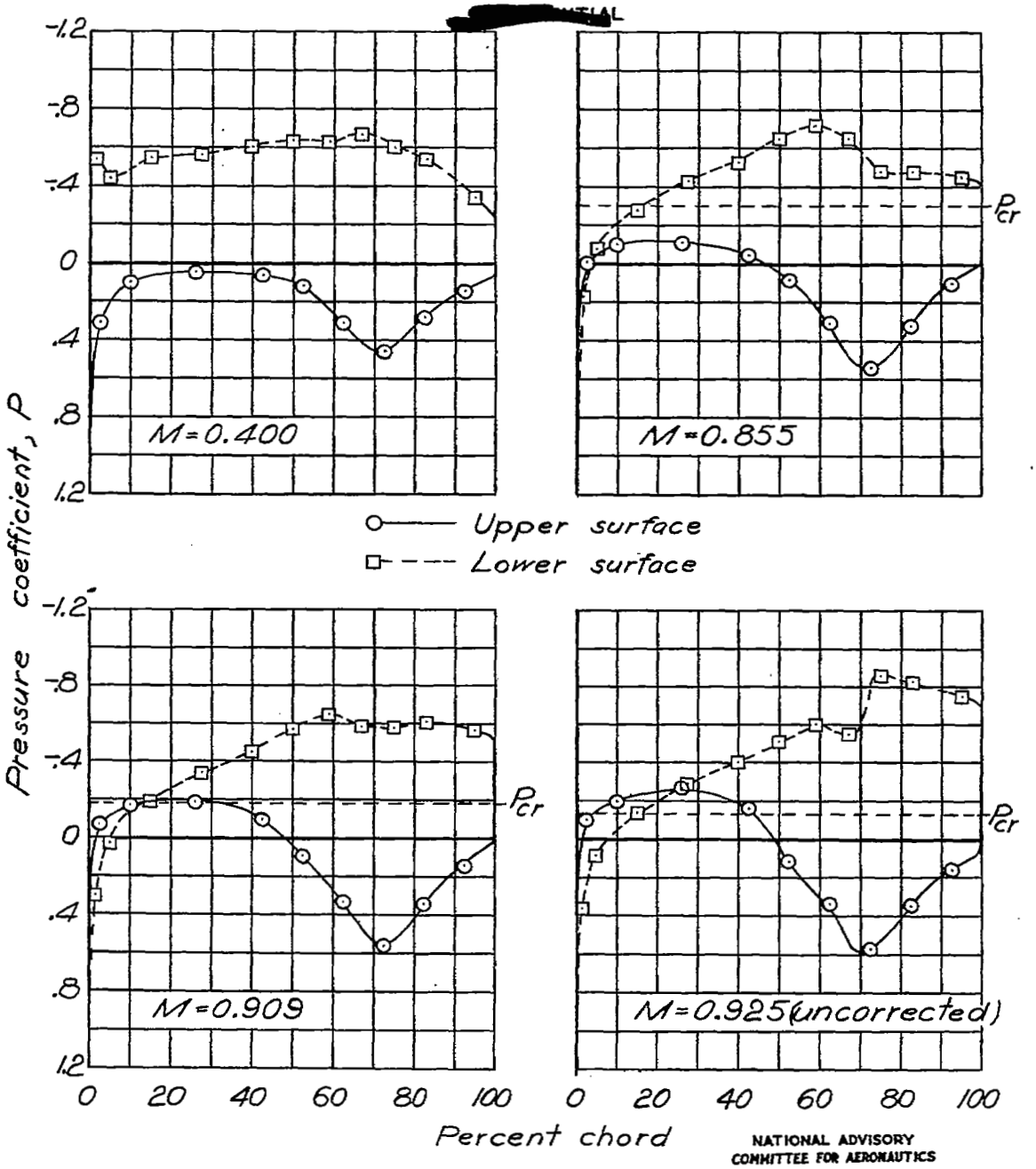

(b) $\alpha = 0°$.

[redacted]

Figure 5.- Continued.

[redacted]

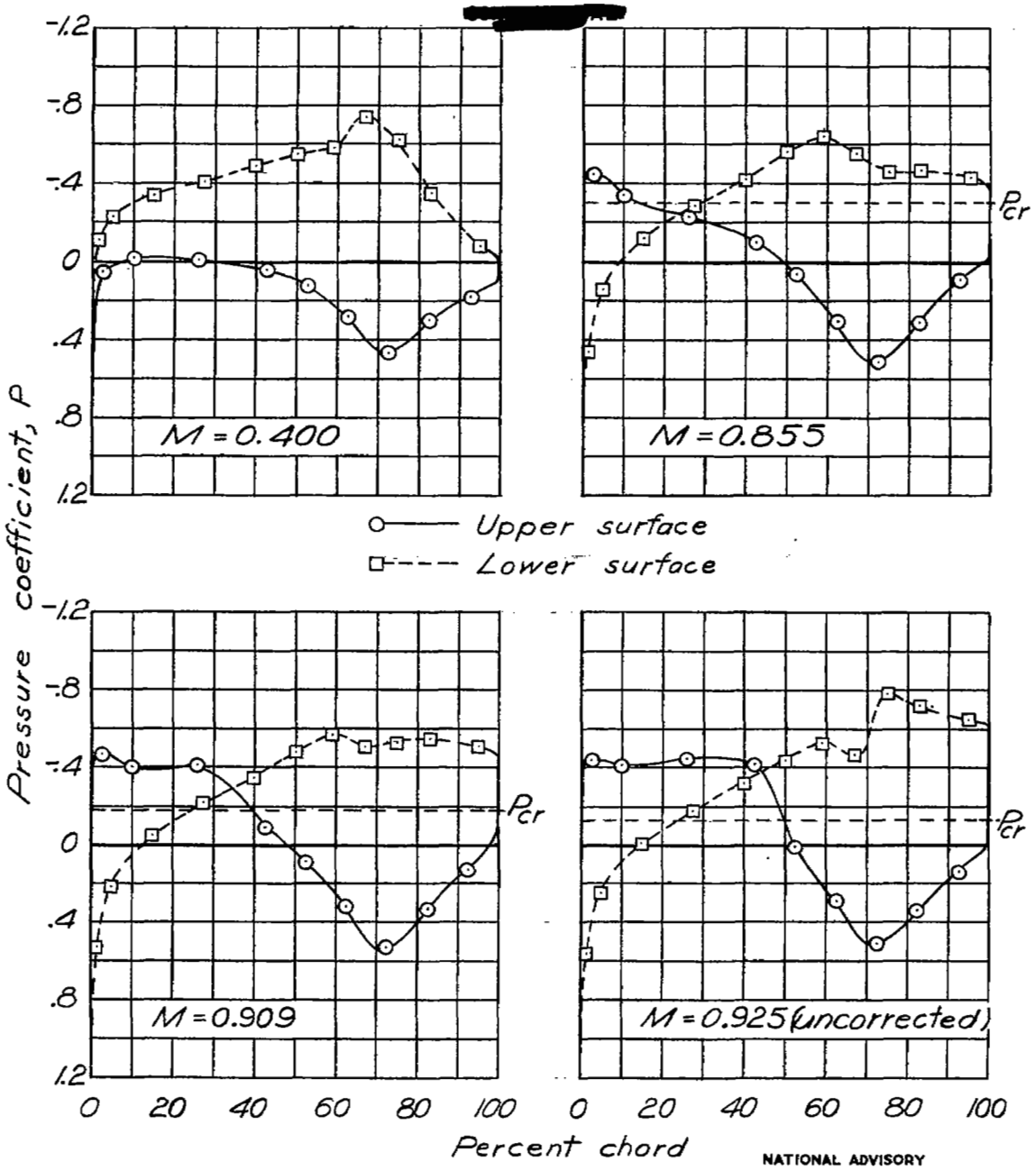

NATIONAL ADVISORY COMMITTEE FOR AERONAUTICS

(c) $\alpha = 2°$.

[redacted]

Figure 5.– Continued.

[redacted]

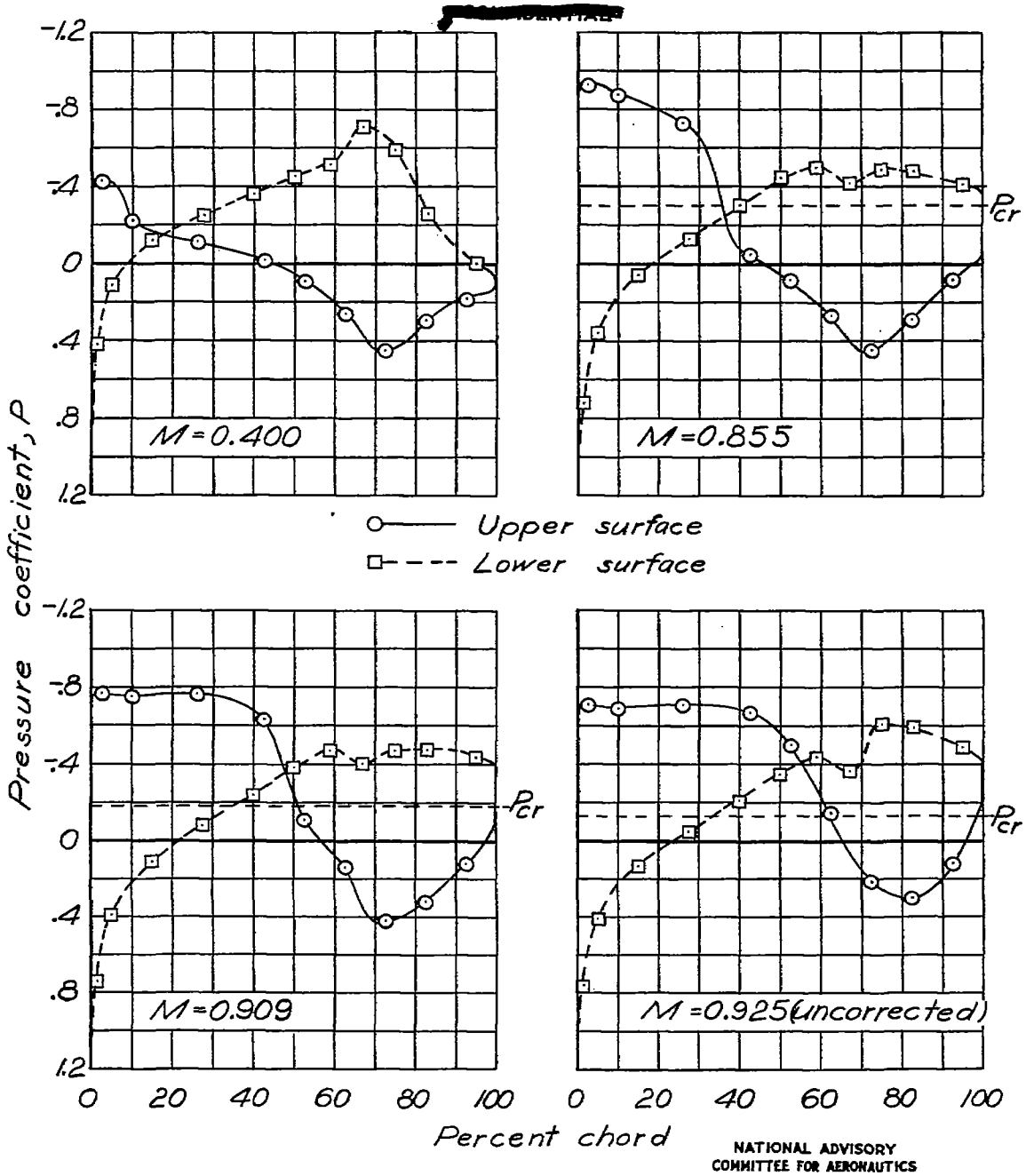

(d) $\alpha = 5^{\circ}$.

[redacted]

Figure 5.- Concluded.

[redacted]

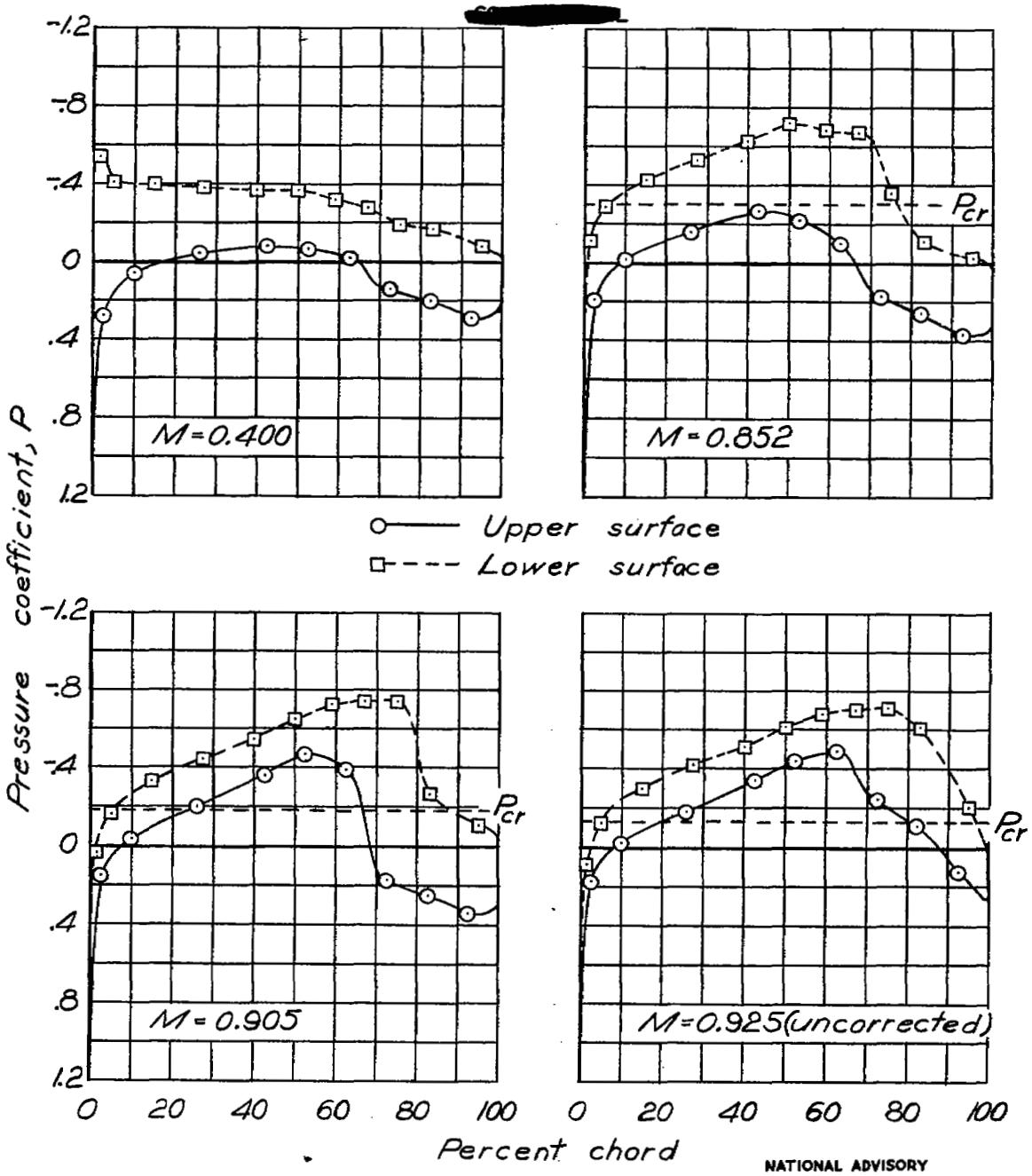

NATIONAL ADVISORY COMMITTEE FOR AERONAUTICS

(a) $\alpha = -2°$.

[redacted]

Figure 6.– Pressure distribution about the horizontal tail at the 40-percent-semispan station. $\delta = 0°$; $\delta_t = -10°$.

[redacted]

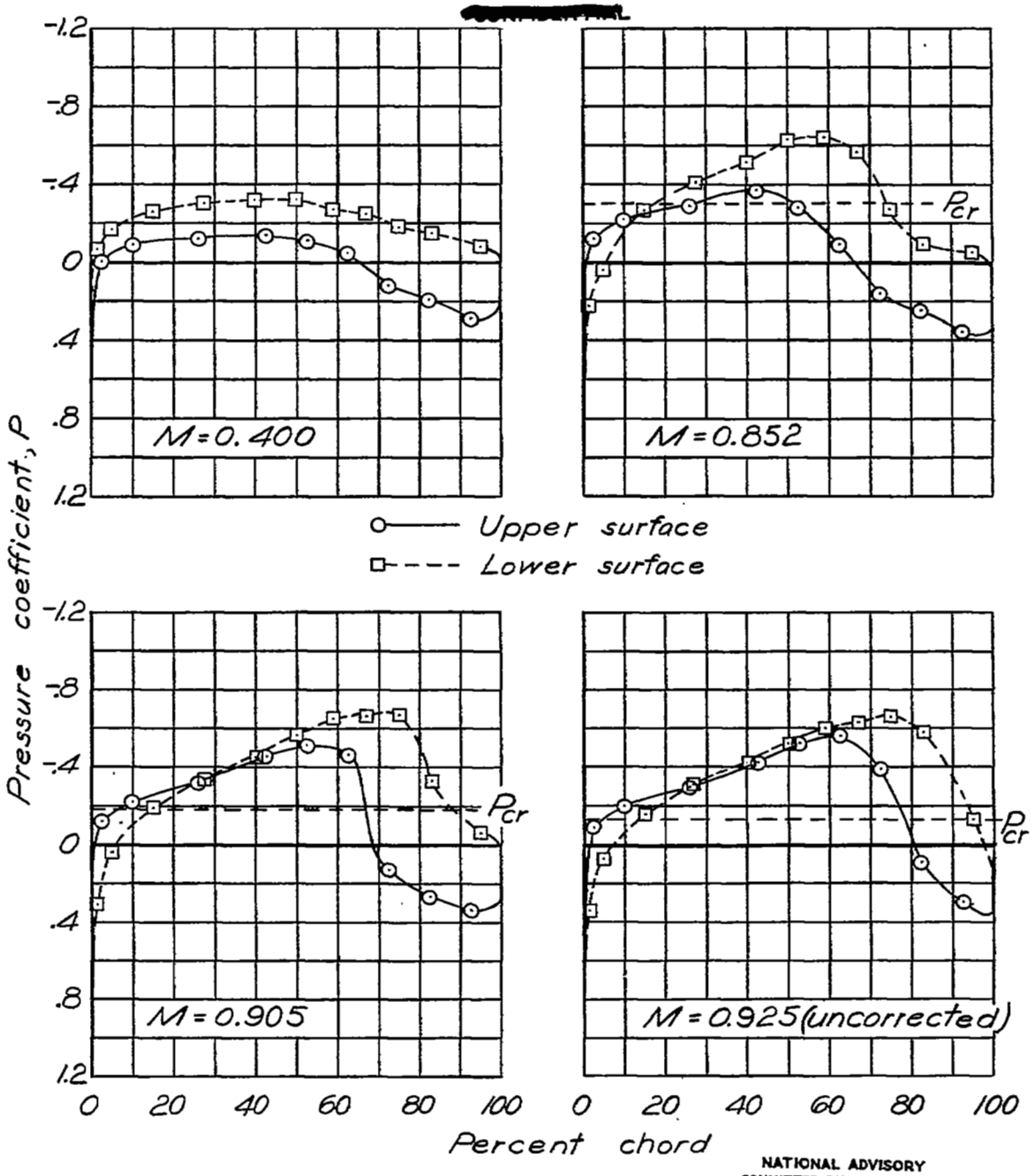

NATIONAL ADVISORY COMMITTEE FOR AERONAUTICS

(b) $\alpha = 0°$.

[redacted]

Figure 6.– Continued.

[redacted]

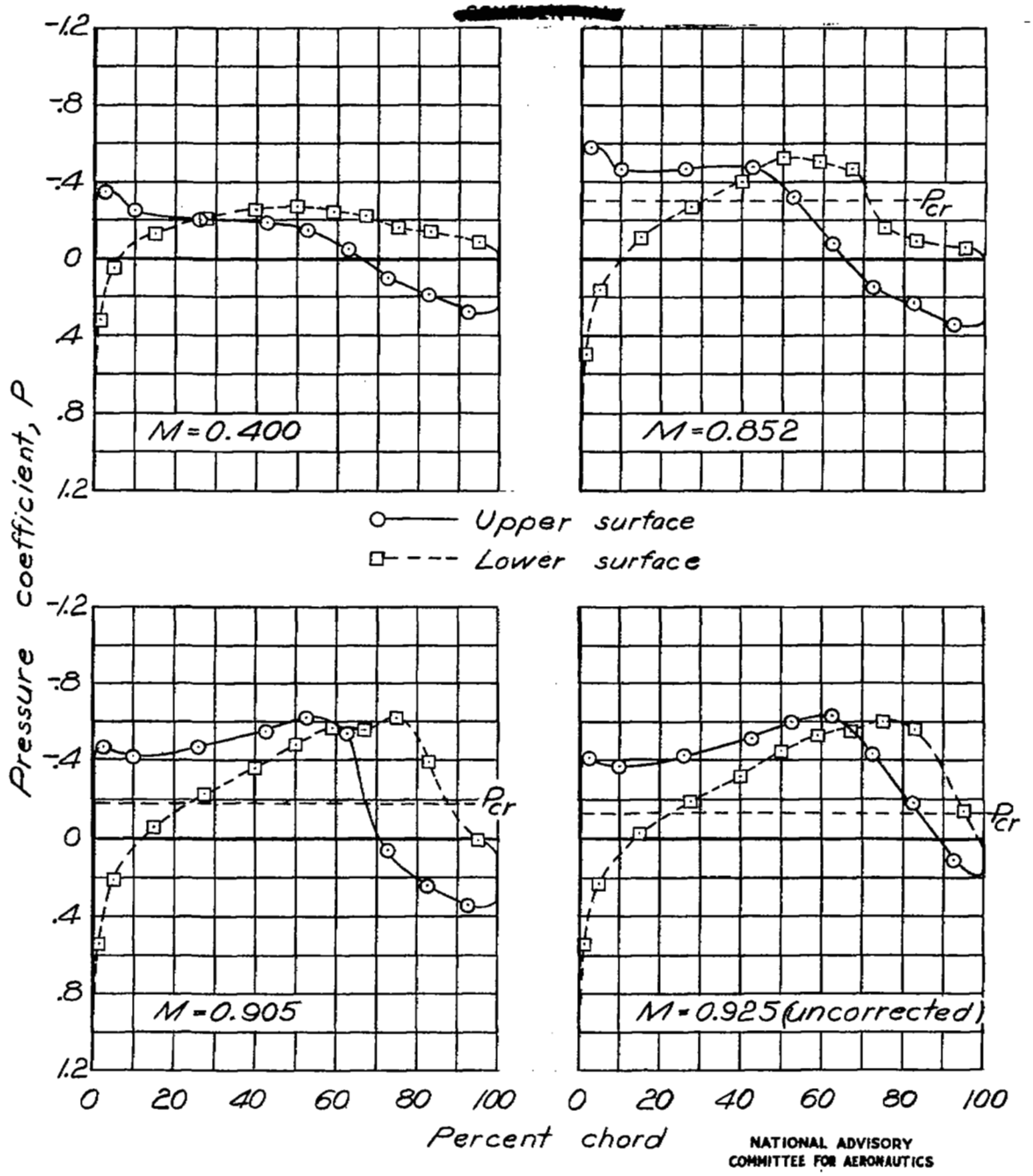

(c) $\alpha = 2°$.

[redacted]

Figure 6 .– Continued.

[redacted]

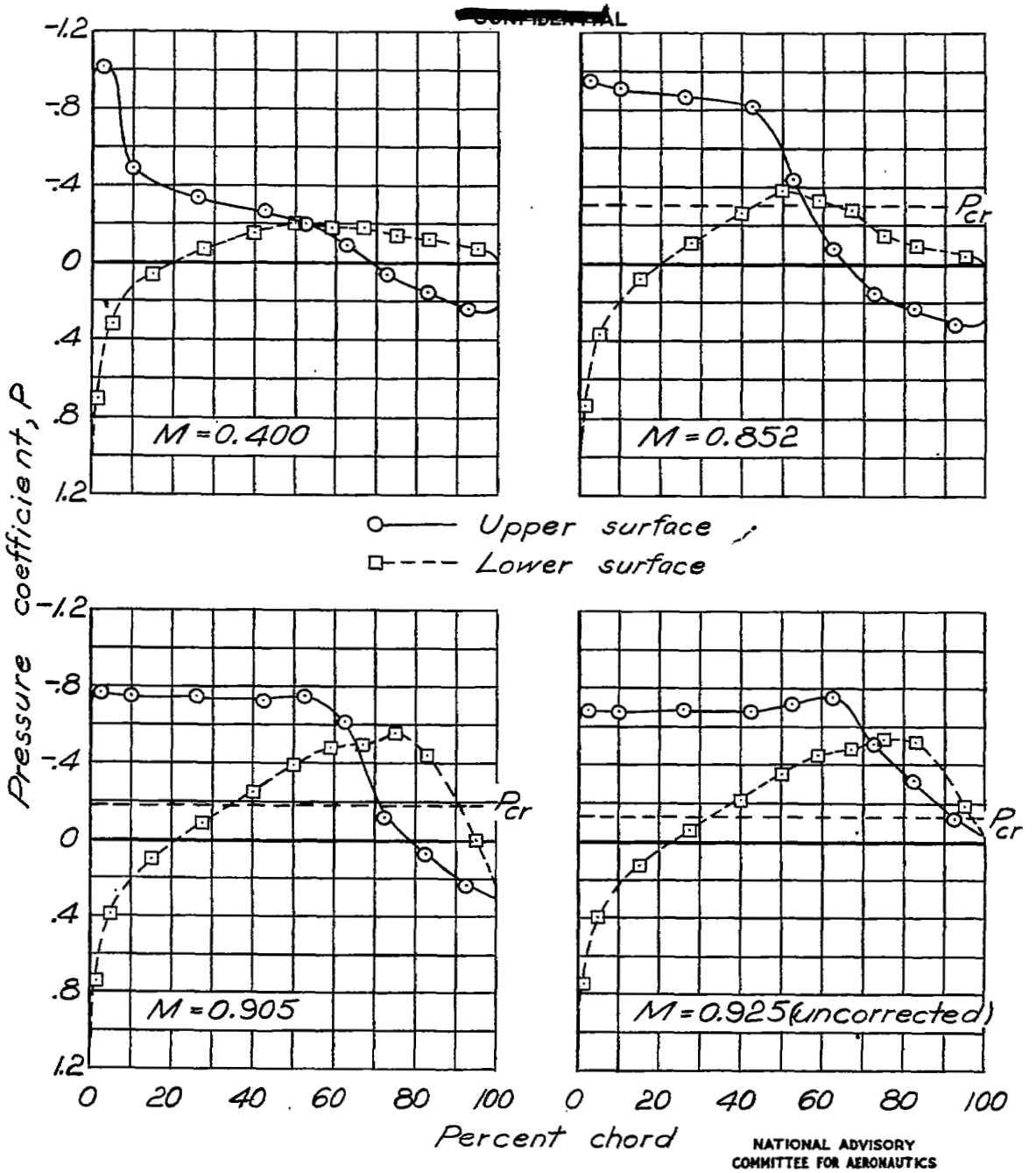

(d) $\alpha = 5°$.

[redacted]

Figure 6.– Concluded.

[redacted]

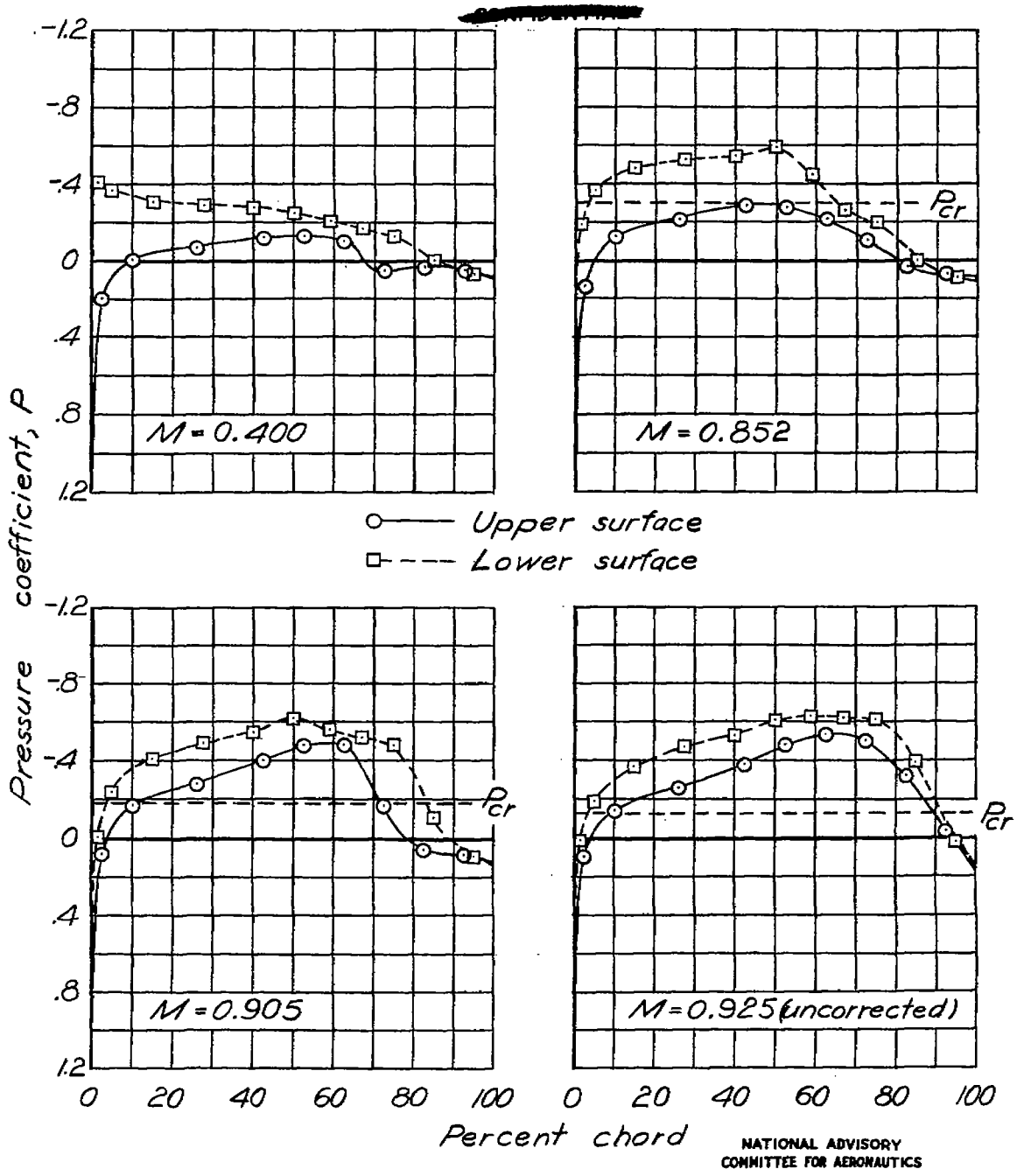

(a) $\alpha = -2°$.

[redacted]

Figure 7.- Pressure distribution about the horizontal tail at the 90-percent-semispan station. $\delta = 0°$; $\delta_f = -10°$.

[redacted]

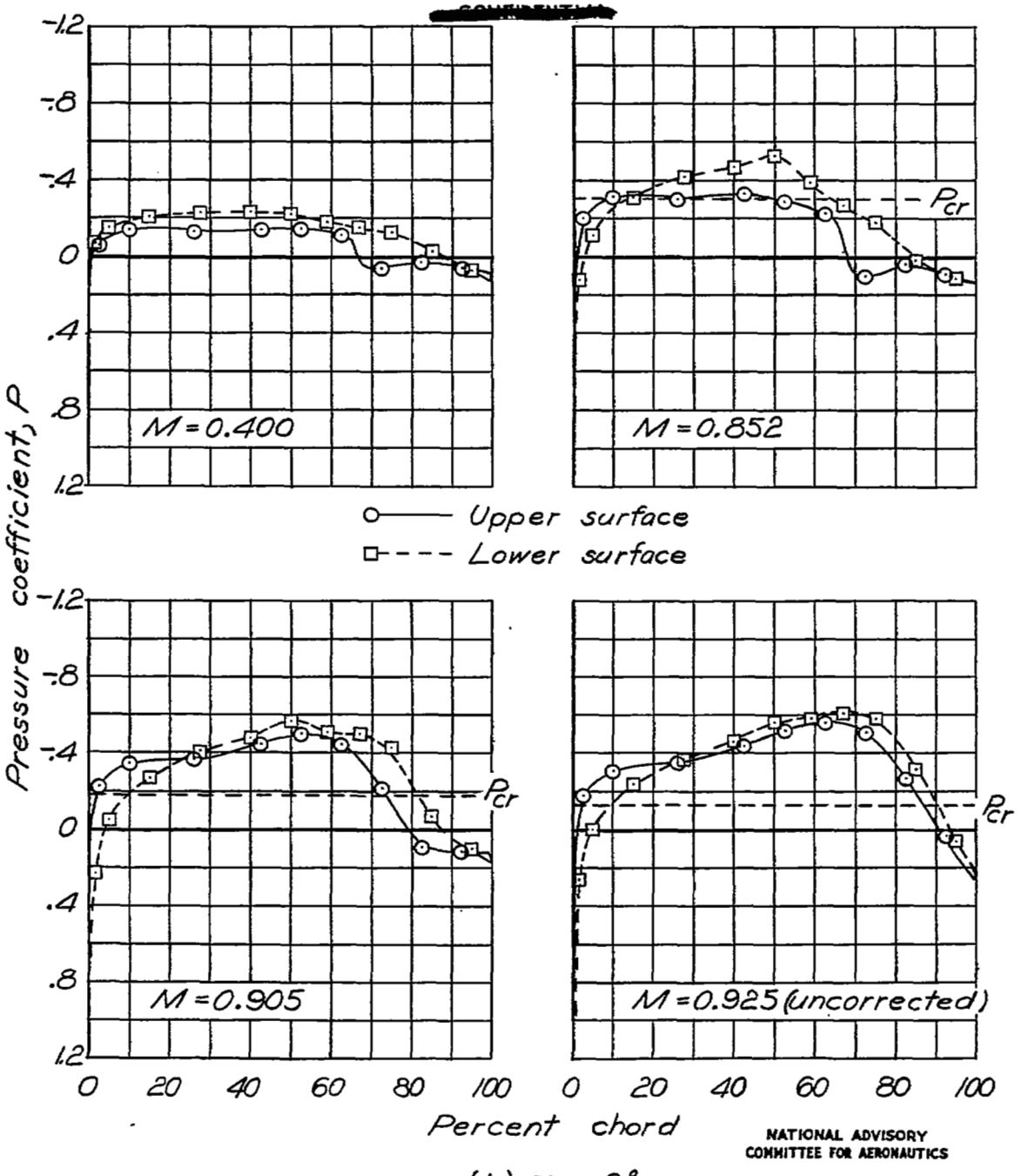

(b) $\alpha = 0°$.

[redacted]

Figure 7.—Continued.

[redacted]

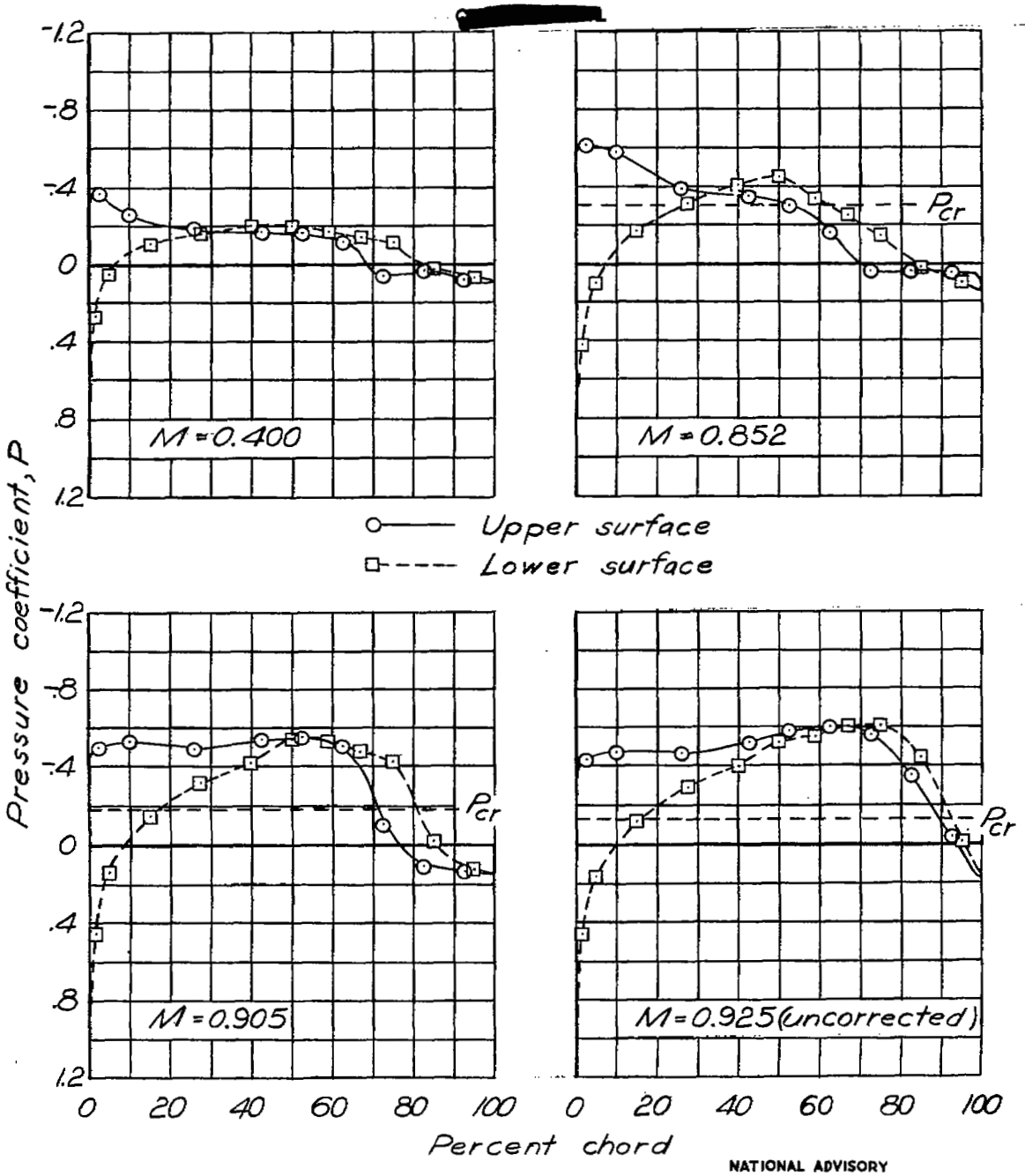

NATIONAL ADVISORY COMMITTEE FOR AERONAUTICS

(c) $\alpha = 2°$.

[redacted]

Figure 7.- Continued.

[redacted]

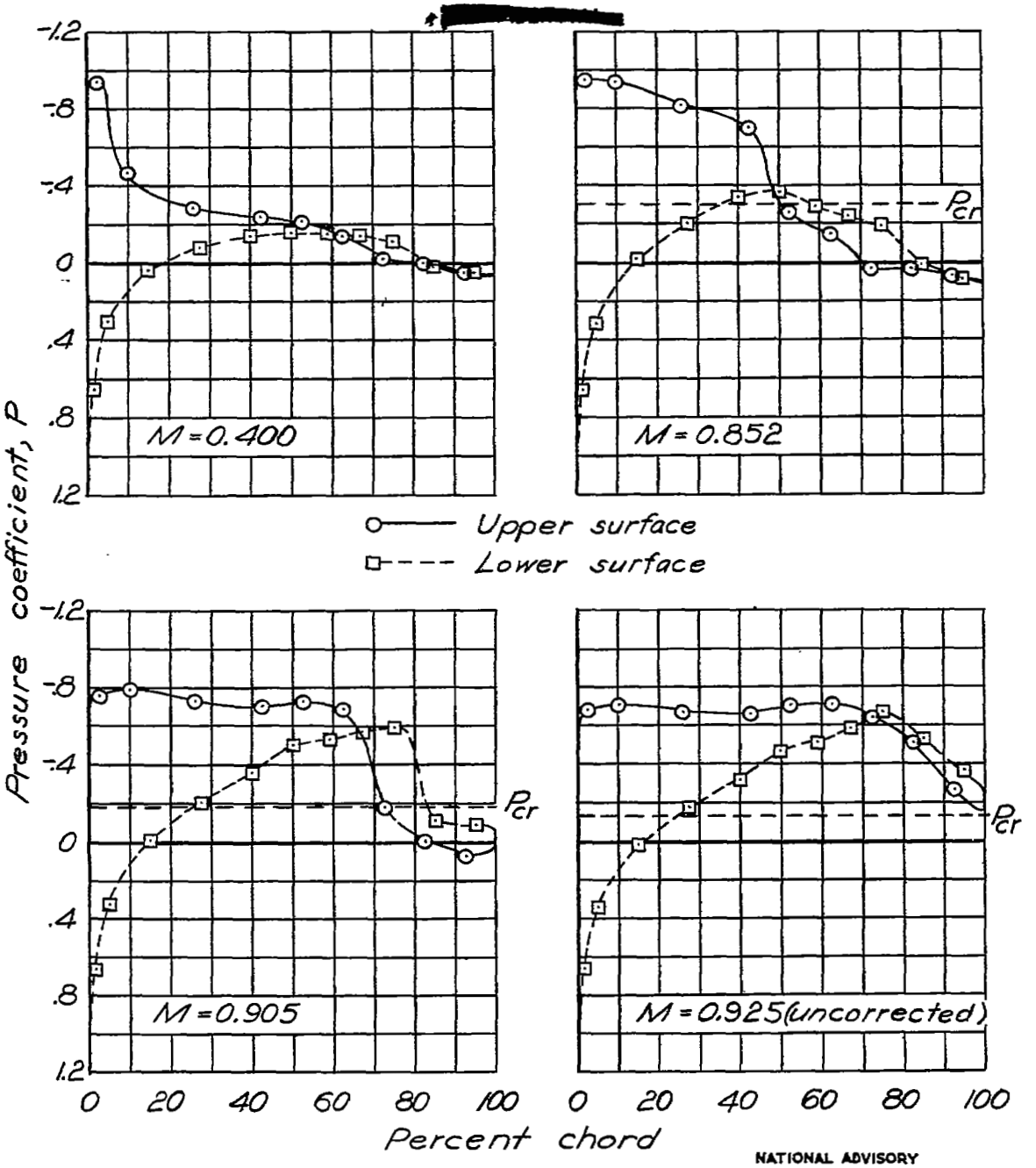

NATIONAL ADVISORY COMMITTEE FOR AERONAUTICS

(d) $\alpha = 5°$.

[redacted]

Figure 7.- Concluded.

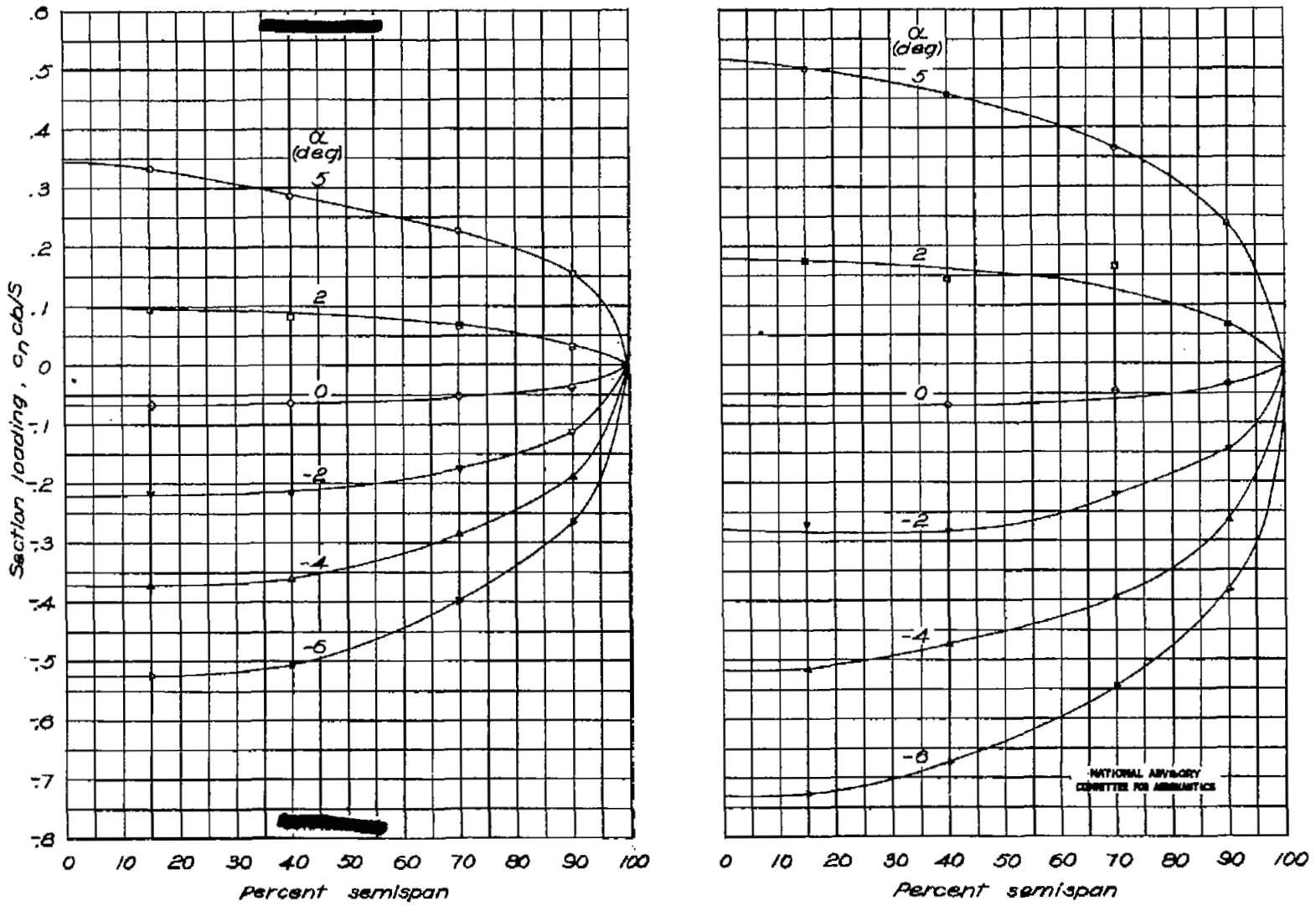

(a) M=0.400.

(b) M=0.852.

Figure 8 .-Spanwise variation in section loading. $\delta=0°$; $\delta_f=0°$.

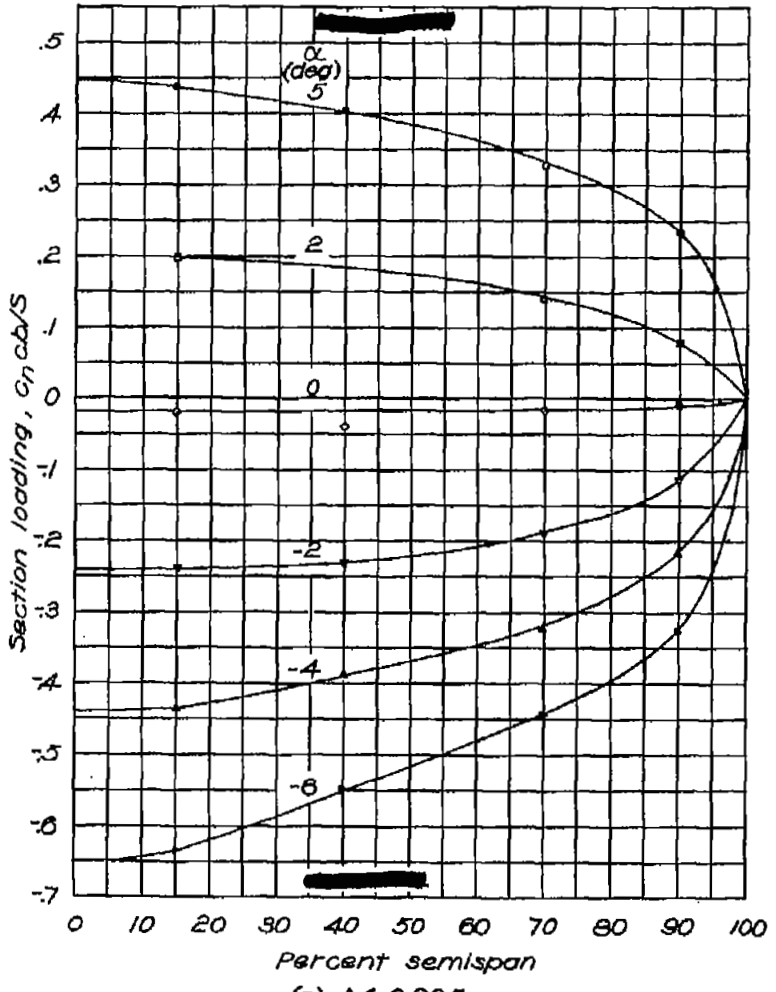

(c) M=0.905.

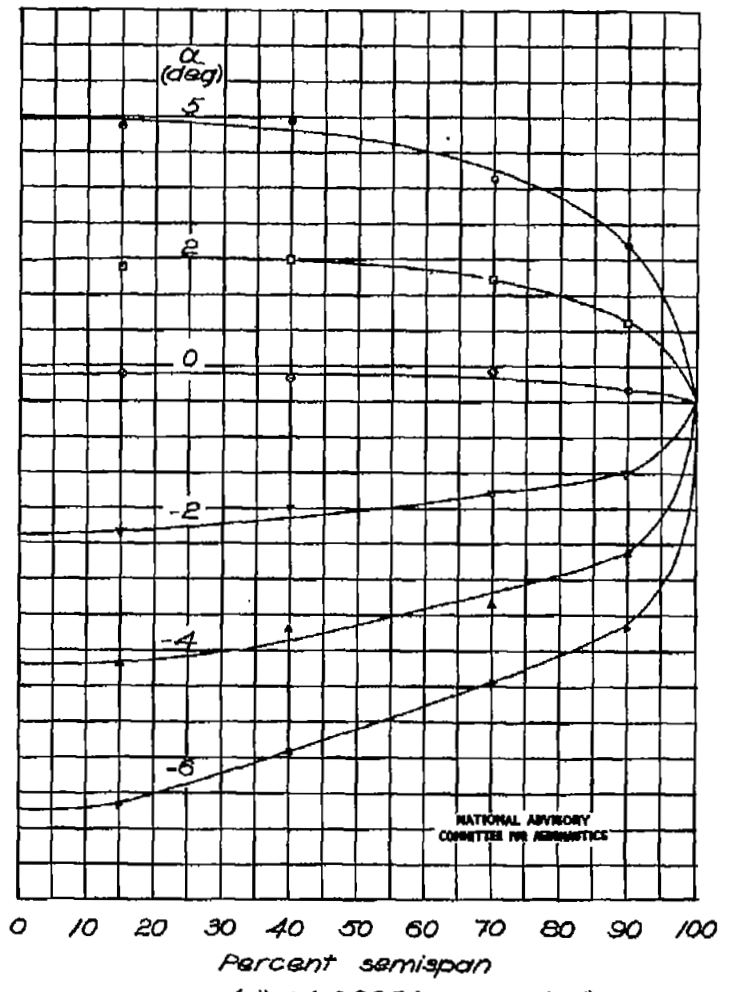

(d) M=0.925 (uncorrected).

Figure 8.- Concluded.

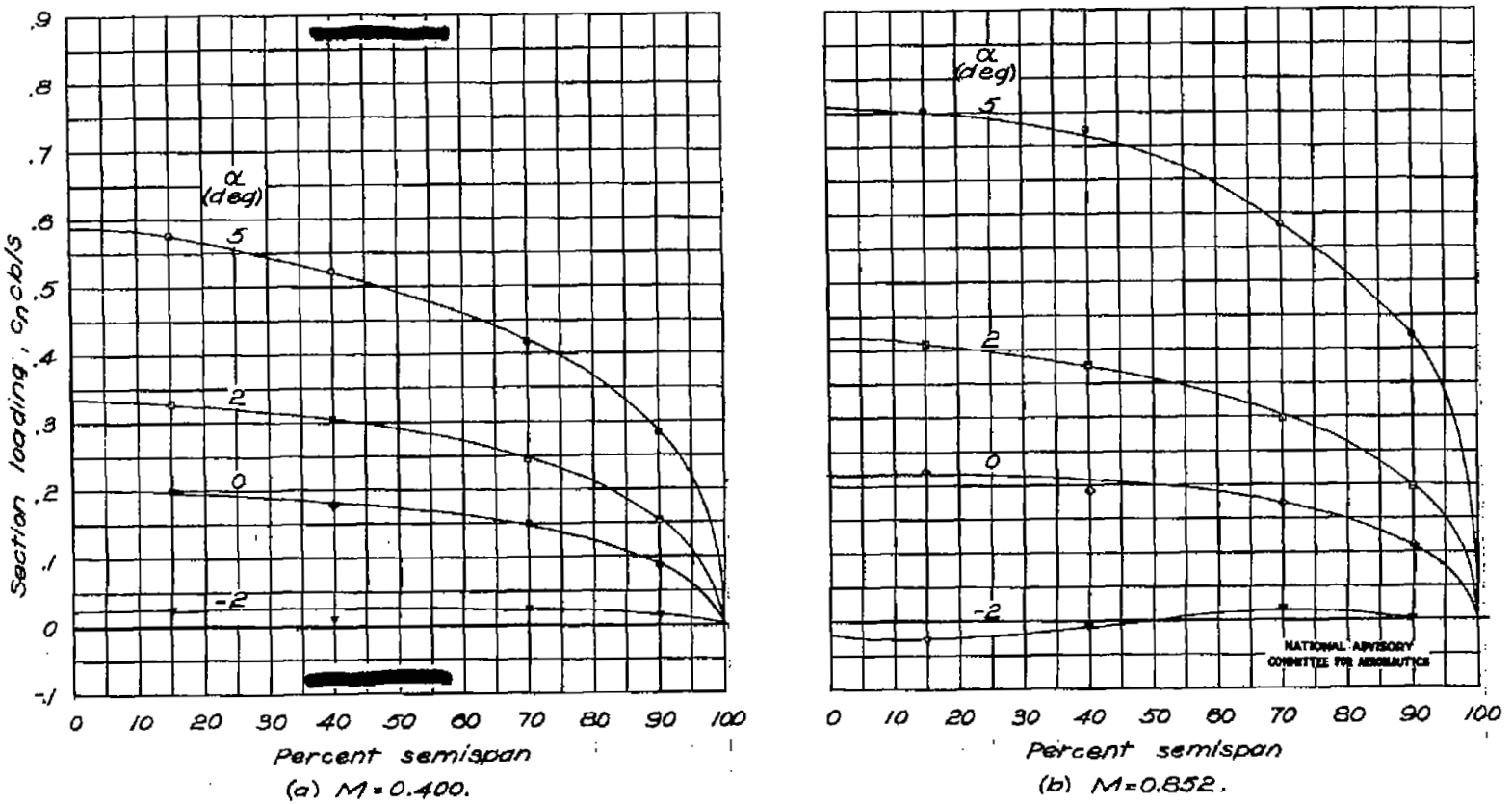

Figure 9.- Spanwise variation in section loading. $\delta = 5°$; $\delta_f = 0°$.

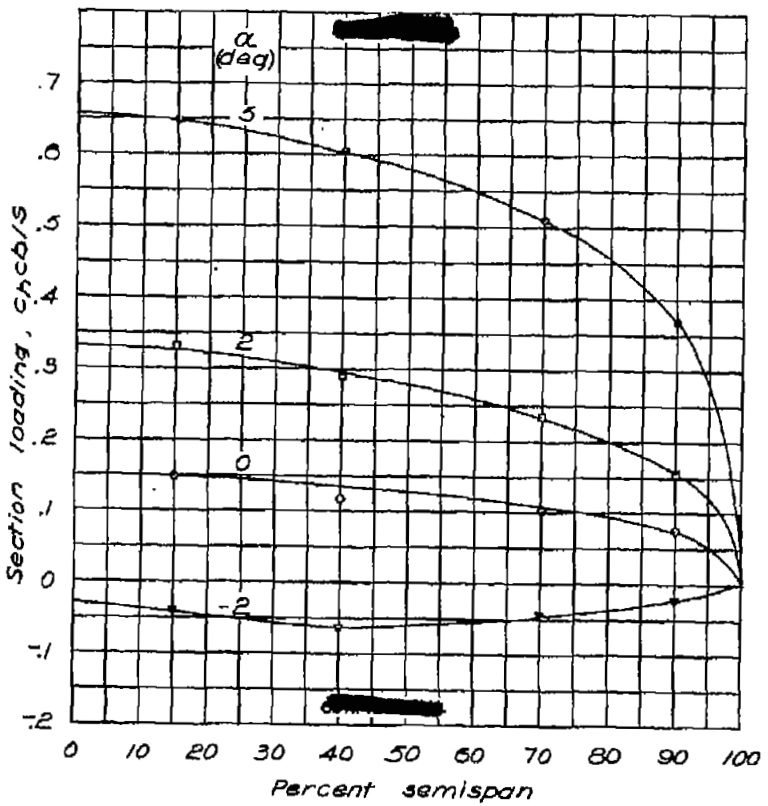

(c) $M = 0.905$.

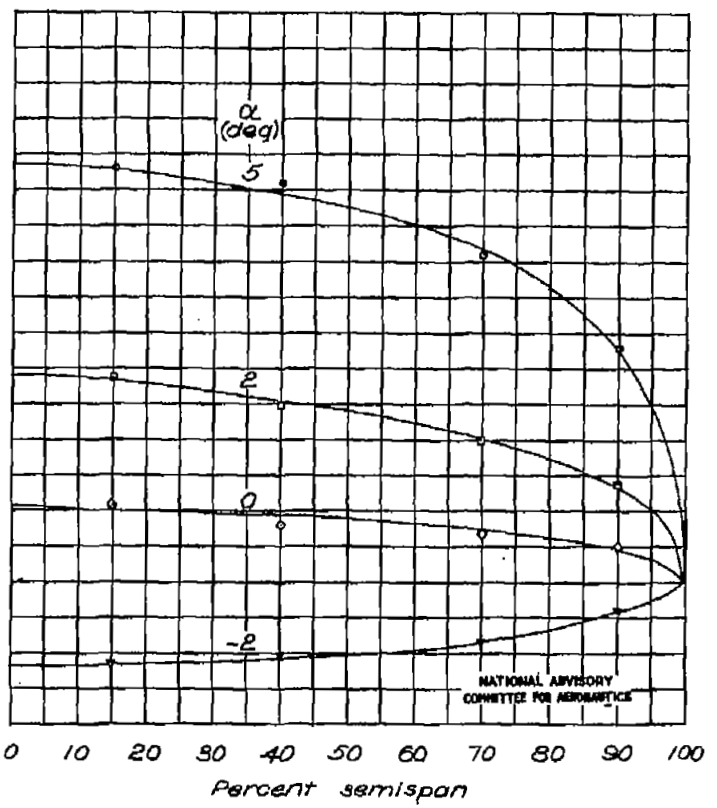

(d) $M = 0.925$ (uncorrected).

Figure 9.– Concluded.

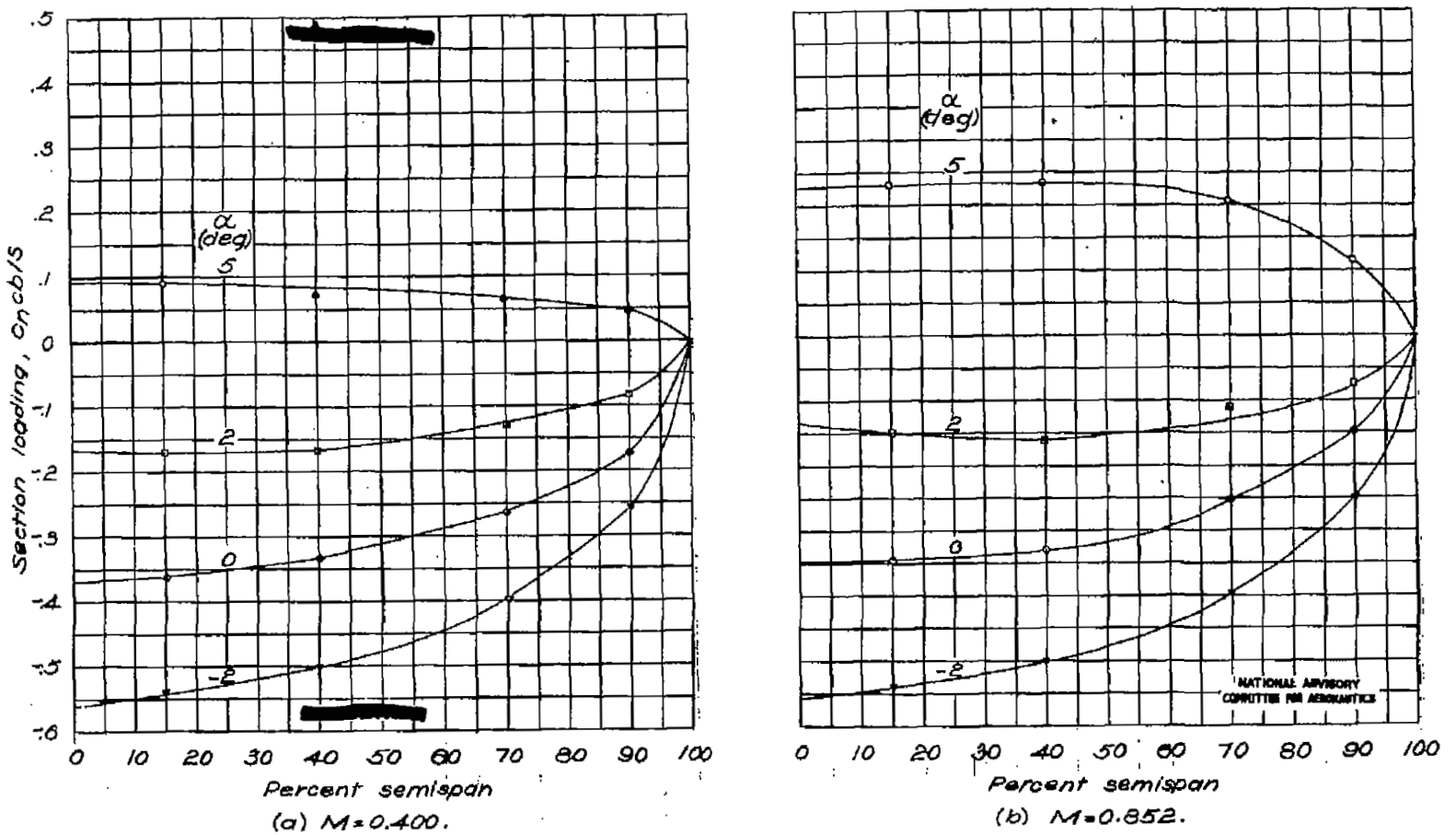

Figure 10.-Spanwise variation in section loading. $\delta = -5°$; $\delta_f = 0°$.

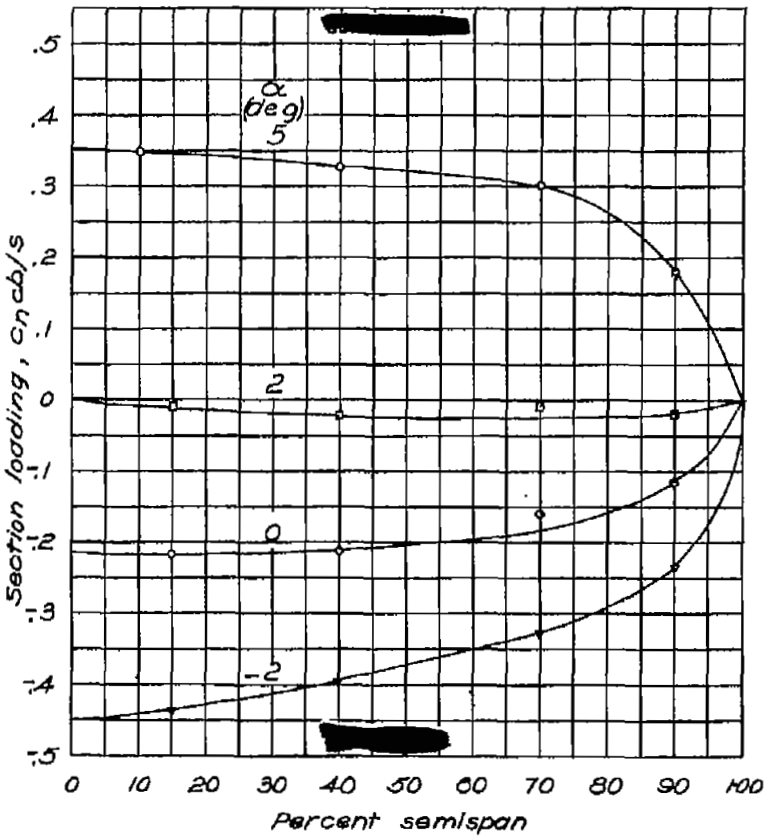

(c) $M = 0.905$.

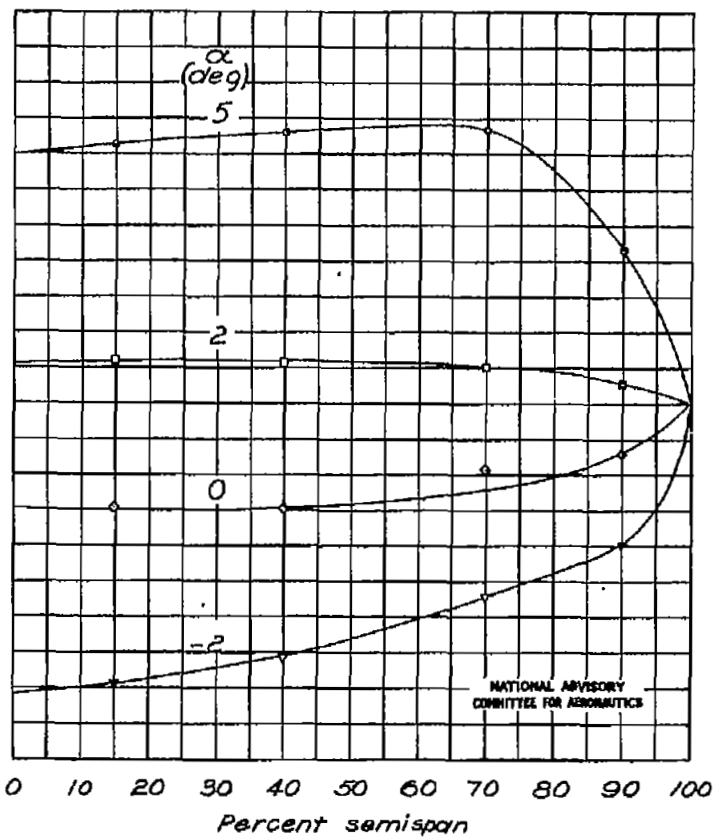

(d) $M = 0.925$ (uncorrected).

Figure 10.- Concluded.

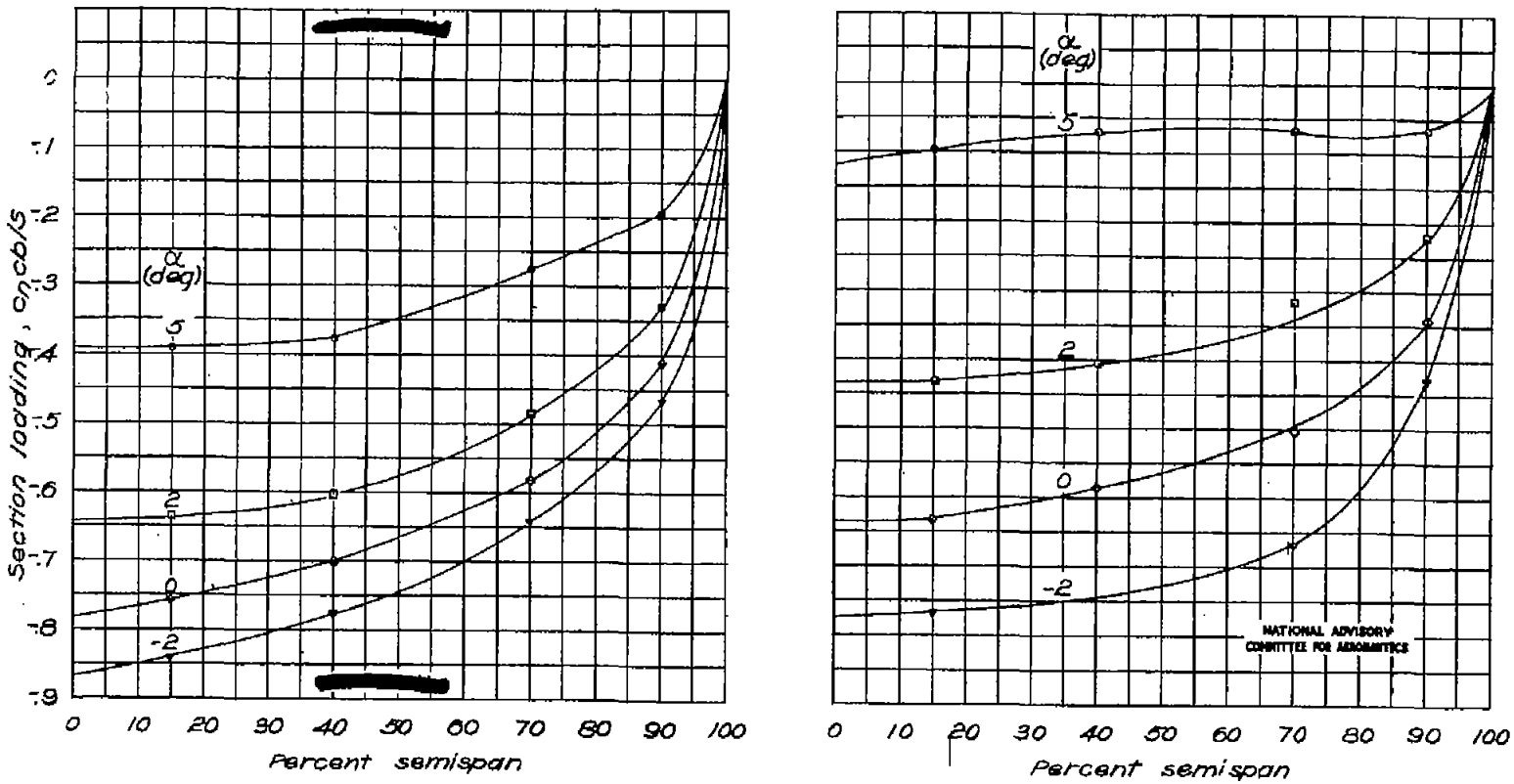

(a) $M = 0.400$.

(b) $M = 0.855$.

Figure 11 .- Spanwise variation in section loading. $\delta = -15°$; $\delta_f = 0°$.

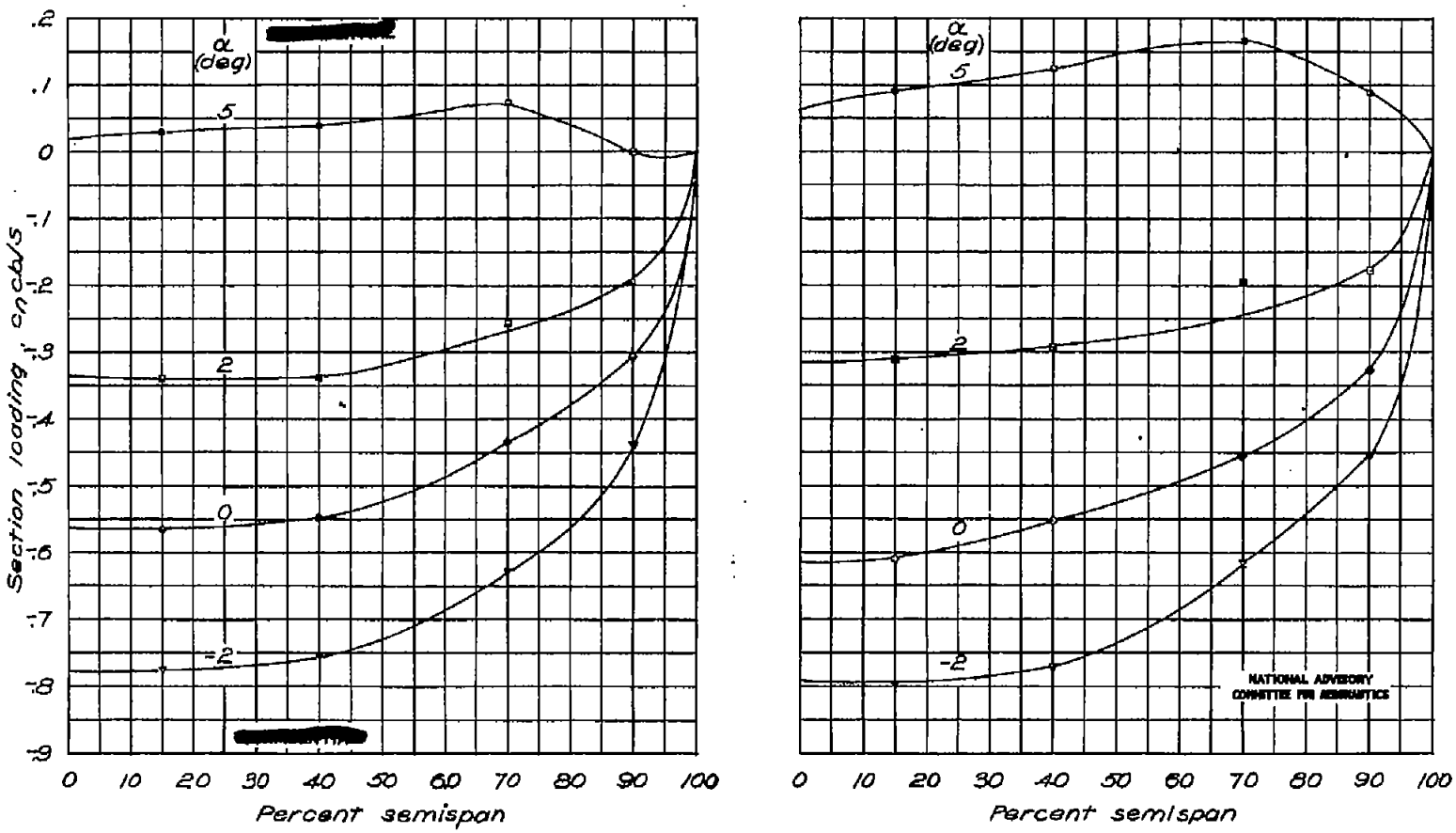

(c) M=0.909.

(d) M=0.925 (uncorrected).

Figure 11 .-Concluded.

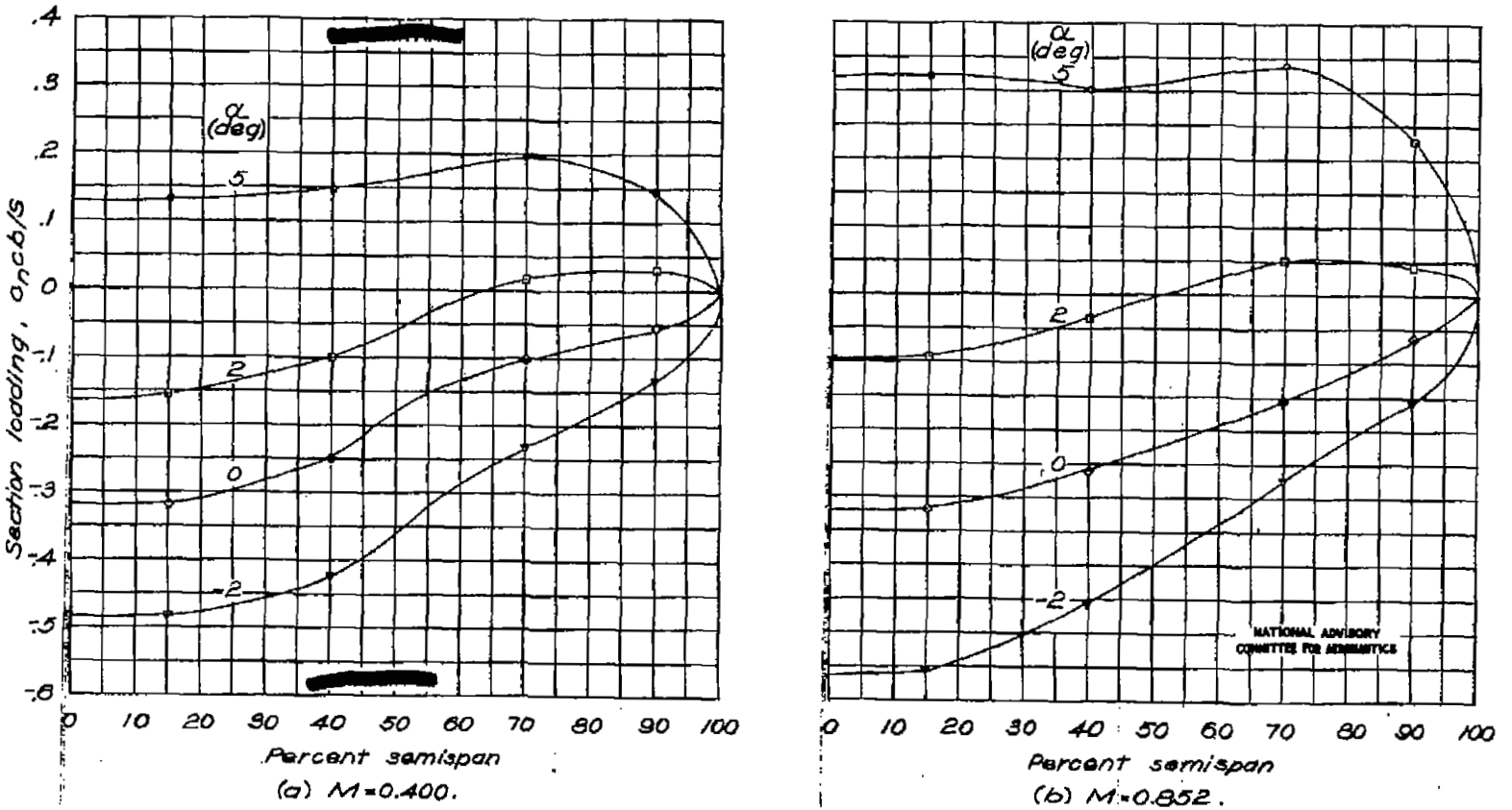

Figure 12 .- Spanwise variation in section loading. $\delta=0°$; $\delta_f=-10°$.

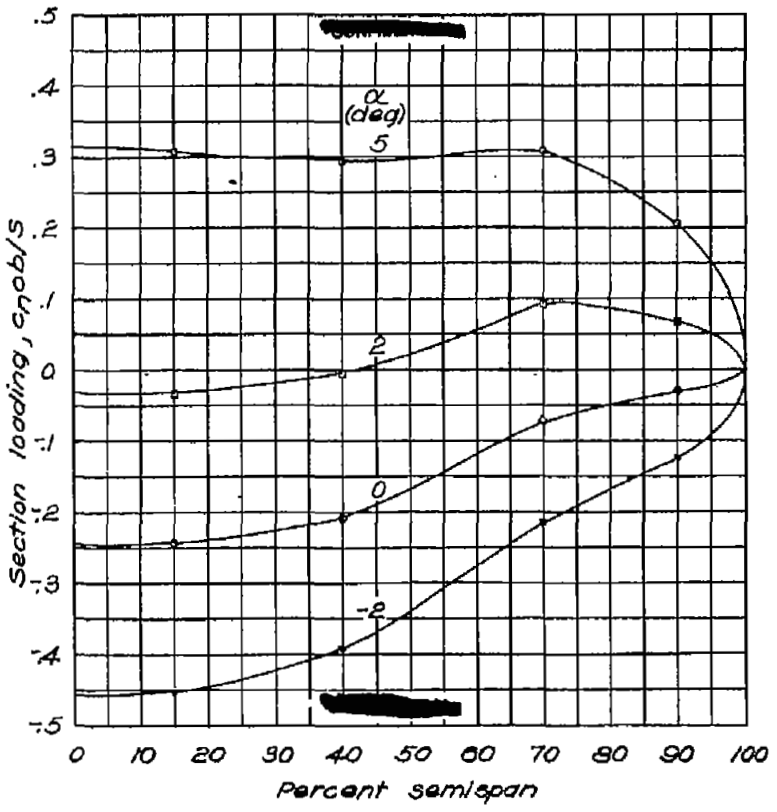

(c) M=0.905.

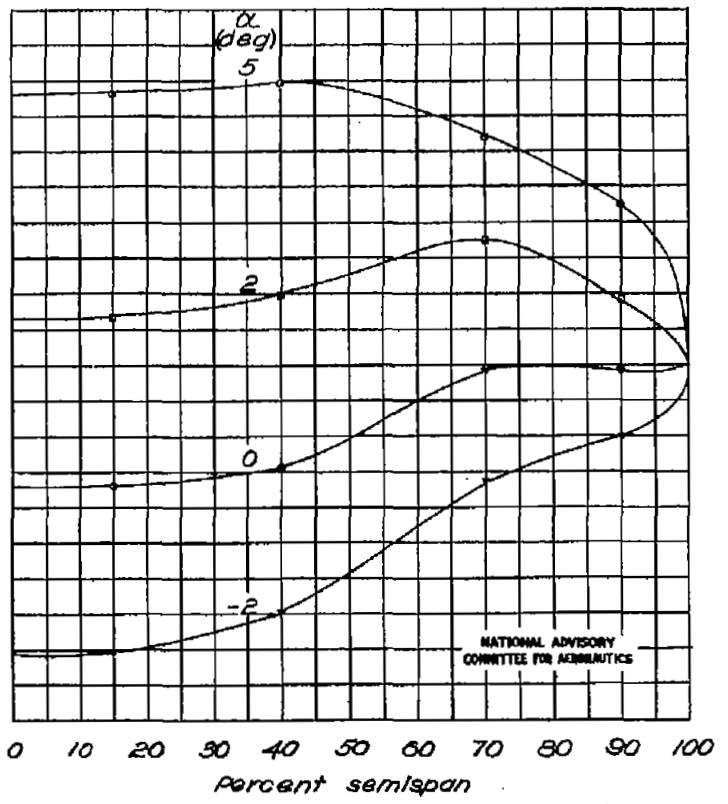

(d) M=0.925 (uncorrected).

Figure 12 .-Concluded.

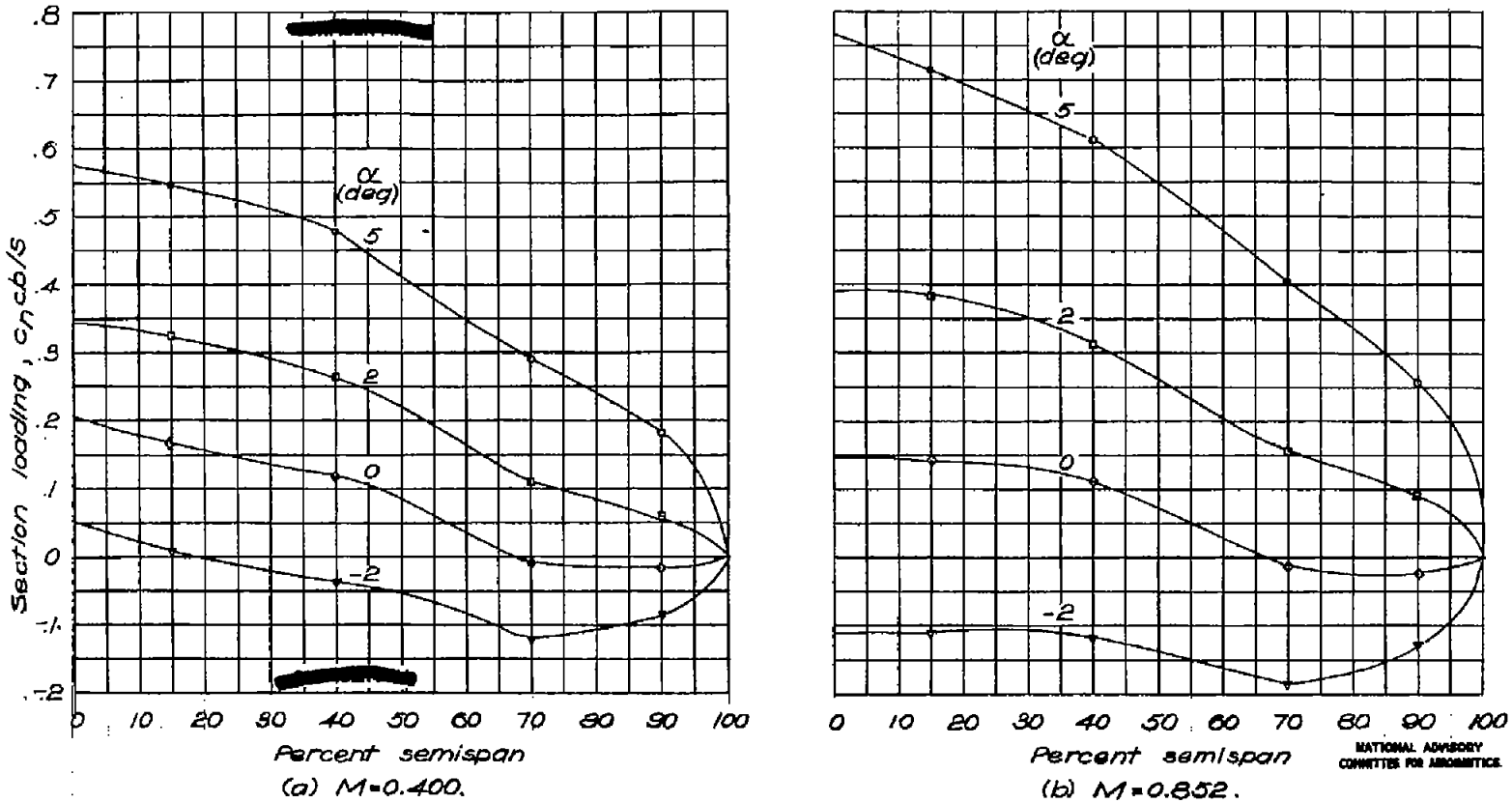

Figure 13.- Spanwise variation in section loading. $\delta = 0°$; $\delta_f = 10°$.

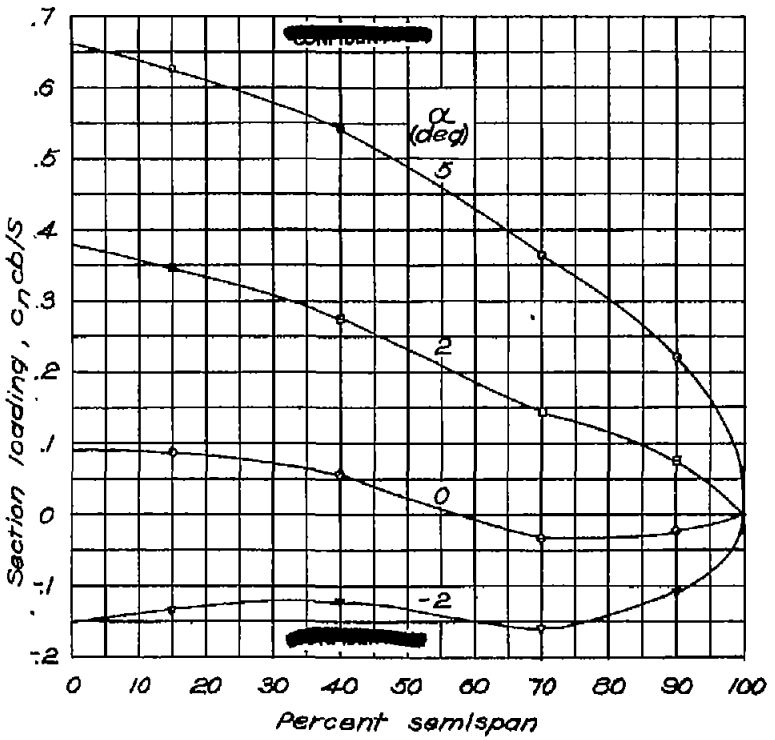

(c) M = 0.905.

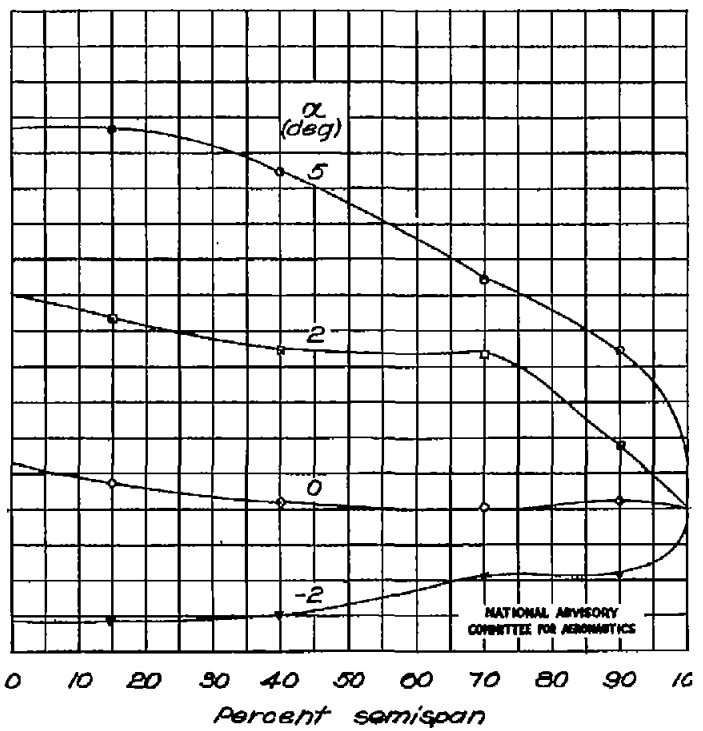

(d) M = 0.925 (uncorrected).

Figure 13.- Concluded.

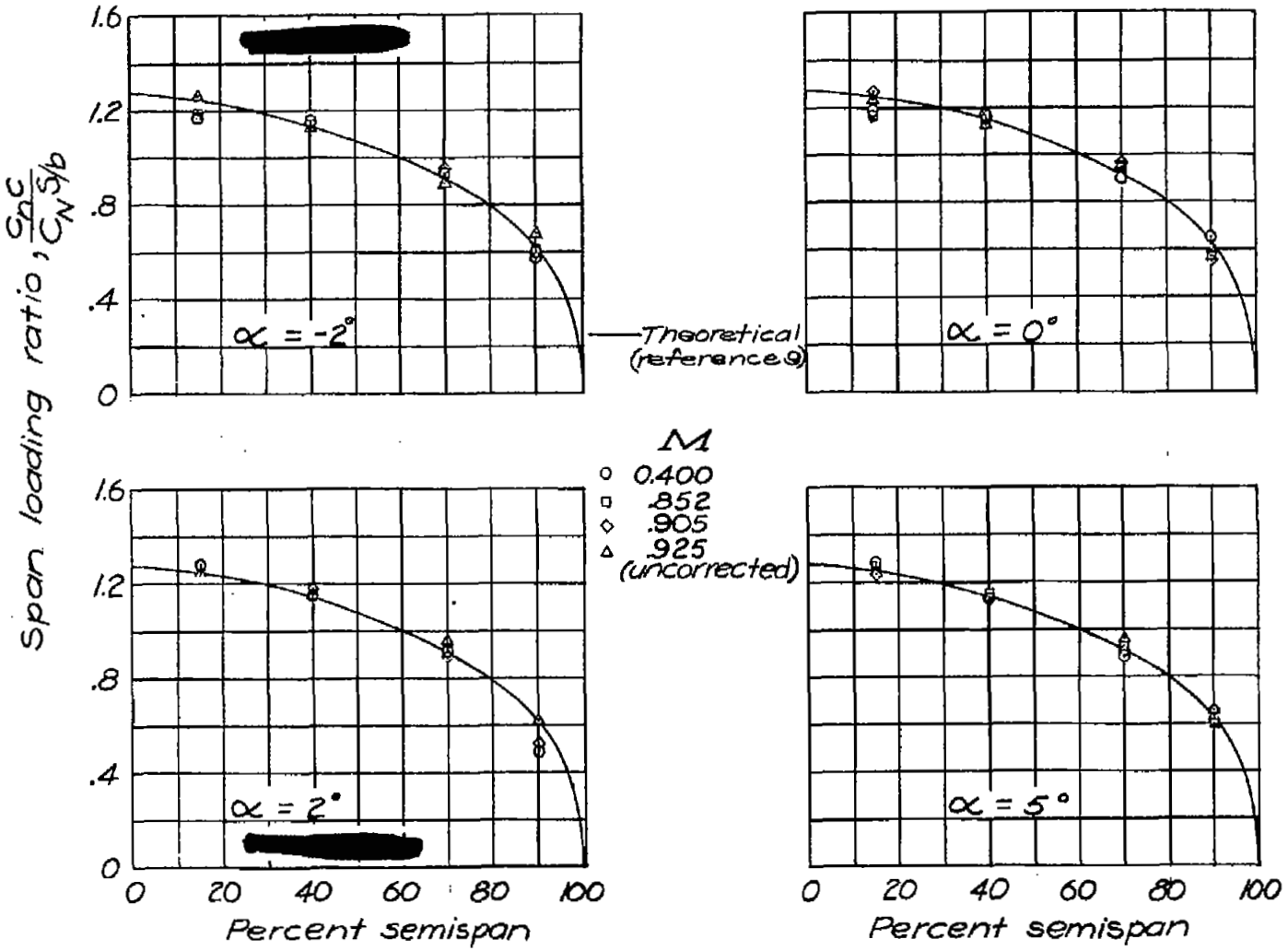

(a) $\delta = 0°$.

NATIONAL ADVISORY COMMITTEE FOR AERONAUTICS

Figure 14.- Effect of Mach number on spanwise load distribution. $\delta_f = 0°$.

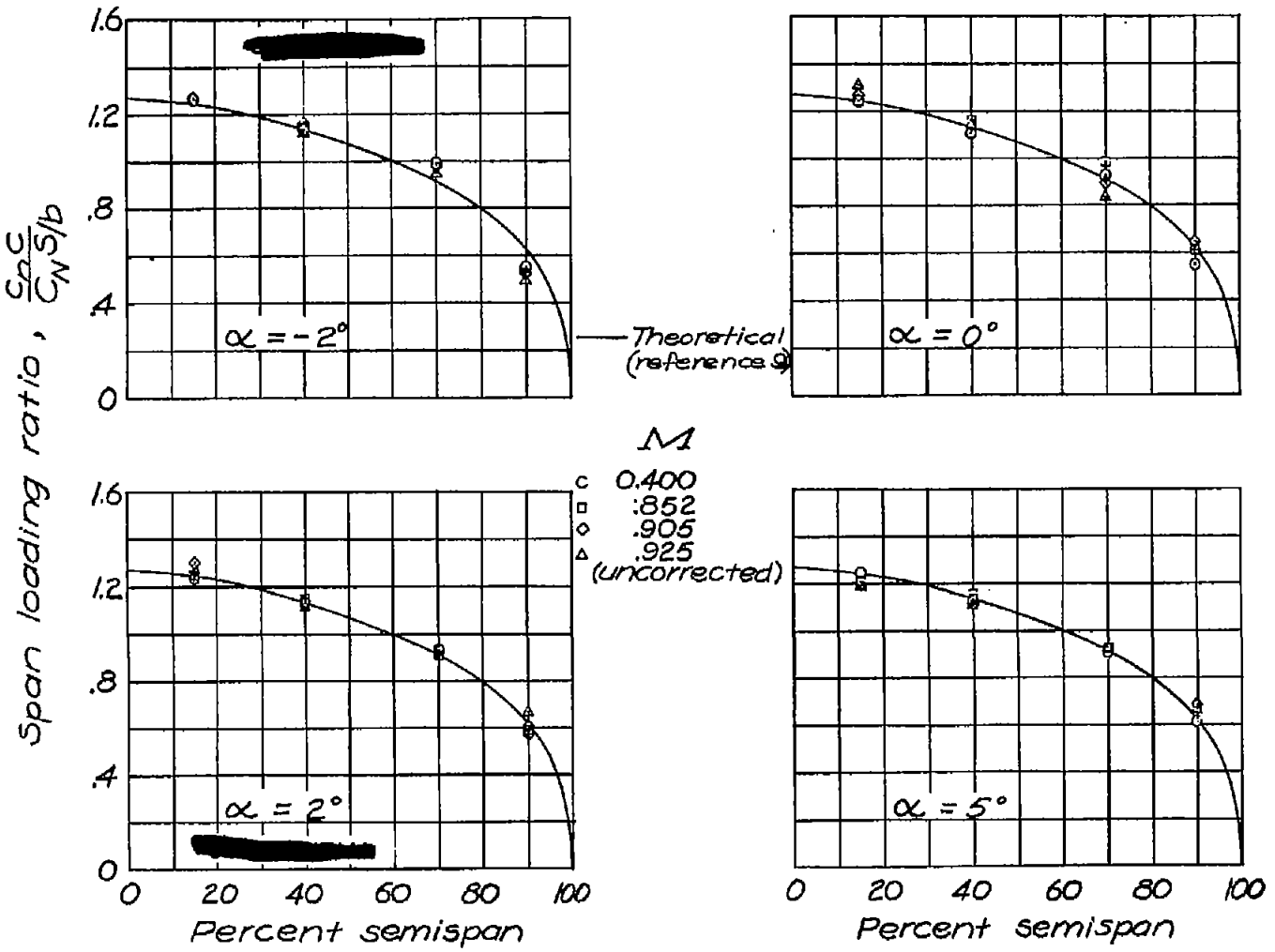

(b) $\delta = 5°$.

NATIONAL ADVISORY COMMITTEE FOR AERONAUTICS

Figure 14.- Continued.

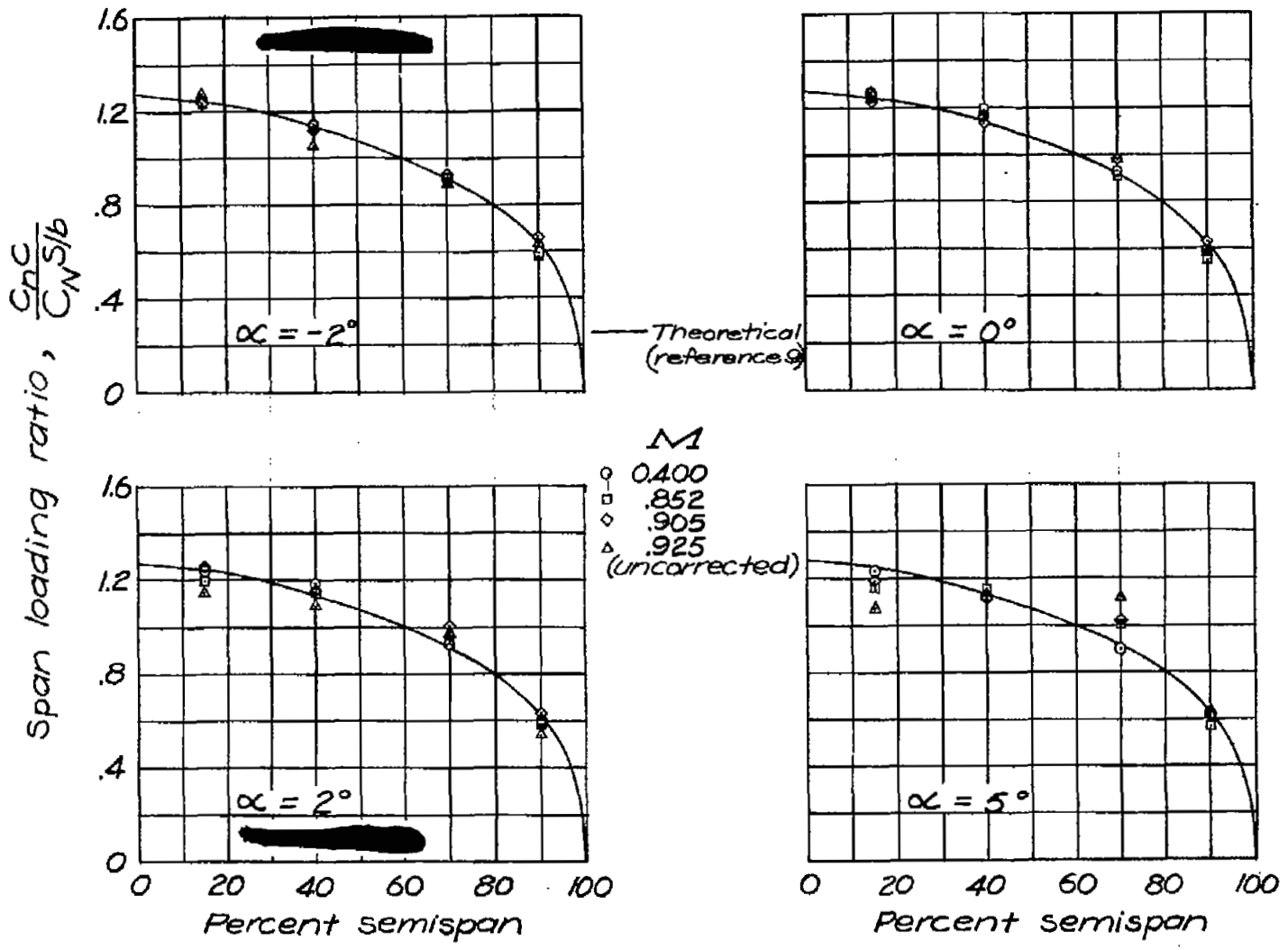

(c) $\delta = -5°$.

NATIONAL ADVISORY COMMITTEE FOR AERONAUTICS

Figure 14.- Concluded.

[redacted]

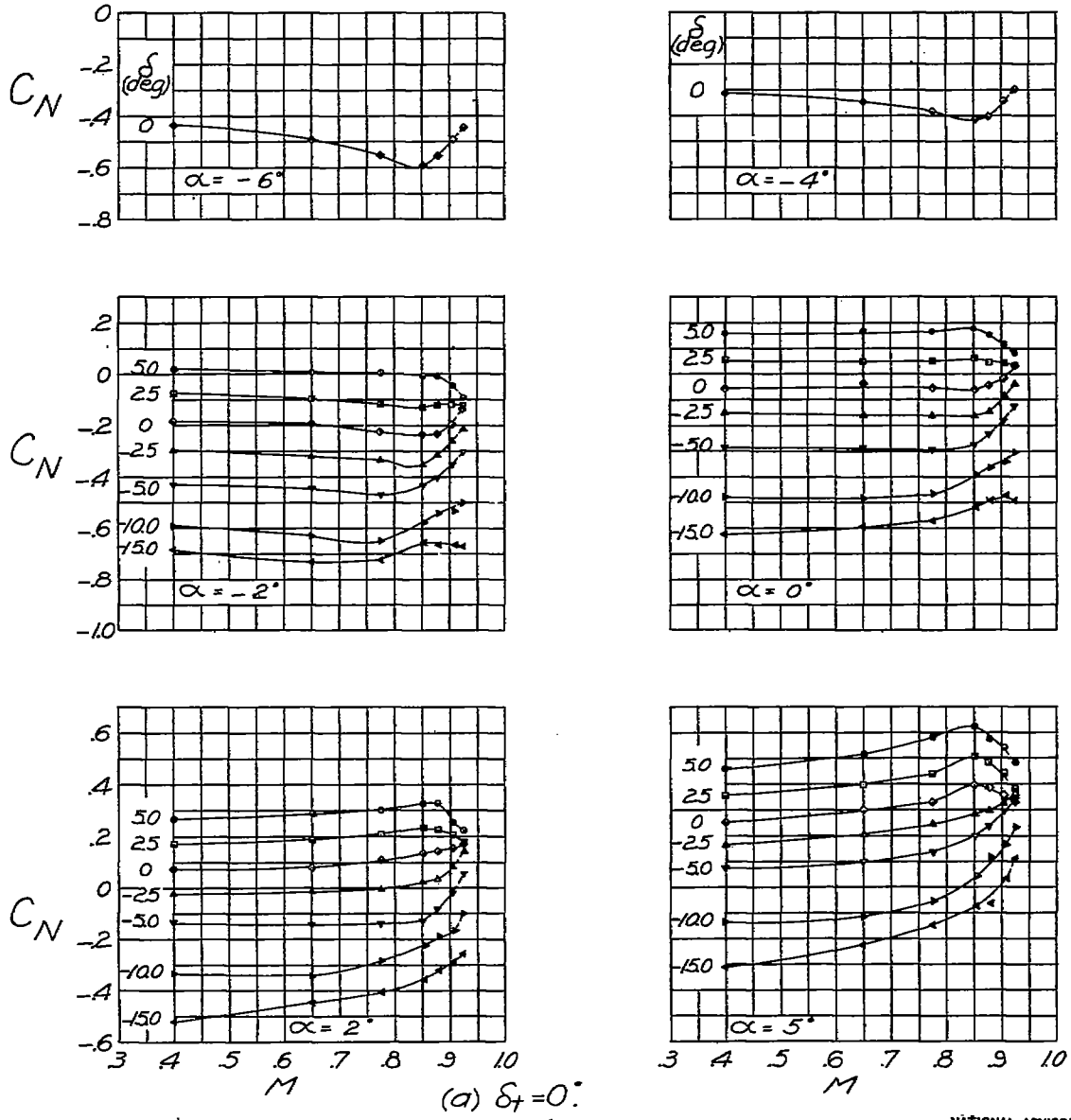

(a) $\delta_t = 0°$.

Figure 15.– Normal-force coefficient data.

NATIONAL ADVISORY COMMITTEE FOR AERONAUTICS

[redacted]

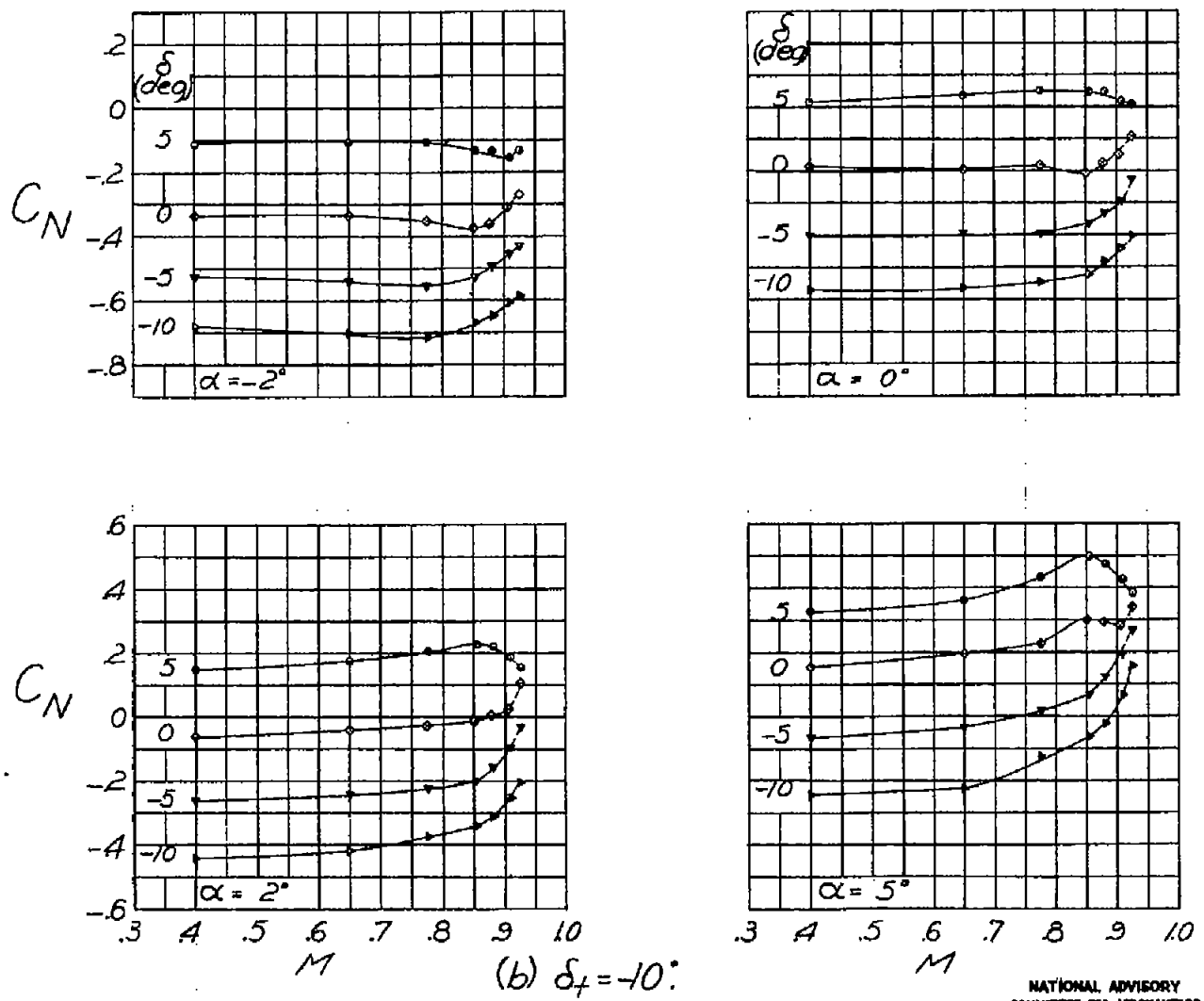

(b) $\delta_f = -10°$.

Figure 15.- Continued.

NATIONAL ADVISORY
COMMITTEE FOR AERONAUTICS

[redacted]

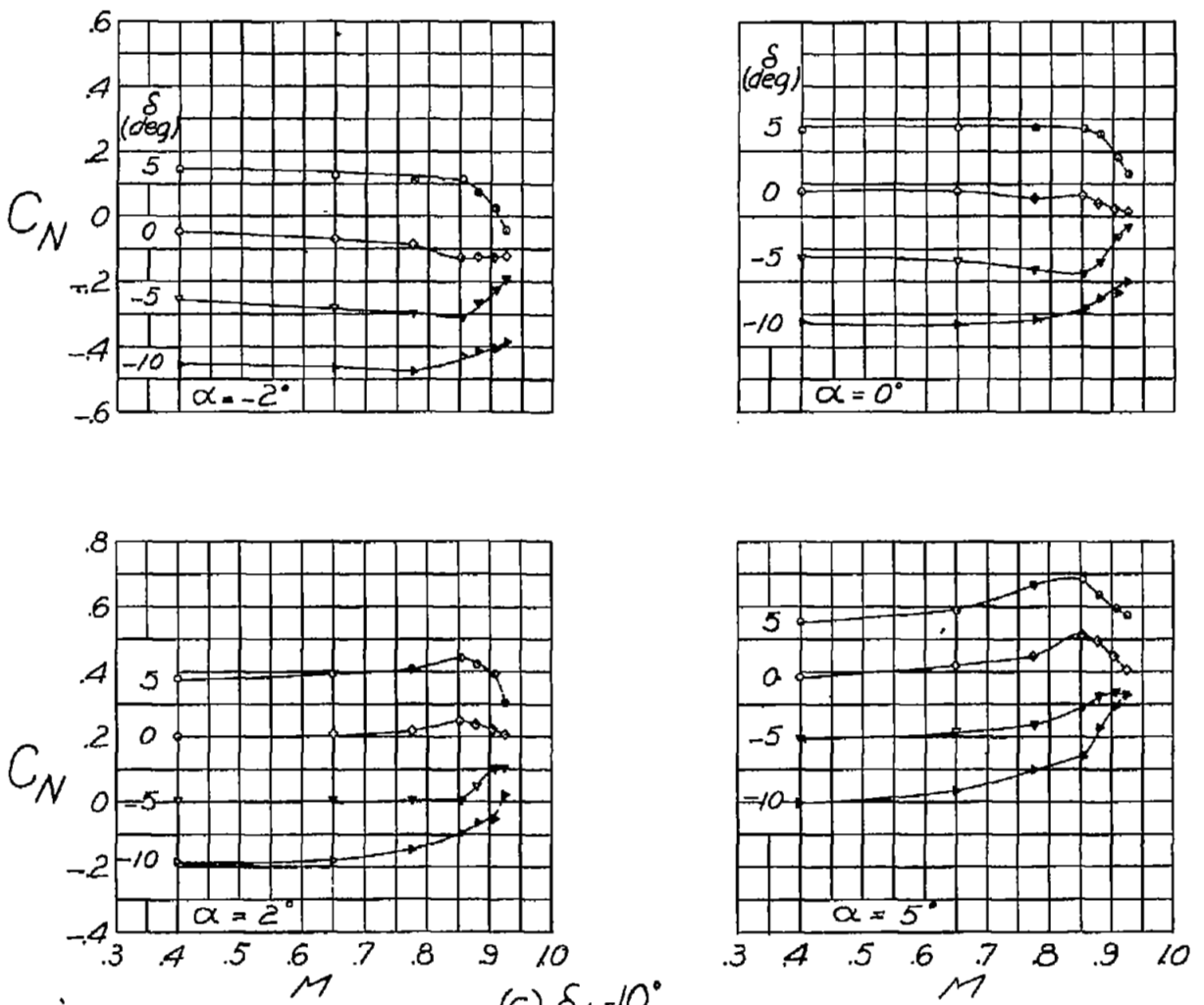

(c) $\delta_f = 10°$.

Figure 15.- Concluded.

NATIONAL ADVISORY COMMITTEE FOR AERONAUTICS

[redacted]

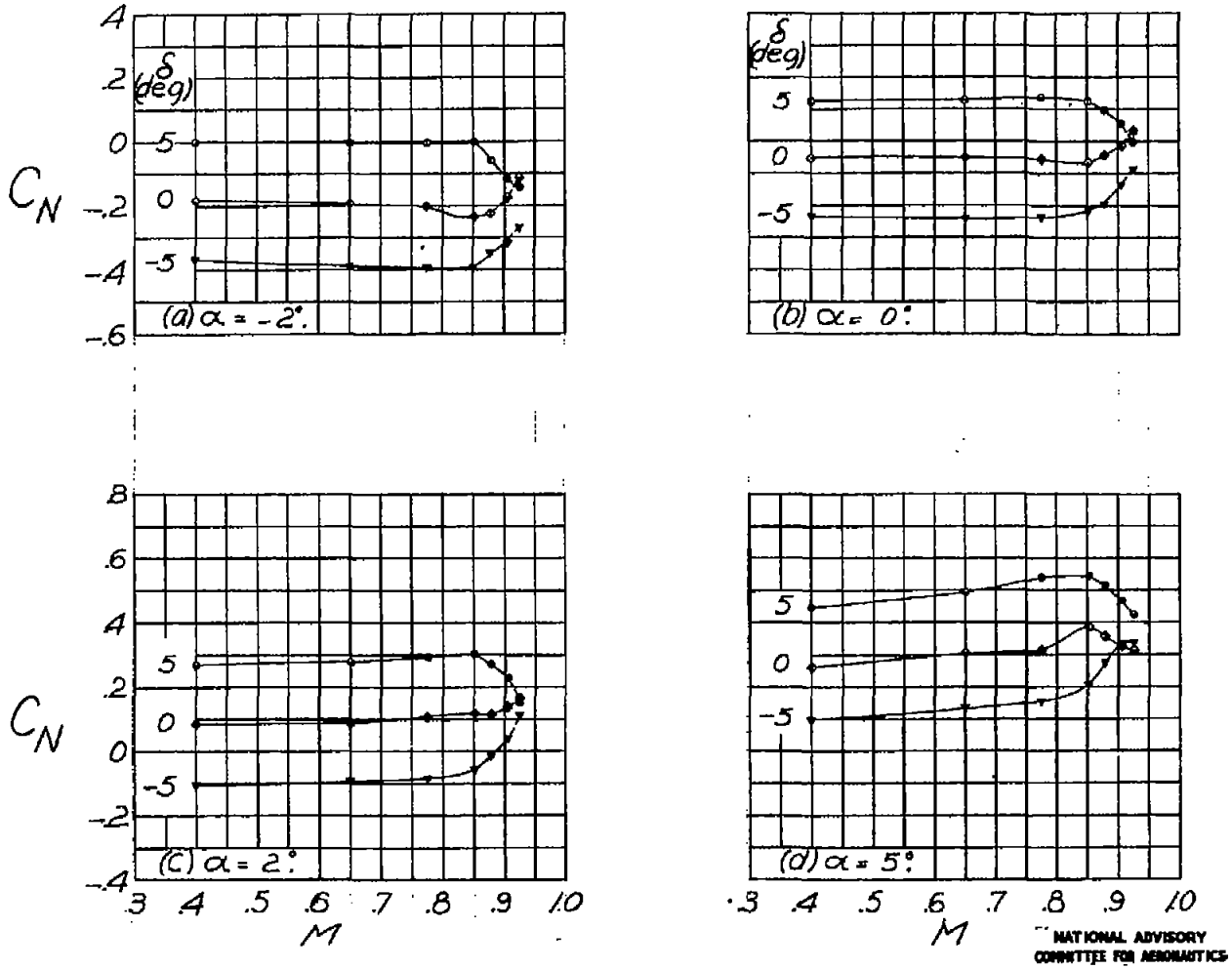

Figure 16.- Normal-force-coefficient data. $\delta_t = 0°$. Transition fixed at 10 percent chord.

[redacted]

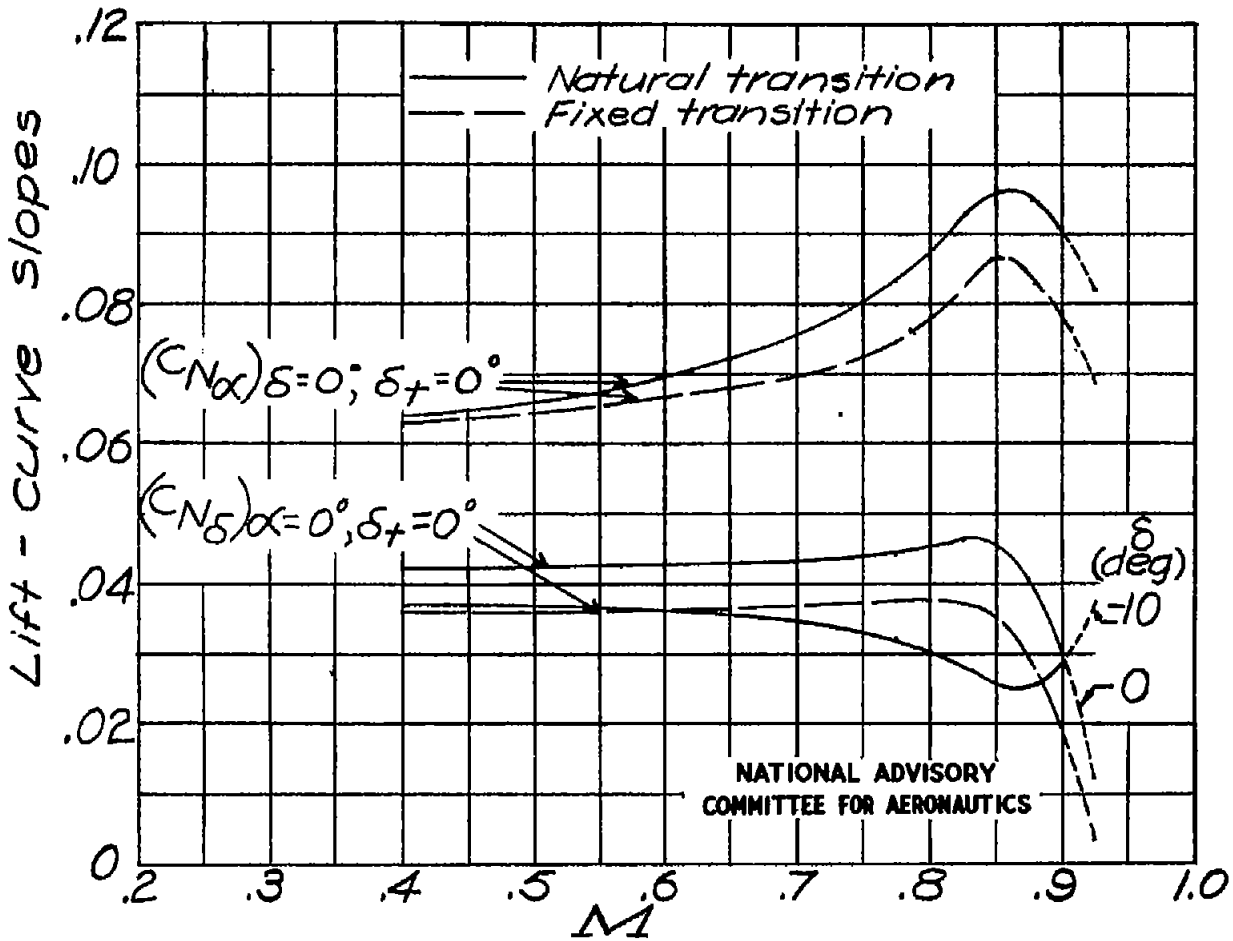

Figure 17.- Variation of lift-curve slopes with Mach number.

[redacted]

[redacted]

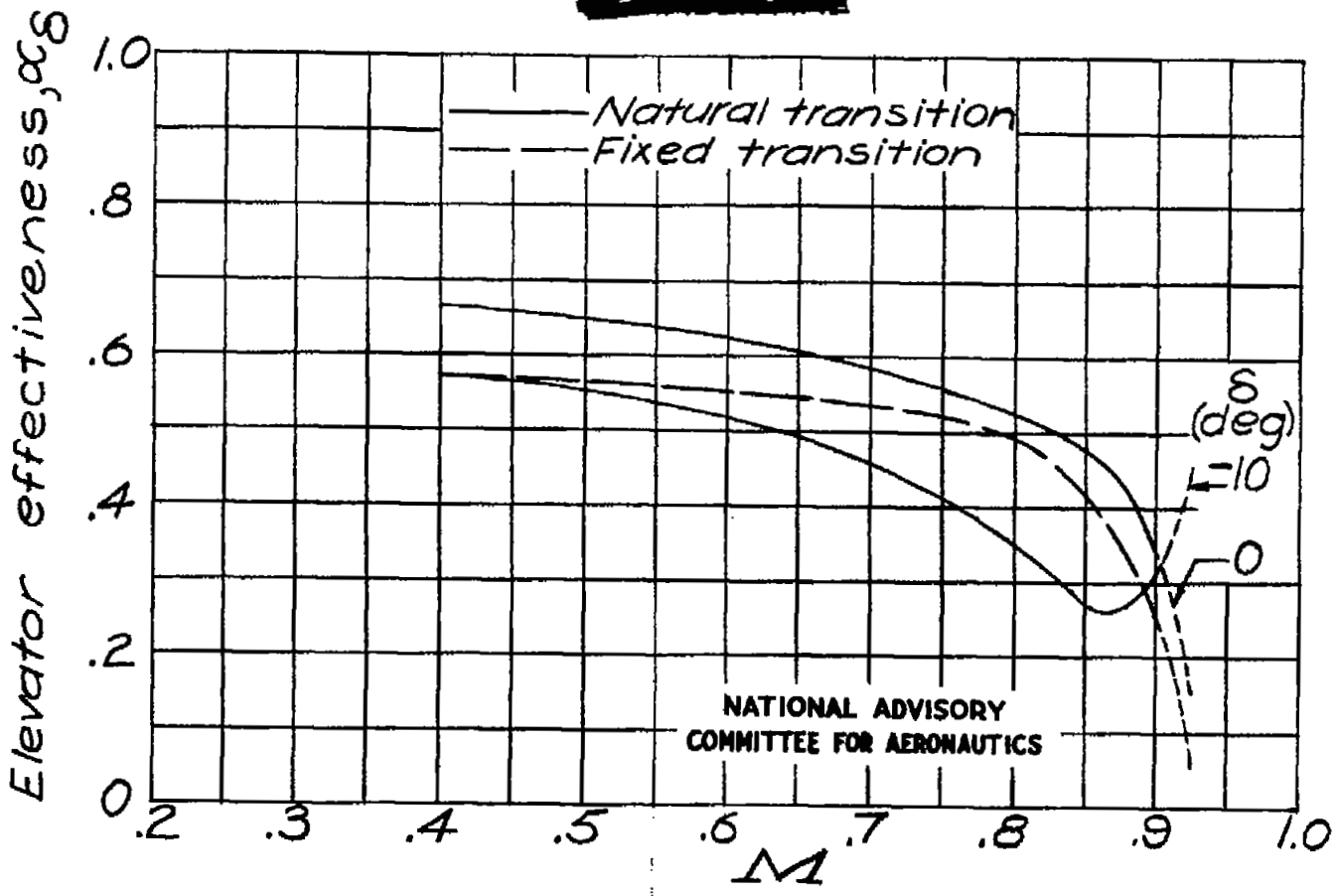

Figure 18.- Variation of elevator effectiveness with Mach number.

[redacted]

[redacted]

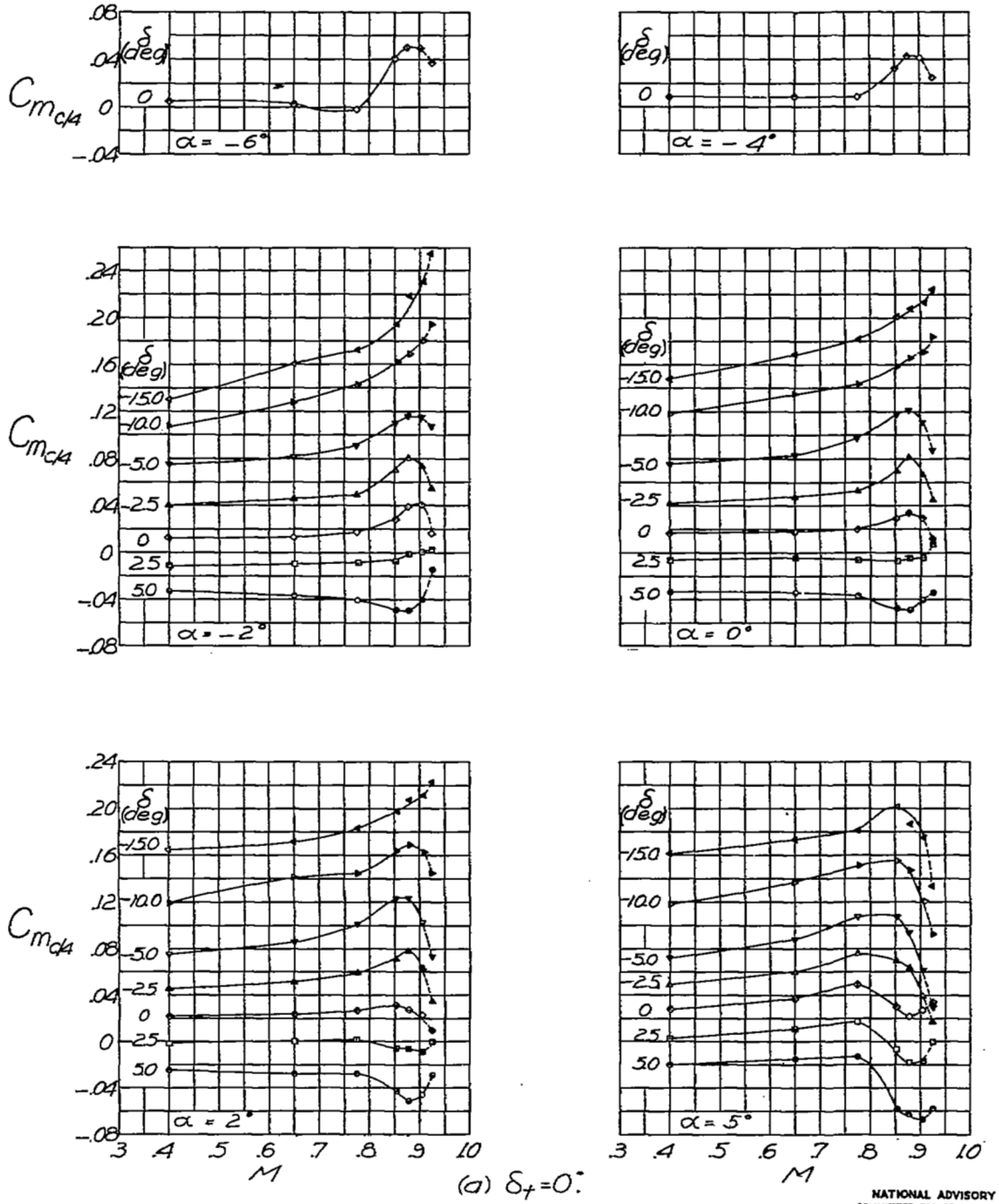

(a) $\delta_f = 0°$.

Figure 19.- Pitching-moment-coefficient data.

NATIONAL ADVISORY COMMITTEE FOR AERONAUTICS

[redacted]

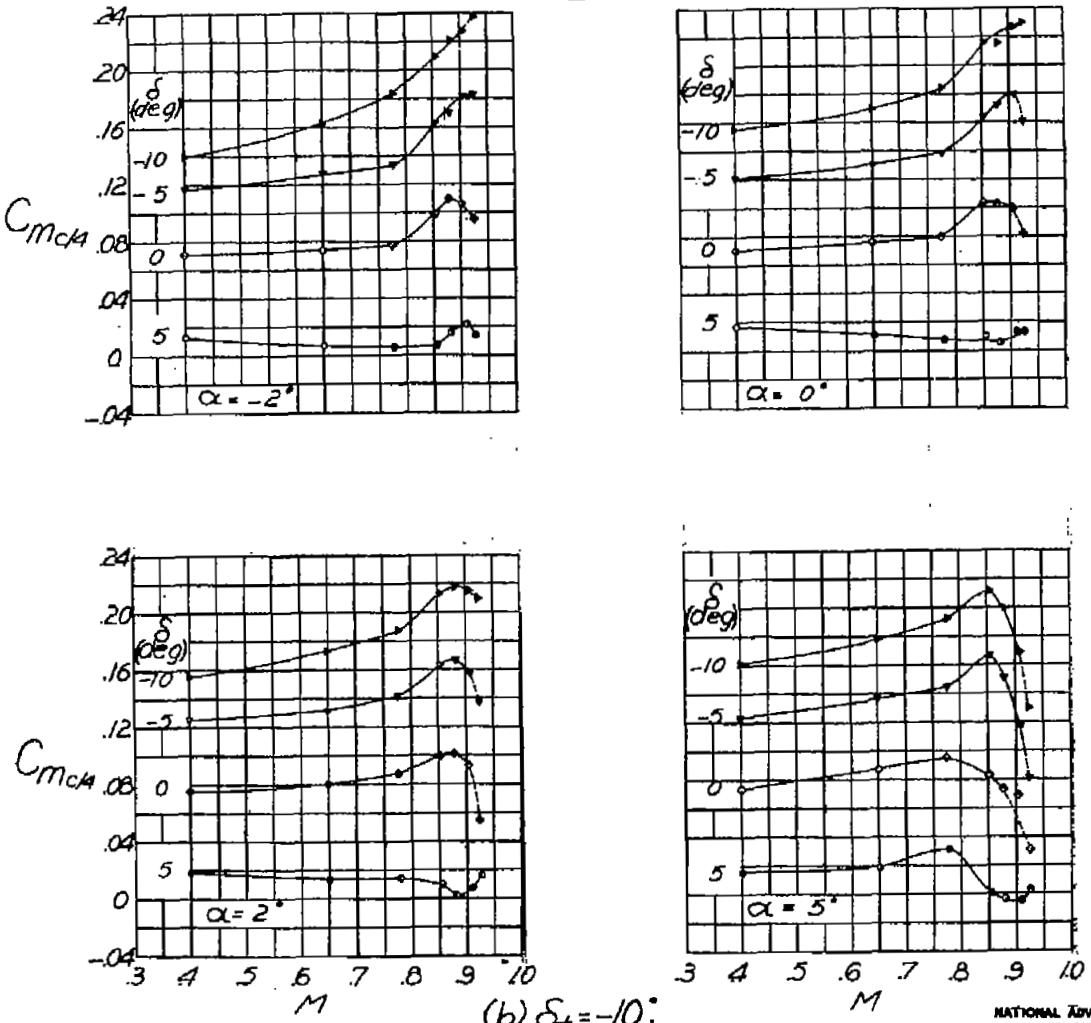

(b) $\delta_f = -10°$

Figure 19.- Continued.

NATIONAL ADVISORY COMMITTEE FOR AERONAUTICS

[redacted]

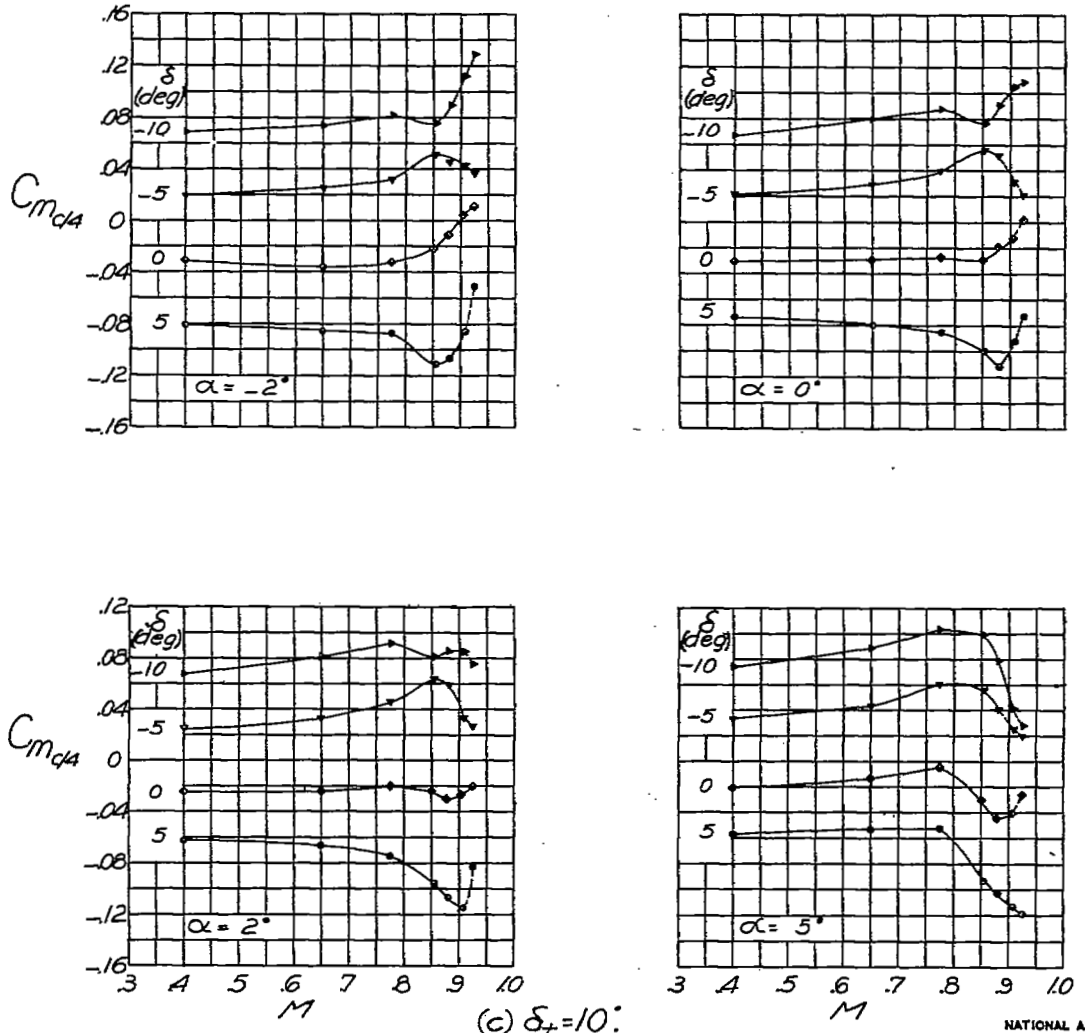

(c) $\delta_f = 10°$.

Figure 19.- Concluded.

NATIONAL ADVISORY COMMITTEE FOR AERONAUTICS

[redacted]

[redacted]

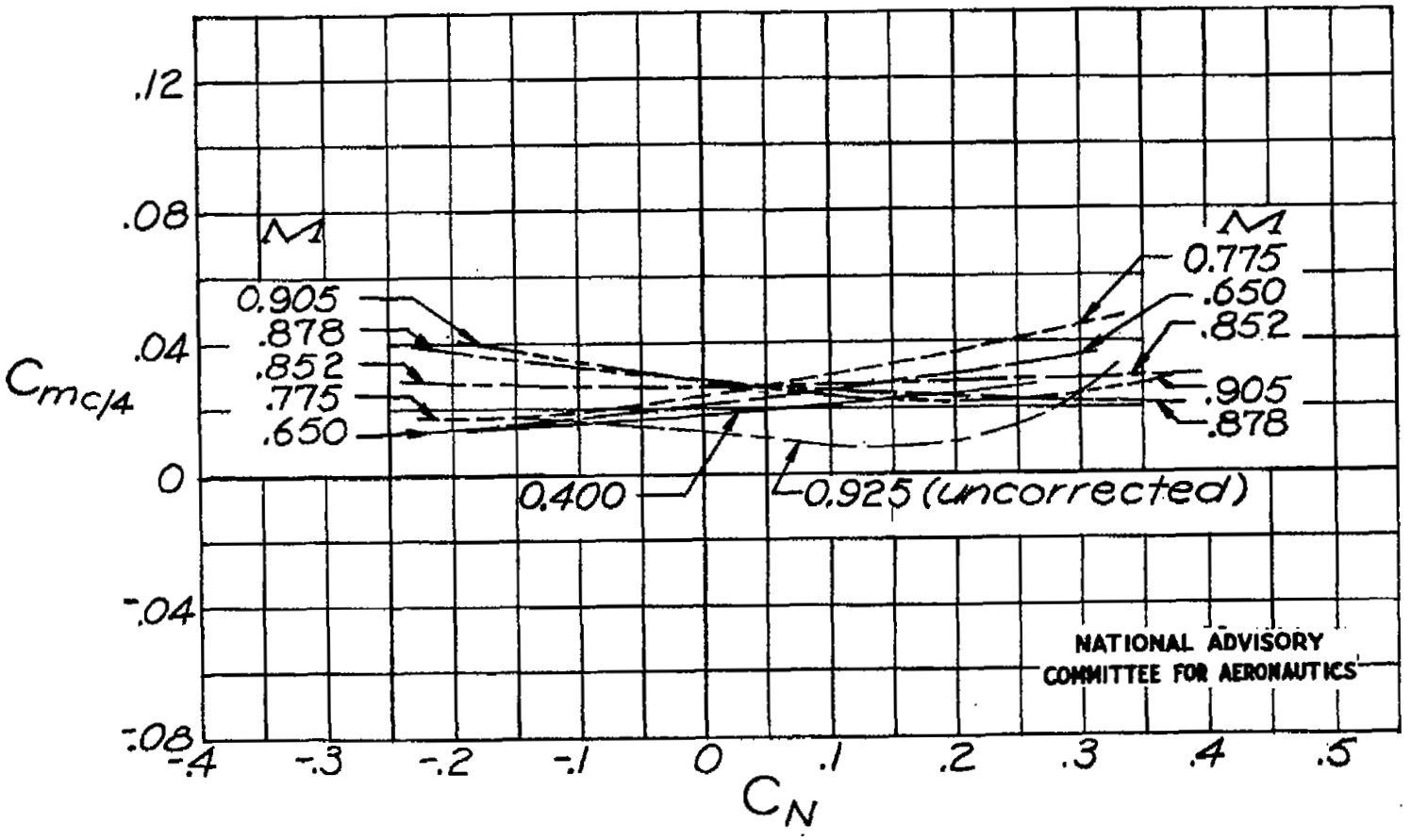

Figure 20.- Variation of pitching-moment coefficient with normal-force coefficient for various Mach numbers. $\delta = 0°$; $\delta_t = 0°$.

[redacted]

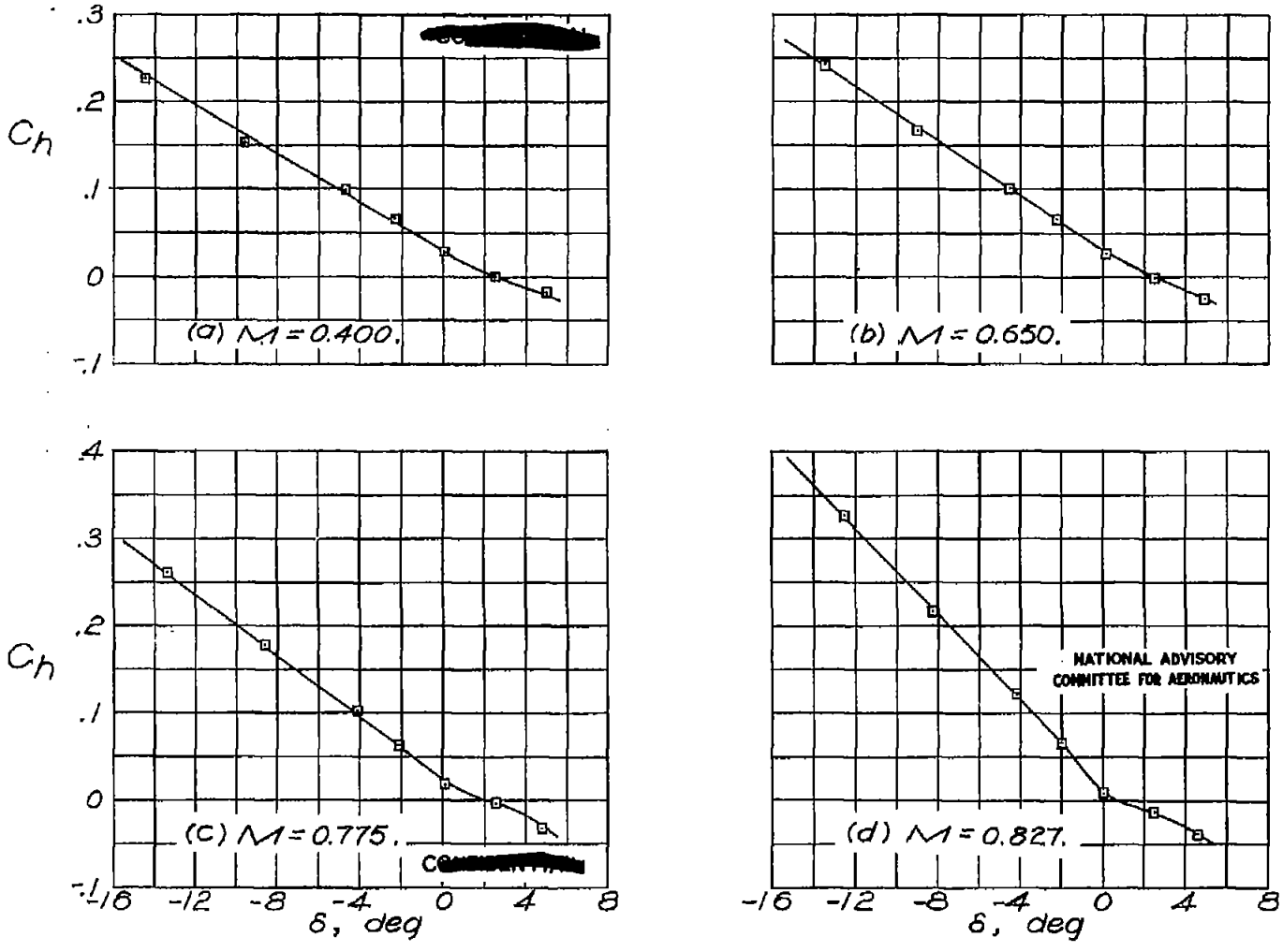

Figure 21.- Variation of elevator hinge-moment coefficient with elevator deflection for various Mach numbers. $\alpha = -6°$; $\delta_f = 0°$.

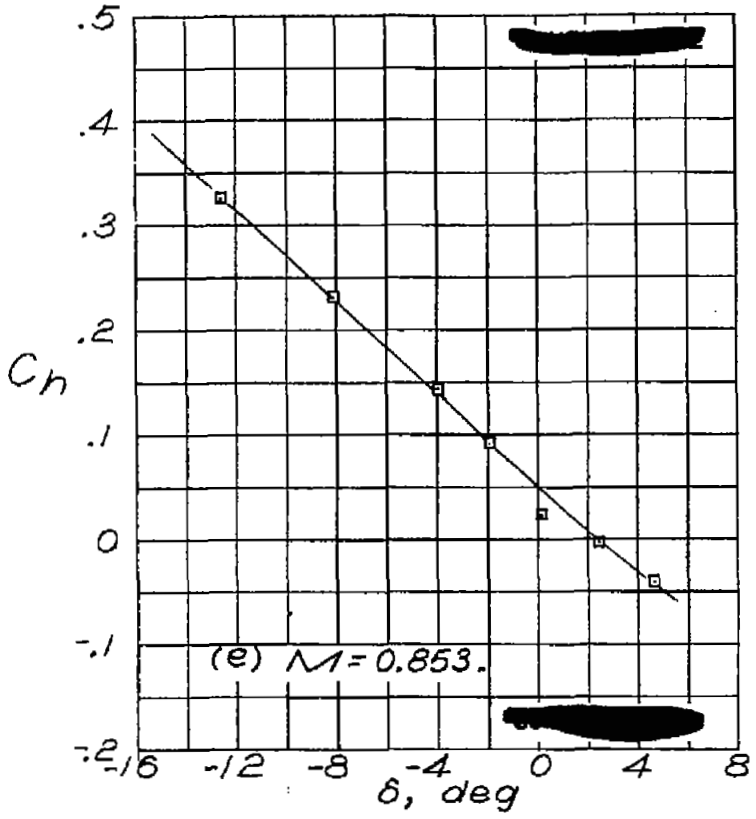

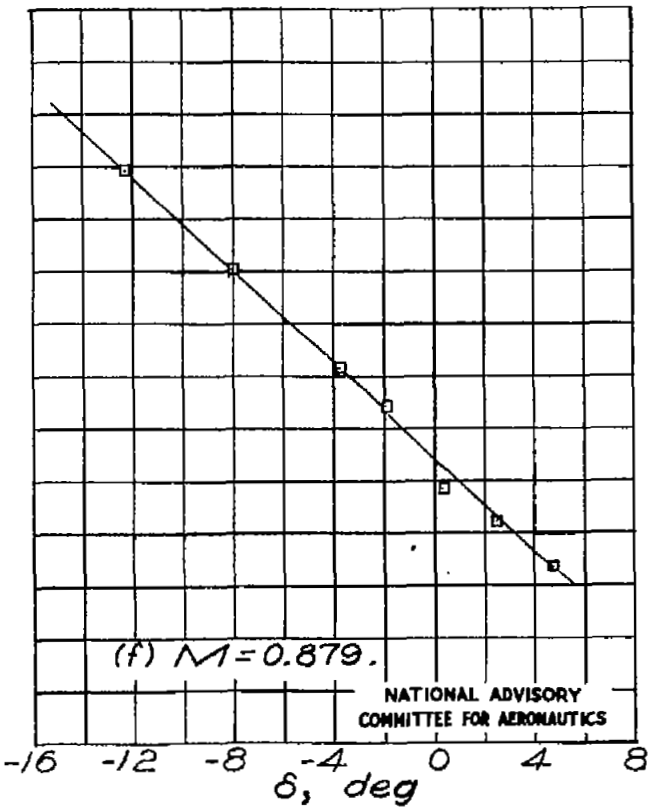

Figure 21 .- Continued.

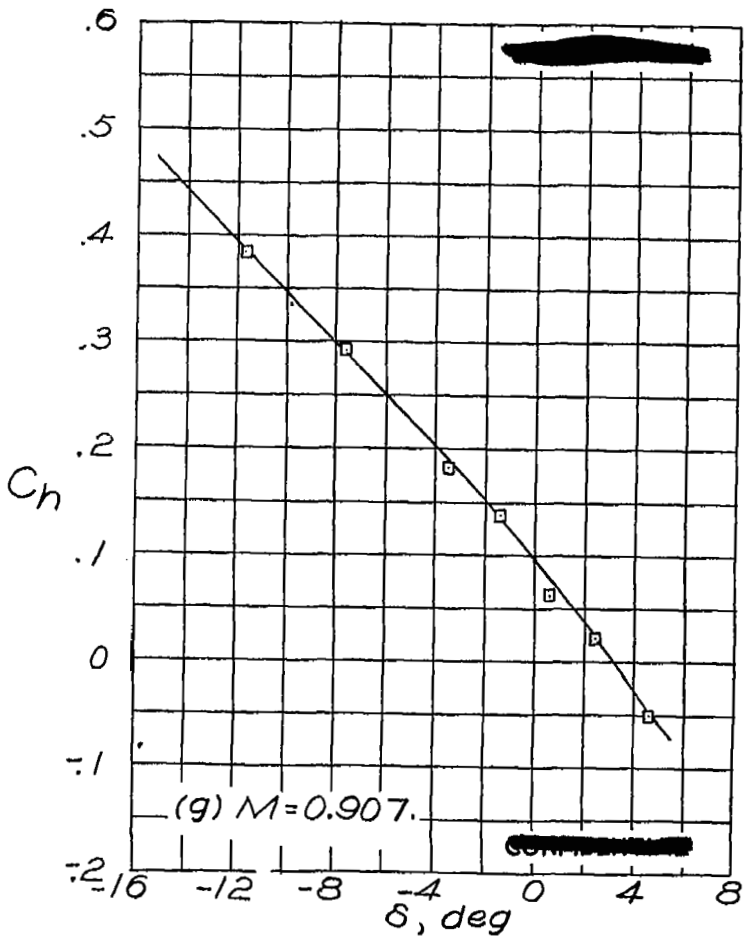

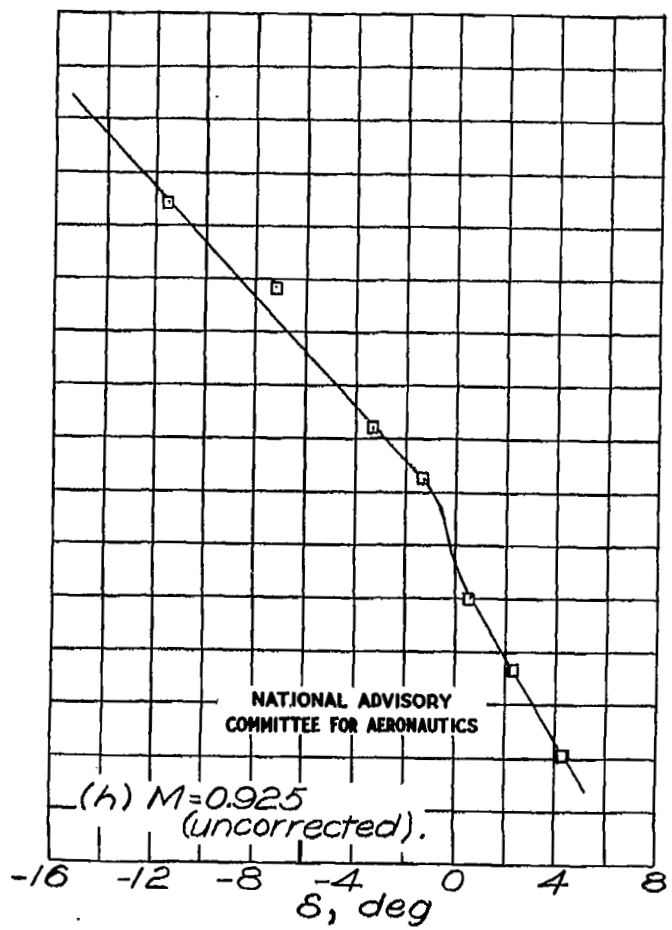

Figure 21 .— Concluded.

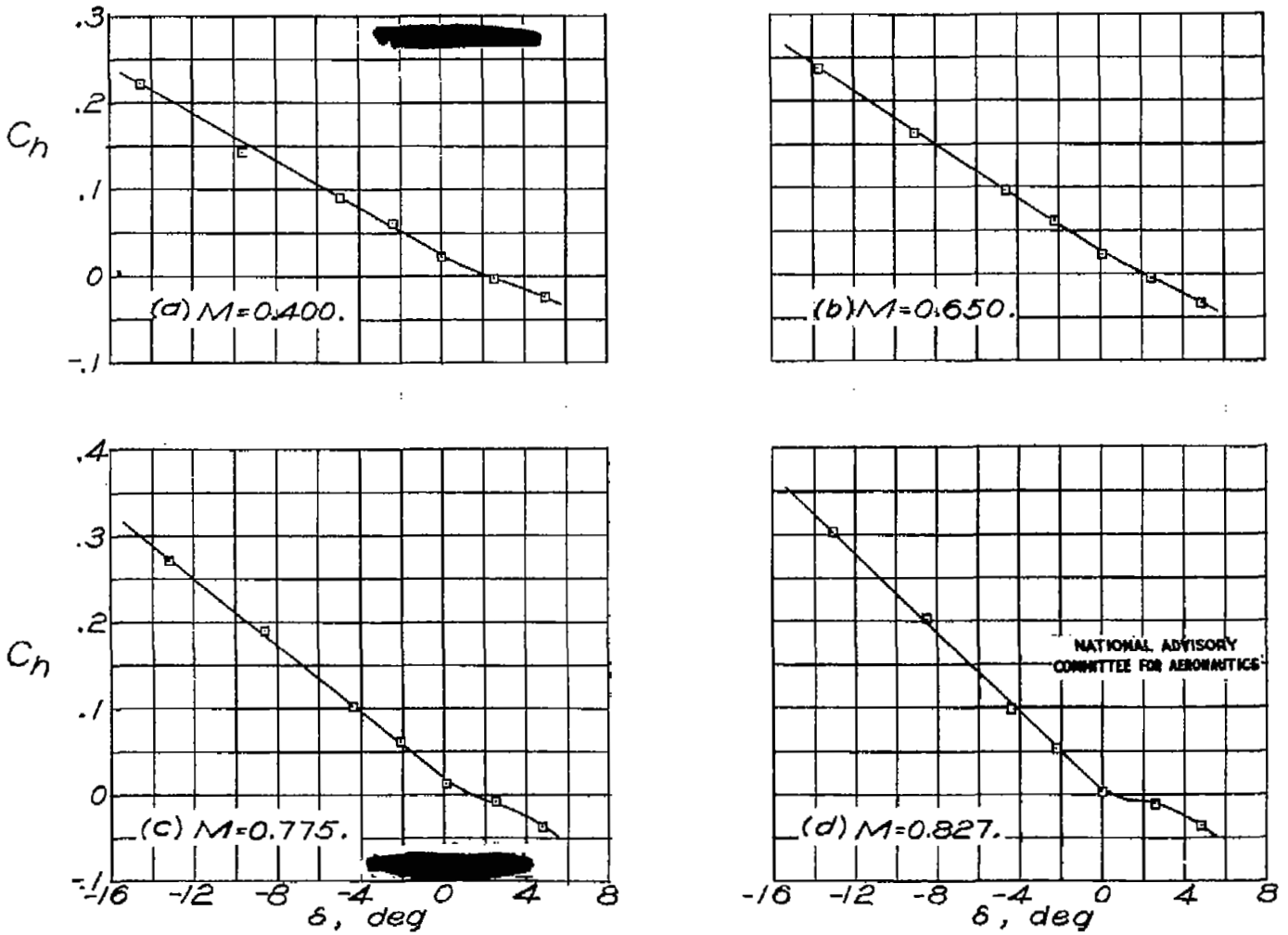

Figure 22.–Variation of elevator hinge-moment coefficient with elevator deflection for various Mach numbers. $\alpha=-4^\circ$; $\delta_t=0^\circ$.

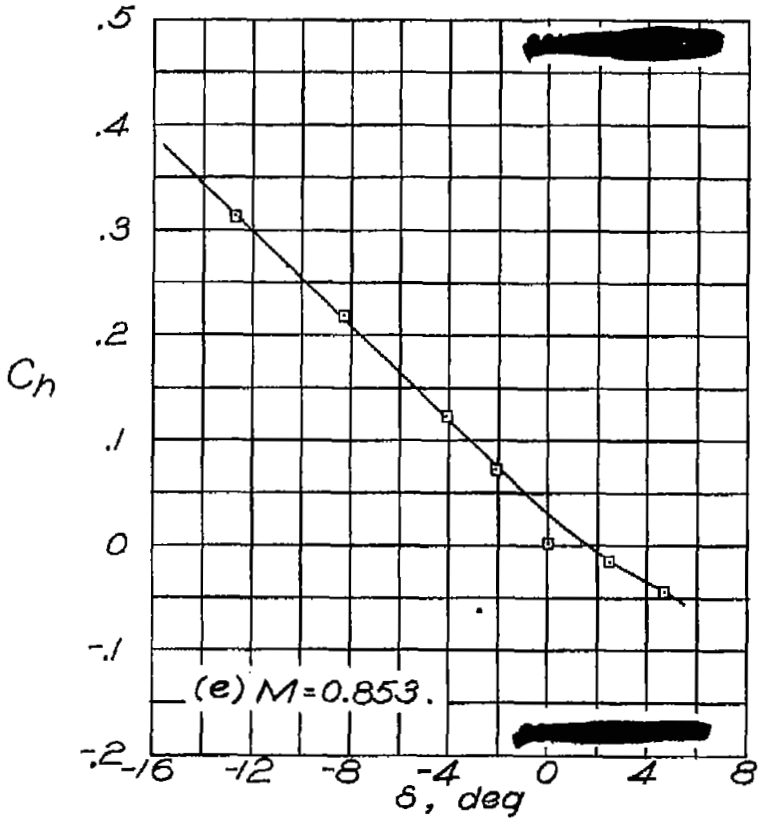

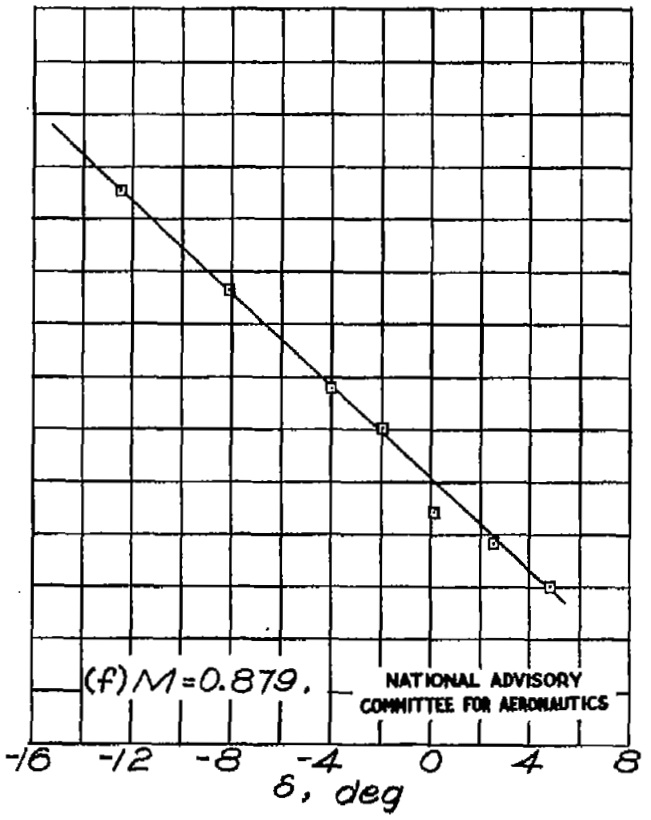

Figure 22.-Continued.

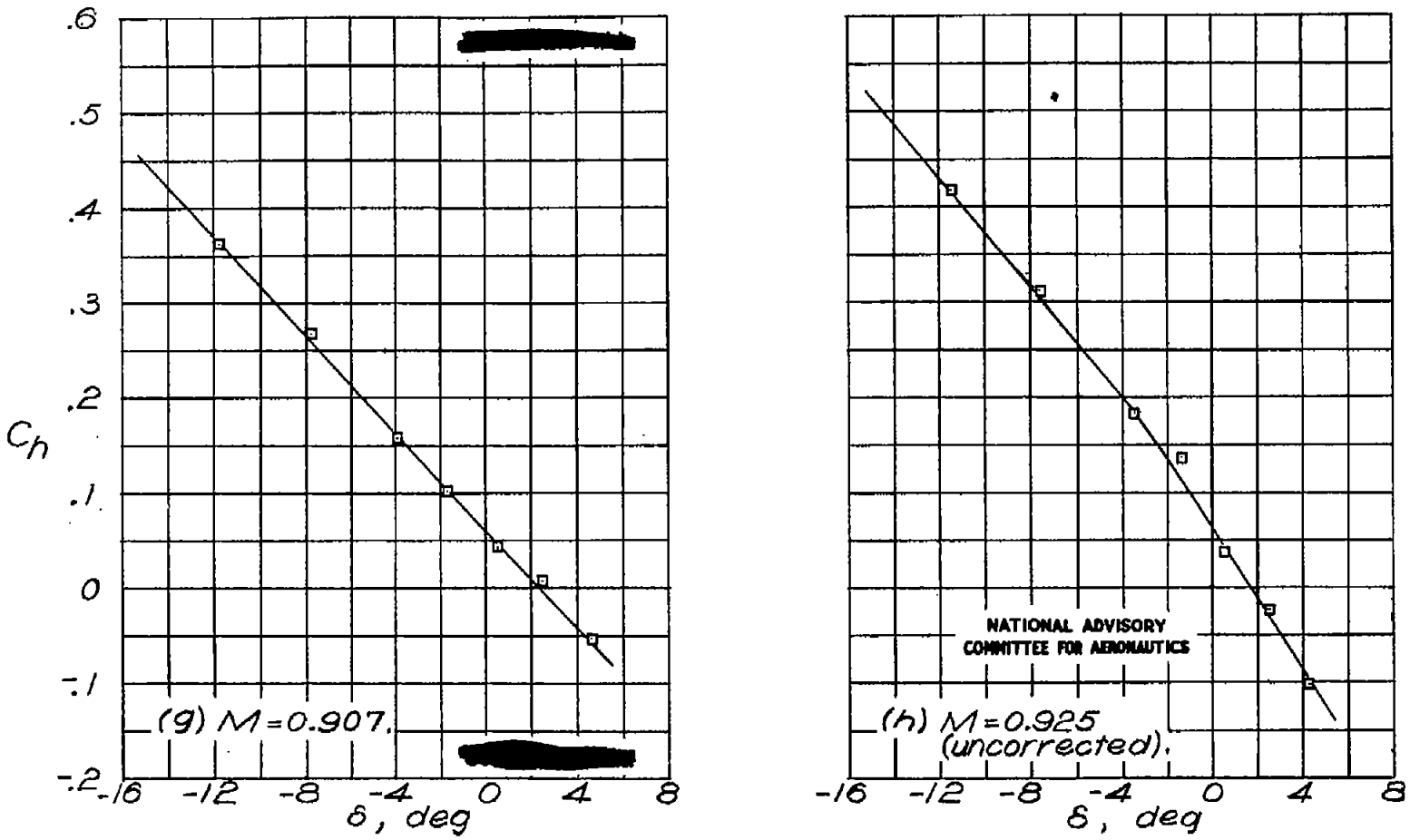

Figure 22.- Concluded.

[redacted]

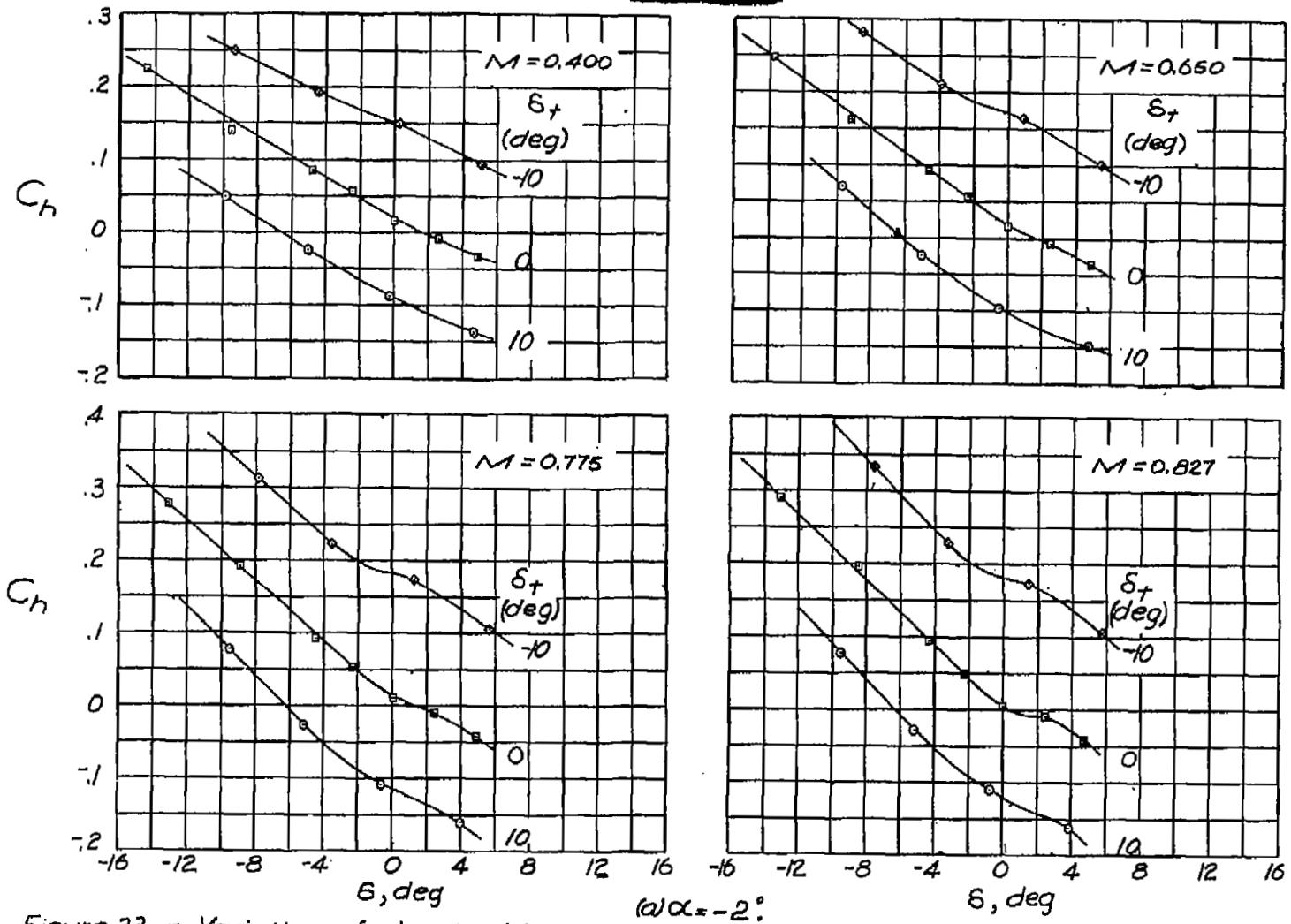

(a) $\alpha = -2°$.

Figure 23.- Variation of elevator hinge-moment coefficient with elevator deflection for various trim-tab deflections and Mach numbers.

[redacted]

NATIONAL ADVISORY COMMITTEE FOR AERONAUTICS

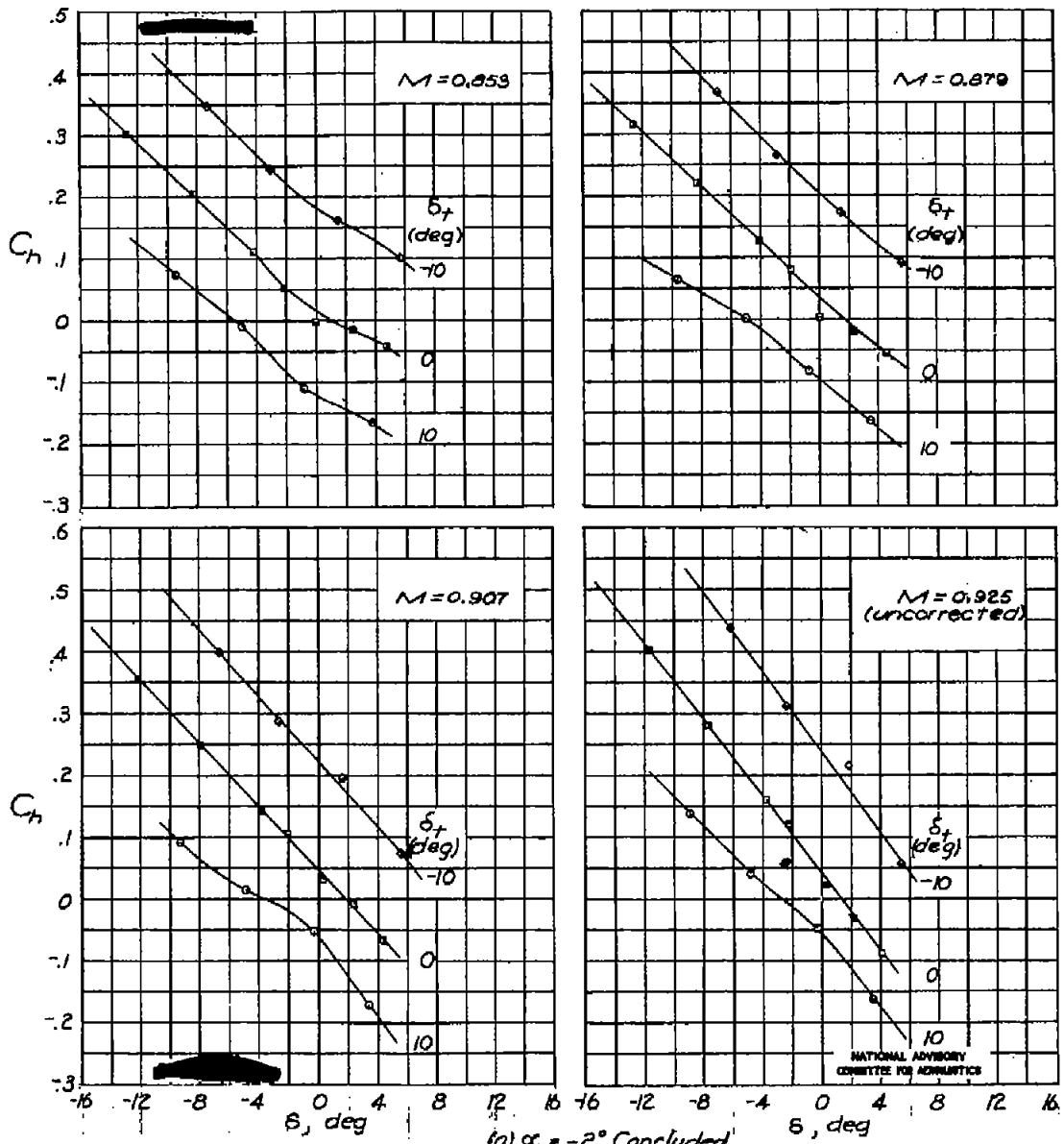

Figure 23.- Continued.

(a) $\alpha = -2°$. Concluded.

[redacted]

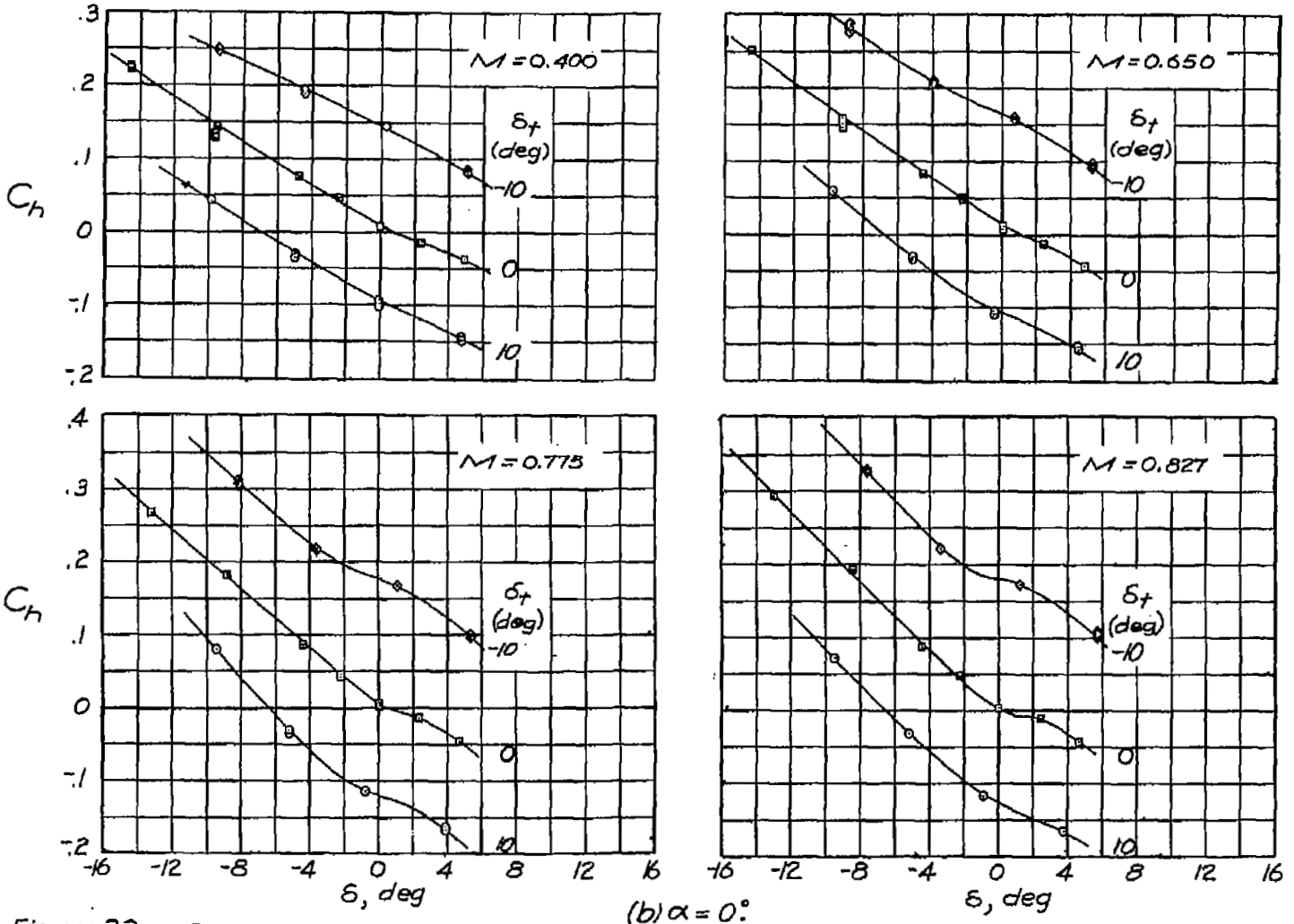

(b) $\alpha = 0°$

Figure 23.- Continued.

NATIONAL ADVISORY COMMITTEE FOR AERONAUTICS

[redacted]

[redacted]

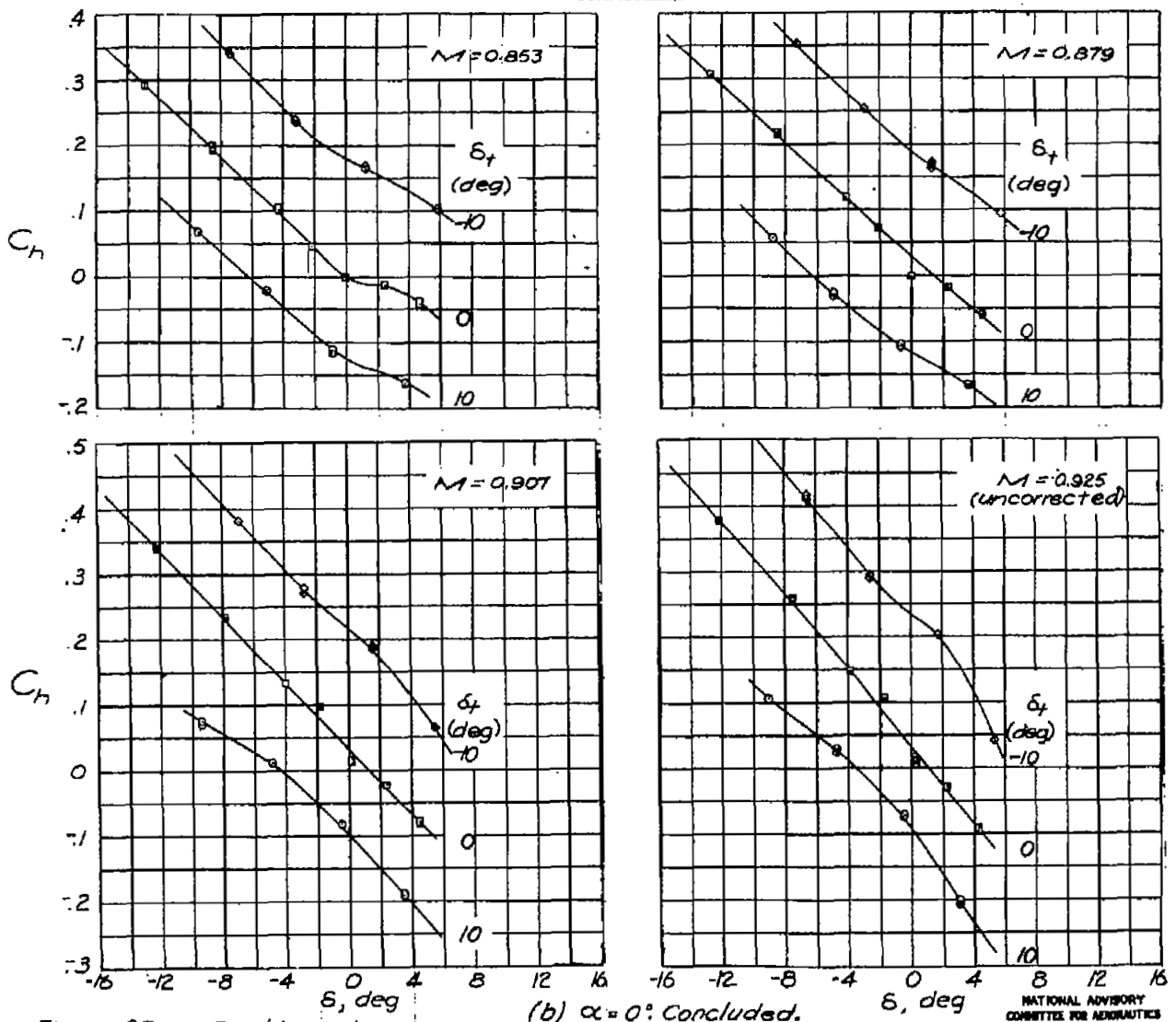

Figure 23.- Continued.

(b) $\alpha = 0°$: Concluded.

[redacted]

[redacted]

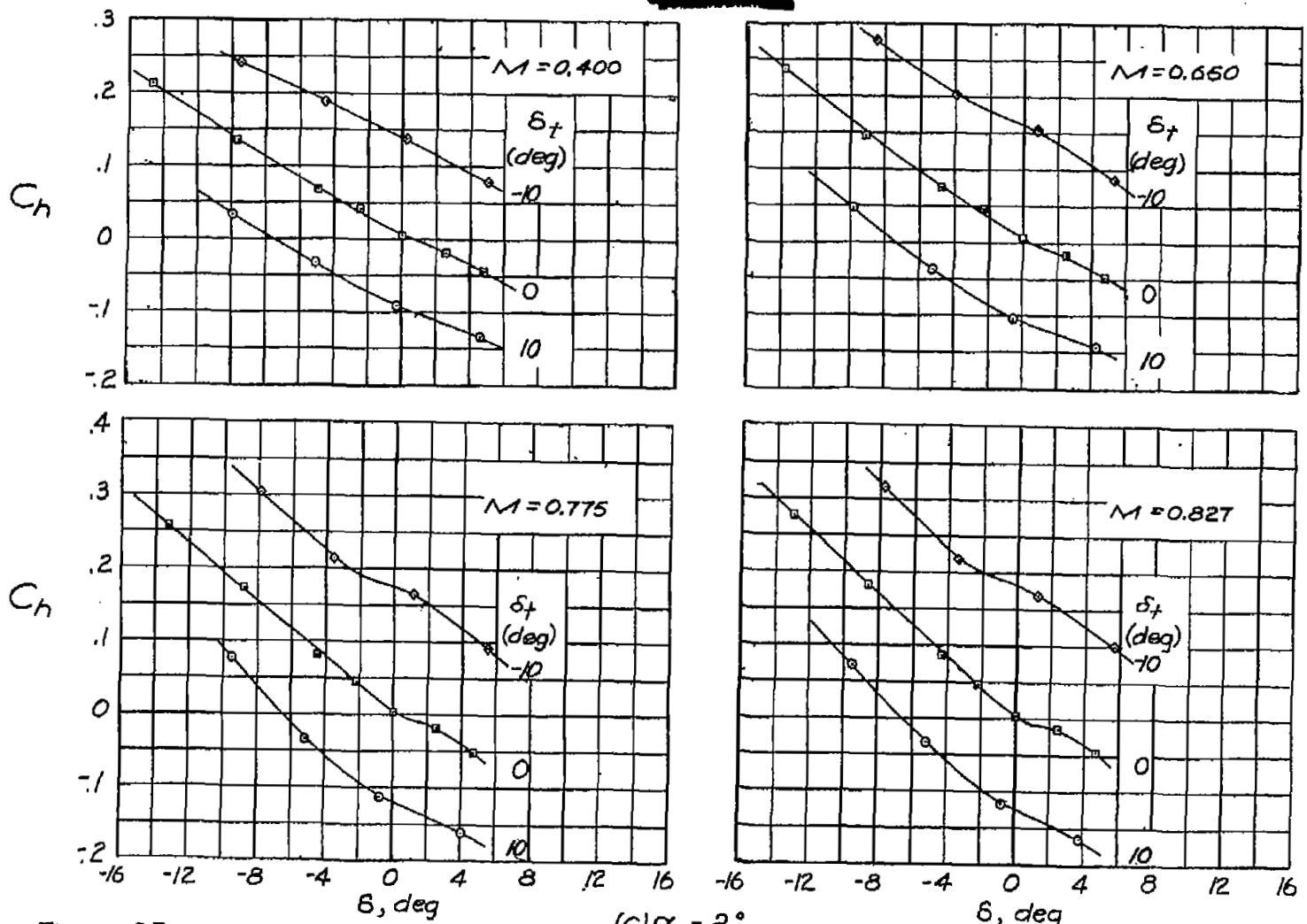

Figure 23.- Continued.

(c) $\alpha = 2°$

[redacted]

NATIONAL ADVISORY COMMITTEE FOR AERONAUTICS

[redacted]

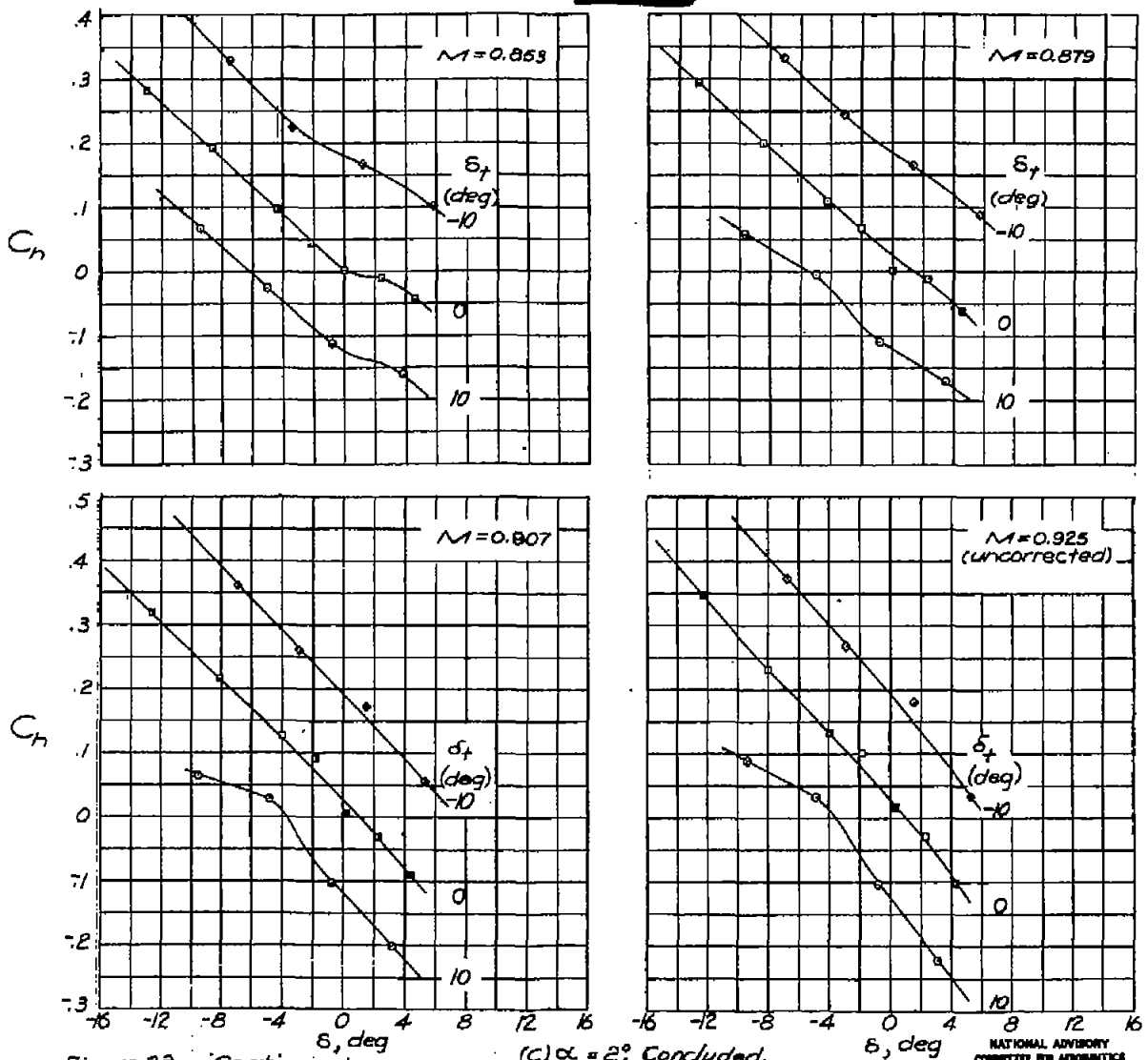

Figure 23.- Continued.

(c) α = 2°. Concluded.

[redacted]

NATIONAL ADVISORY COMMITTEE FOR AERONAUTICS

[redacted]

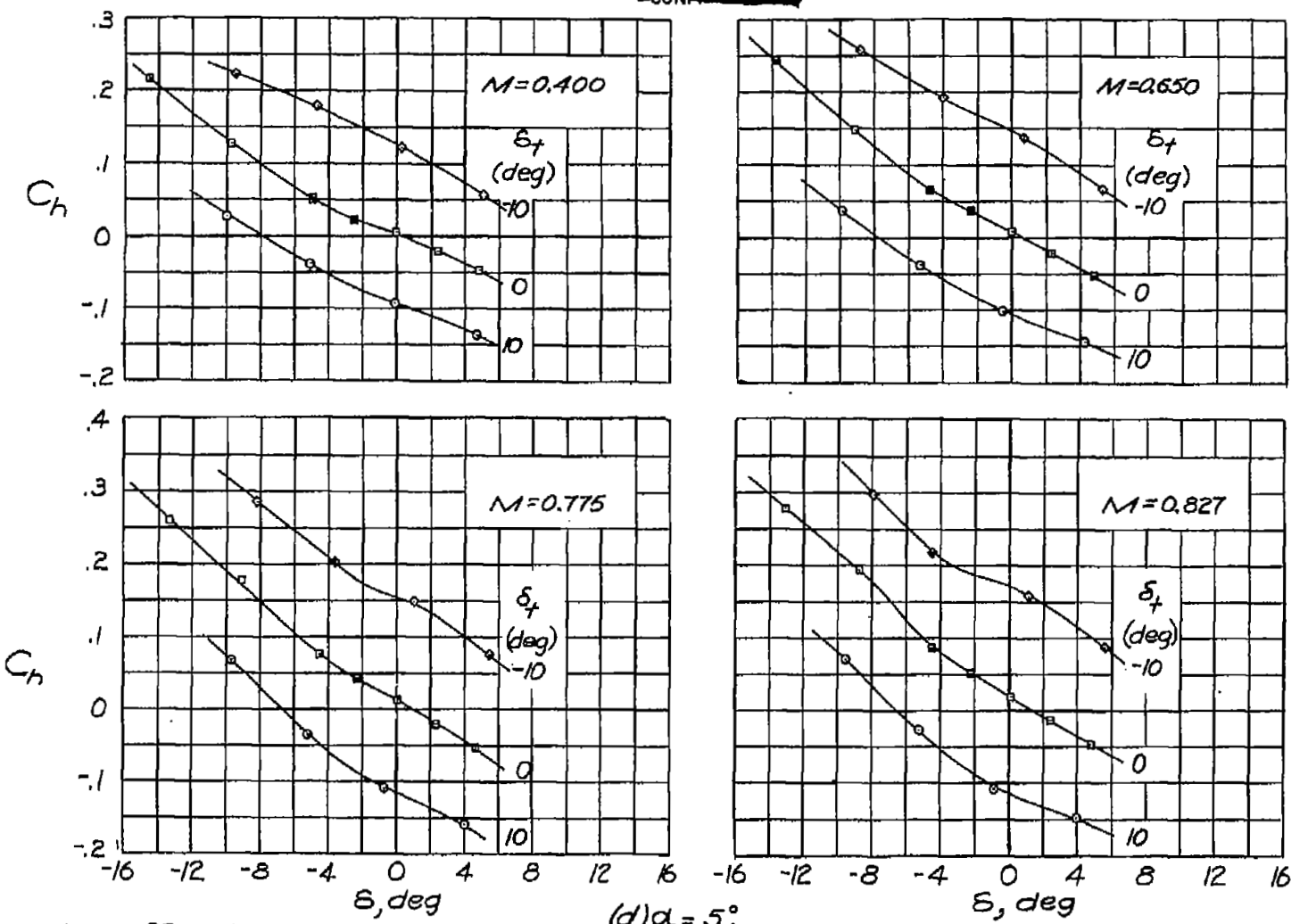

(d) $\alpha = 5°$.

Figure 23.- Continued.

NATIONAL ADVISORY COMMITTEE FOR AERONAUTICS

[redacted]

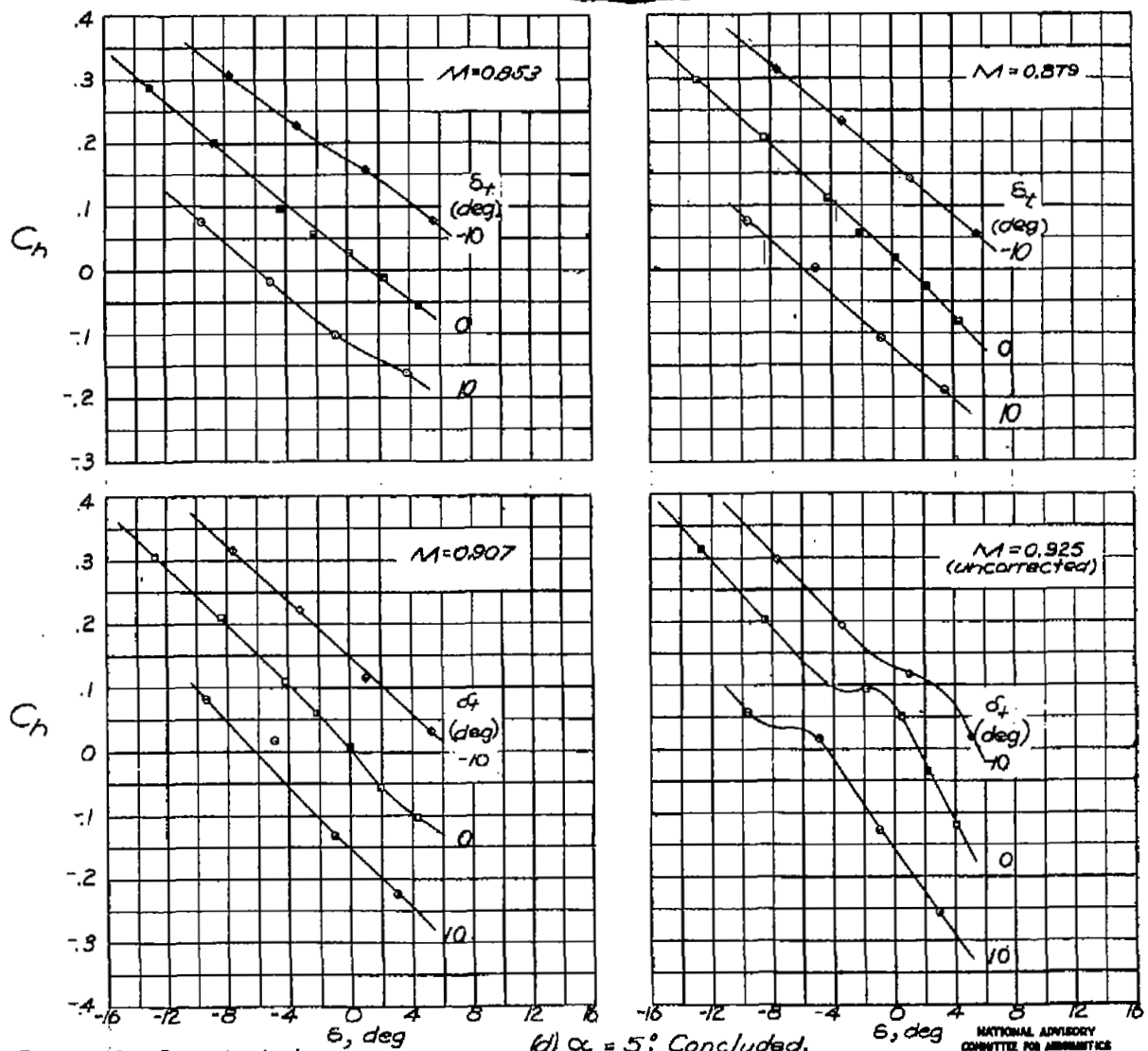

Figure 23.- Concluded.

(d) $\alpha = 5°$. Concluded.

NATIONAL ADVISORY COMMITTEE FOR AERONAUTICS

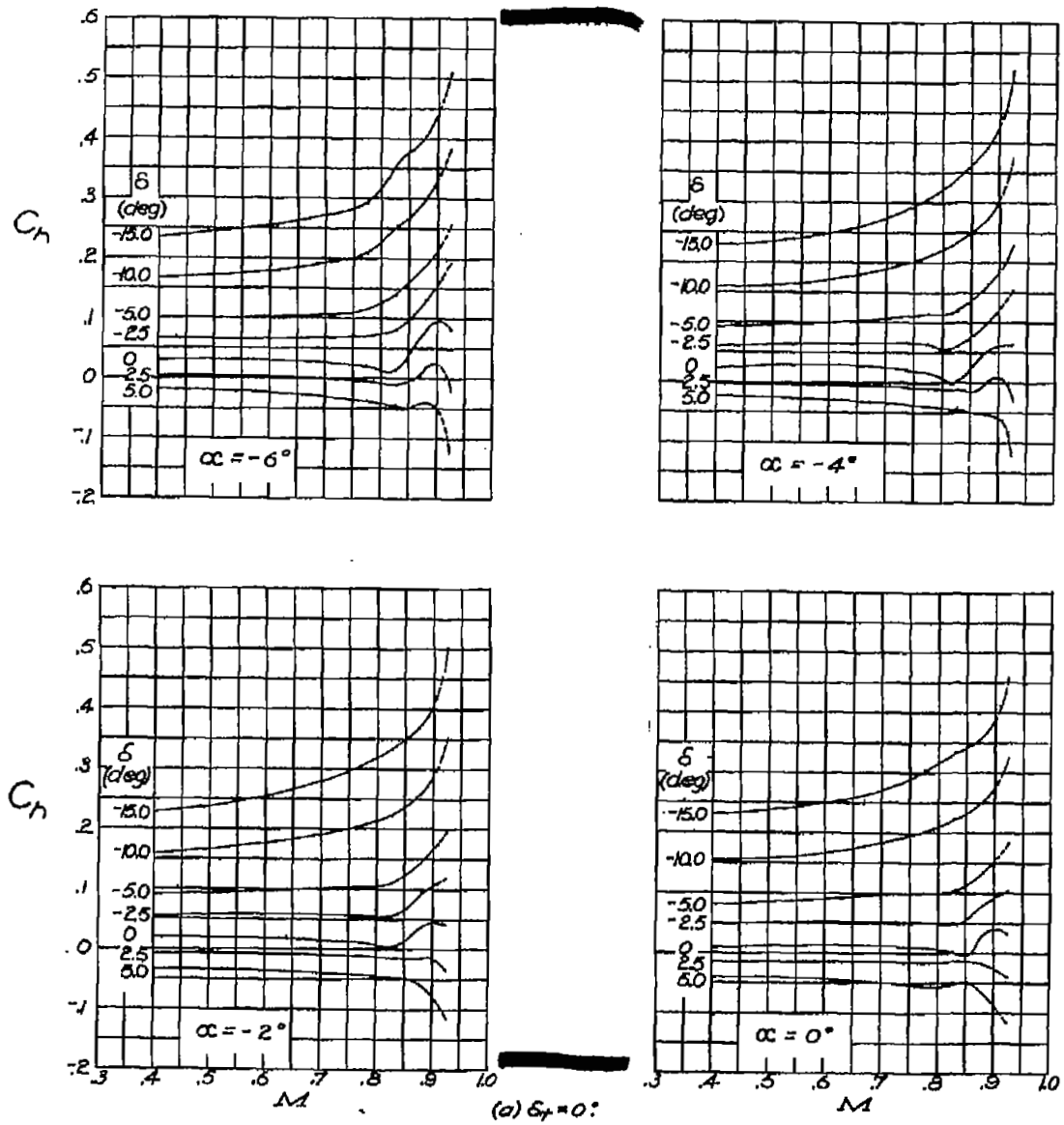

(a) $\delta_f = 0°$.

Figure 24.- Elevator hinge-moment-coefficient data.

NATIONAL ADVISORY COMMITTEE FOR AERONAUTICS

[redacted]

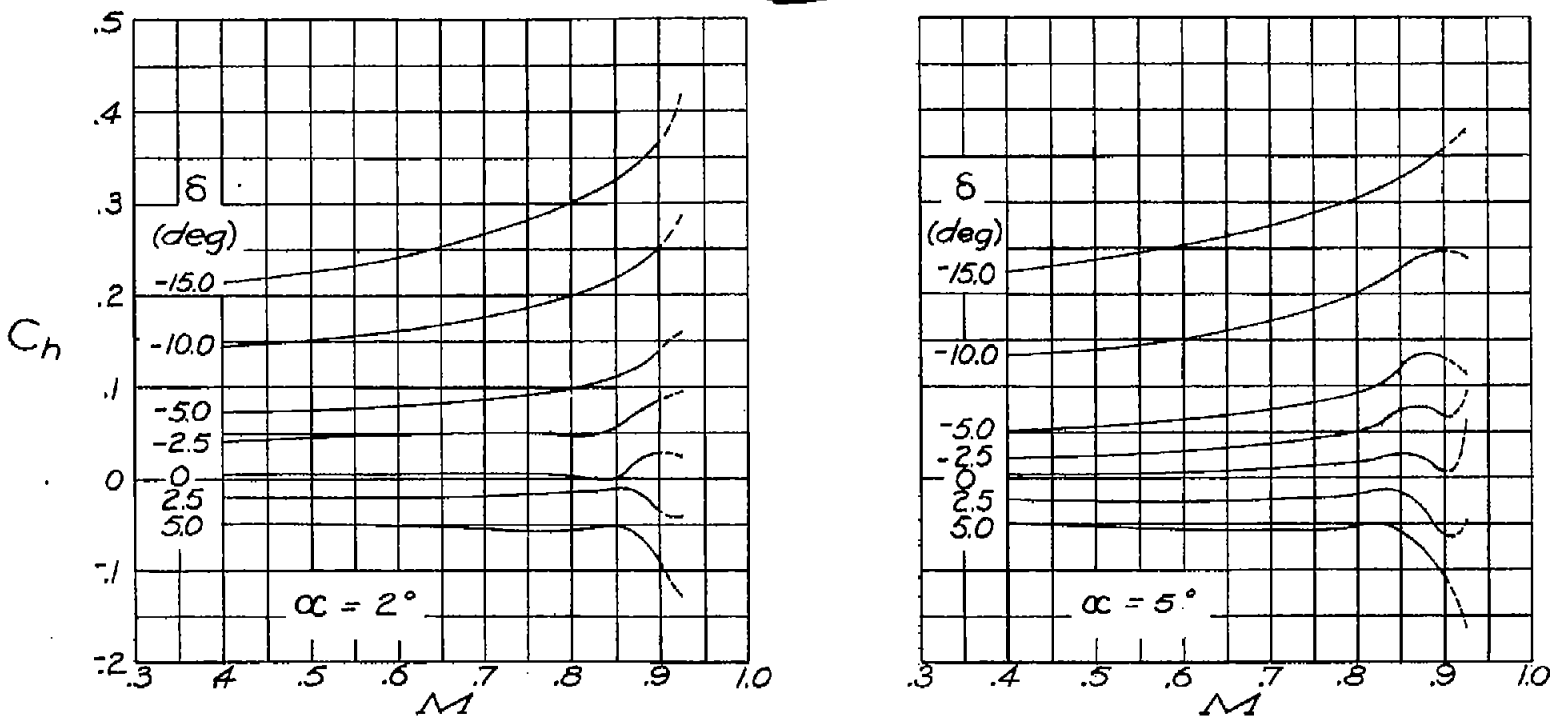

Figure 24.- Continued.

(a) $\delta_f = 0°$. Concluded.

NATIONAL ADVISORY
COMMITTEE FOR AERONAUTICS

[redacted]

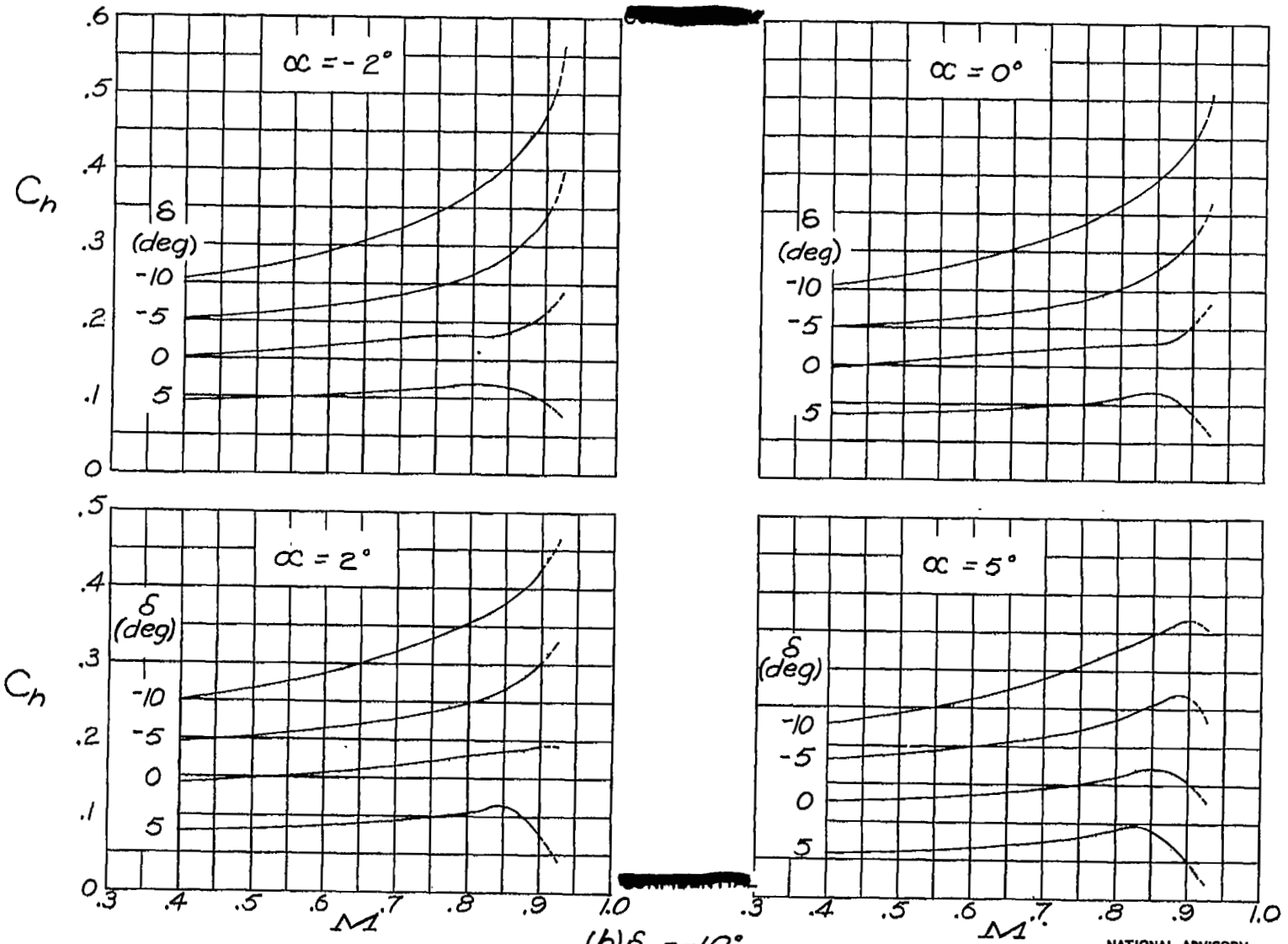

Figure 24.--Continued.

(b) $\delta_f = -10°$

NATIONAL ADVISORY COMMITTEE FOR AERONAUTICS

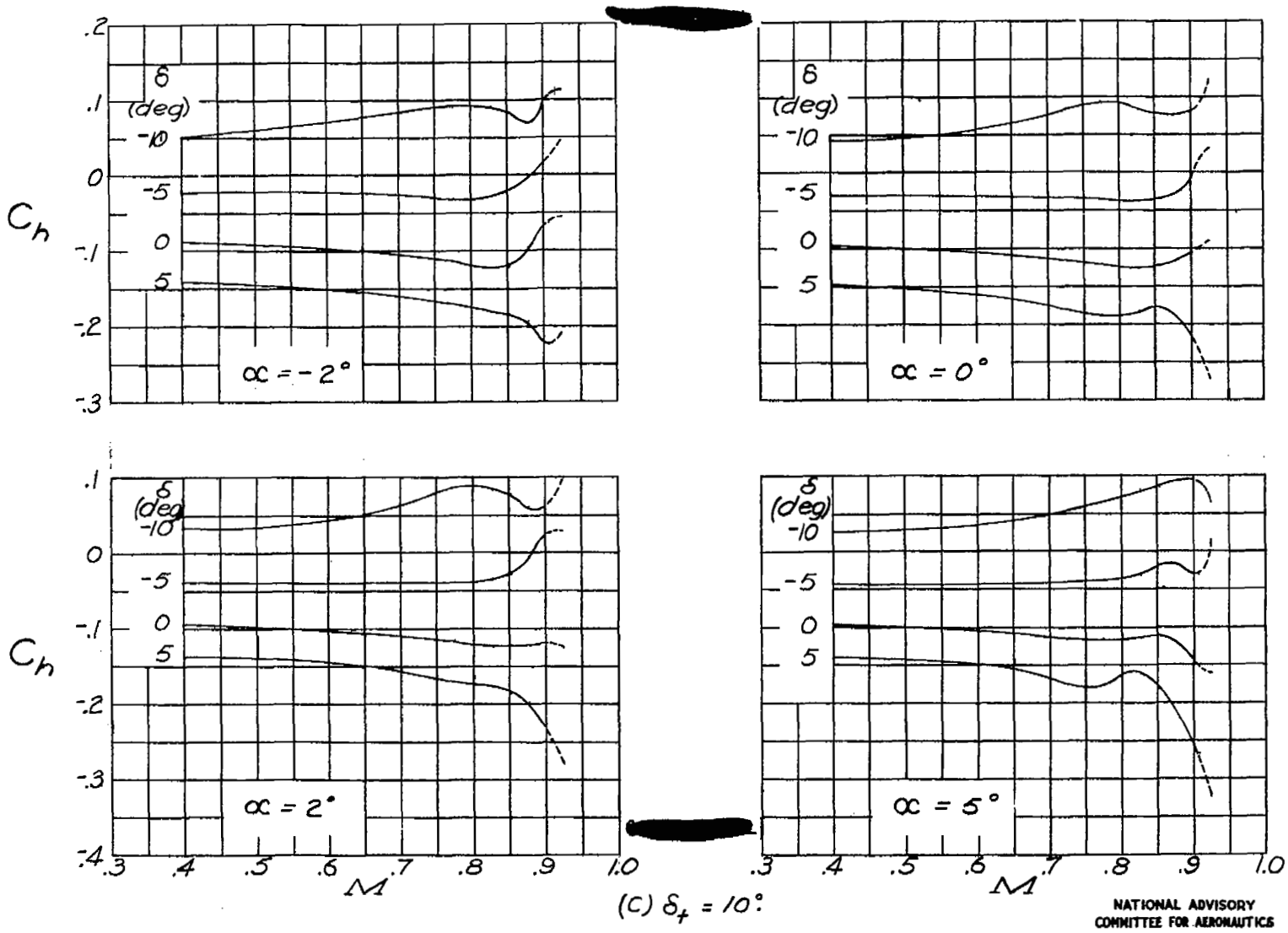

(c) $\delta_t = 10°$

NATIONAL ADVISORY COMMITTEE FOR AERONAUTICS

Figure 24.—Concluded.

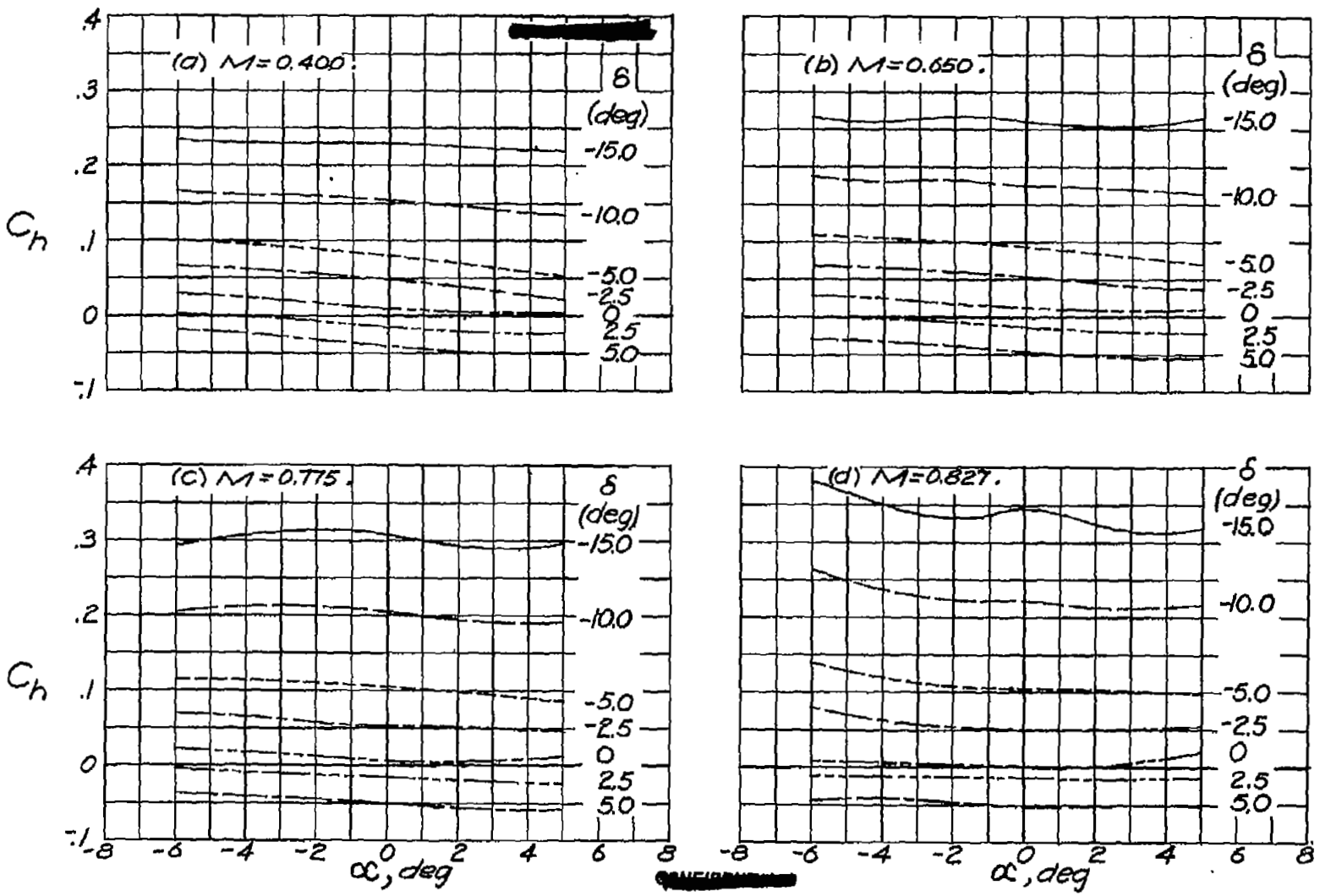

[redacted]

Figure 25.- Variation of elevator hinge-moment coefficient with angle of attack for various elevator deflections and Mach numbers. $\delta_t = 0°$.

NATIONAL ADVISORY COMMITTEE FOR AERONAUTICS

[redacted]

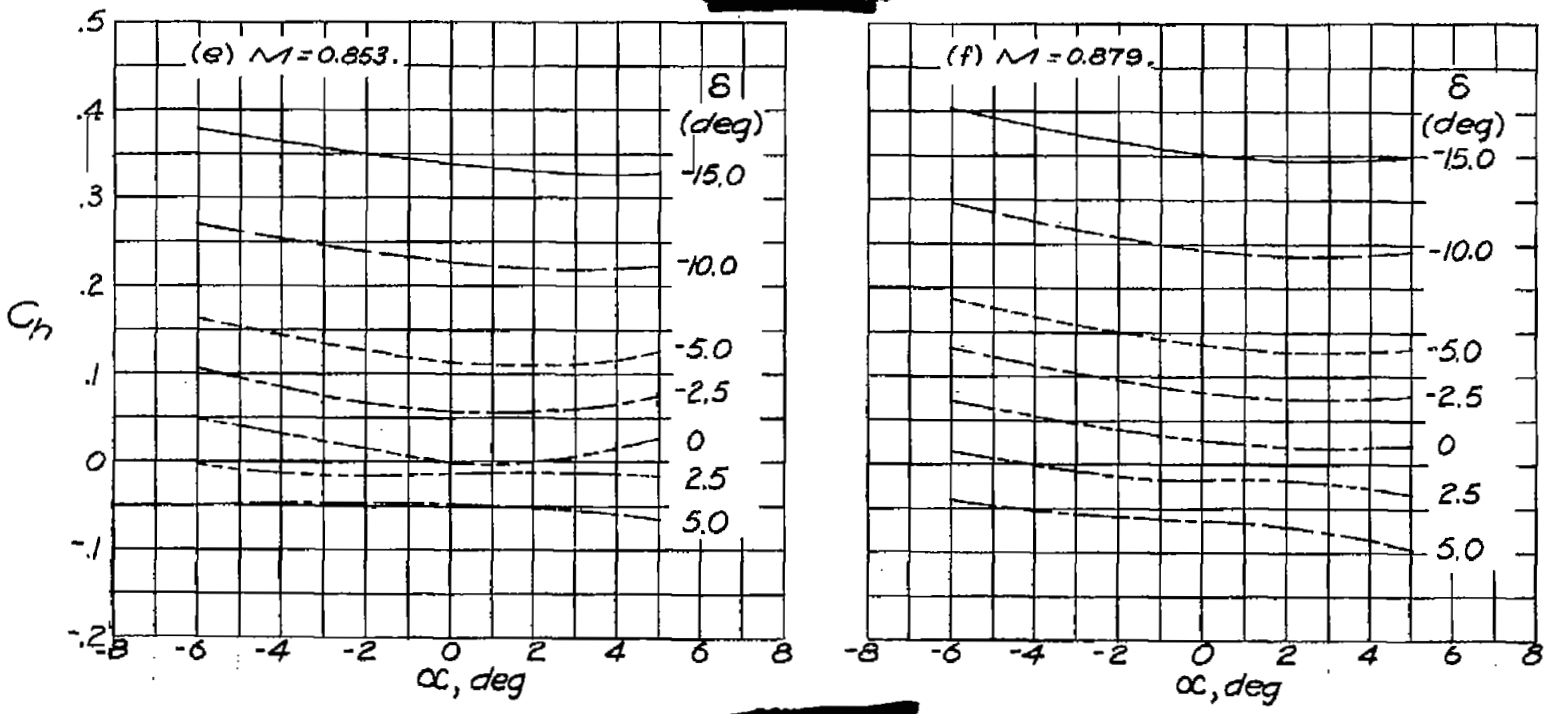

Figure 25.- Continued.

[redacted]

NATIONAL ADVISORY COMMITTEE FOR AERONAUTICS

[redacted]

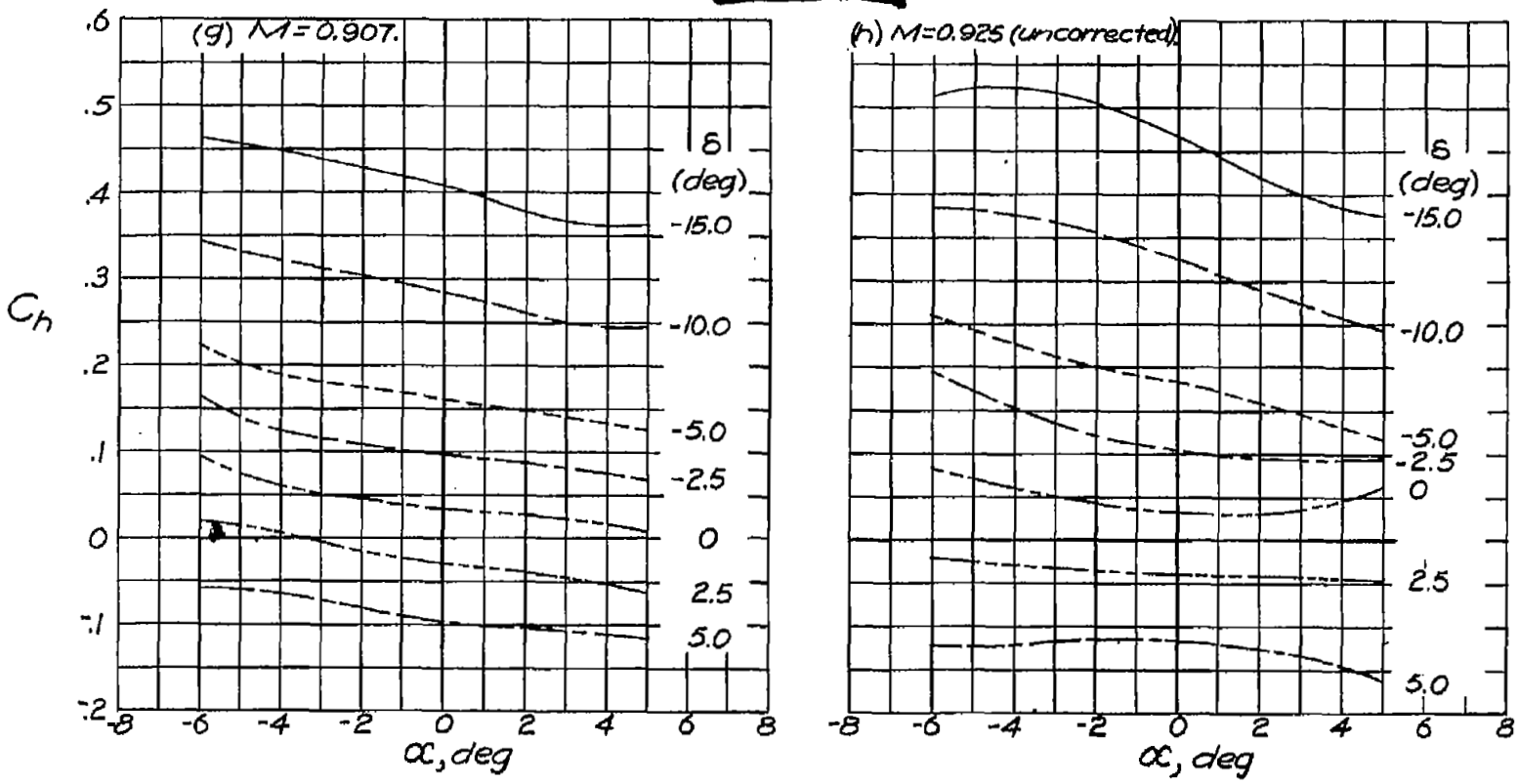

Figure 25.- Concluded.

[redacted]

NATIONAL ADVISORY COMMITTEE FOR AERONAUTICS

[redacted]

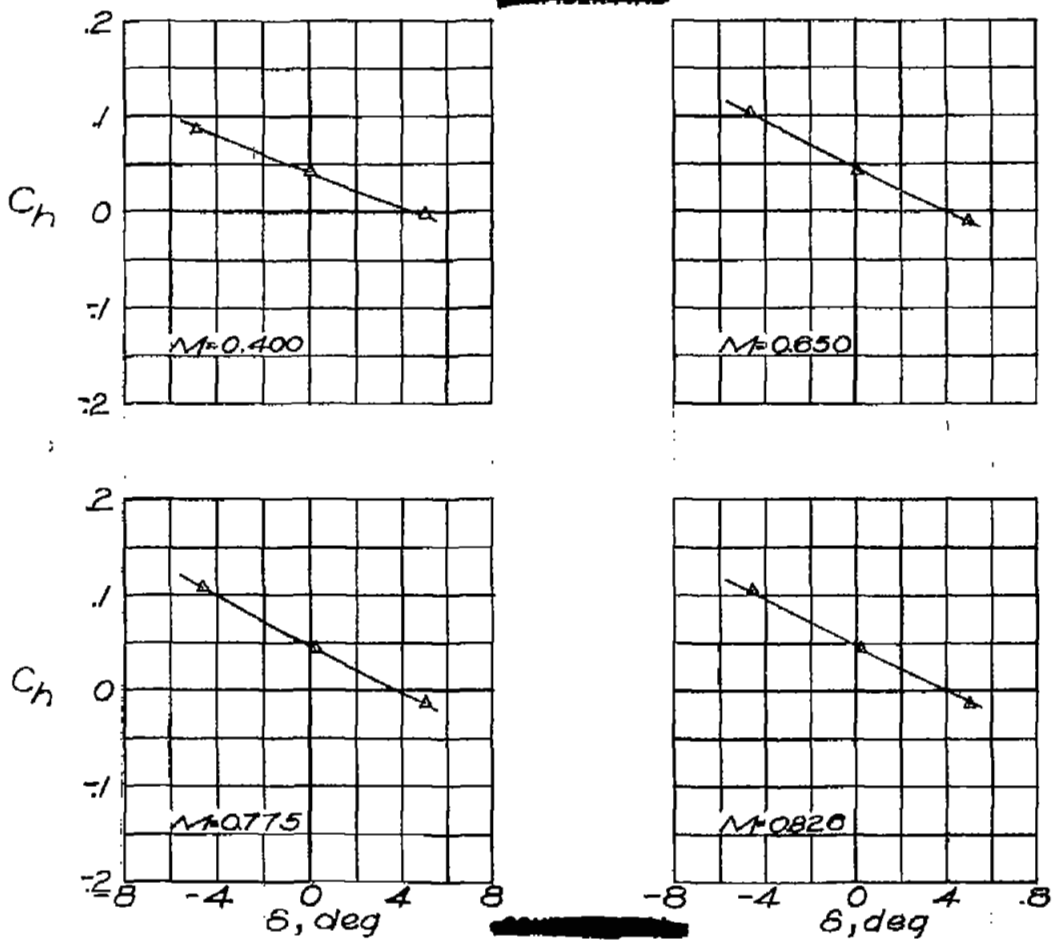

[redacted]

(a) $\alpha = -2°$.

NATIONAL ADVISORY
COMMITTEE FOR AERONAUTICS

Figure 26.- Variation of elevator hinge-moment coefficient with elevator deflection for various Mach numbers. Transition fixed at 10 percent chord; $\delta_f = 0°$.

[redacted]

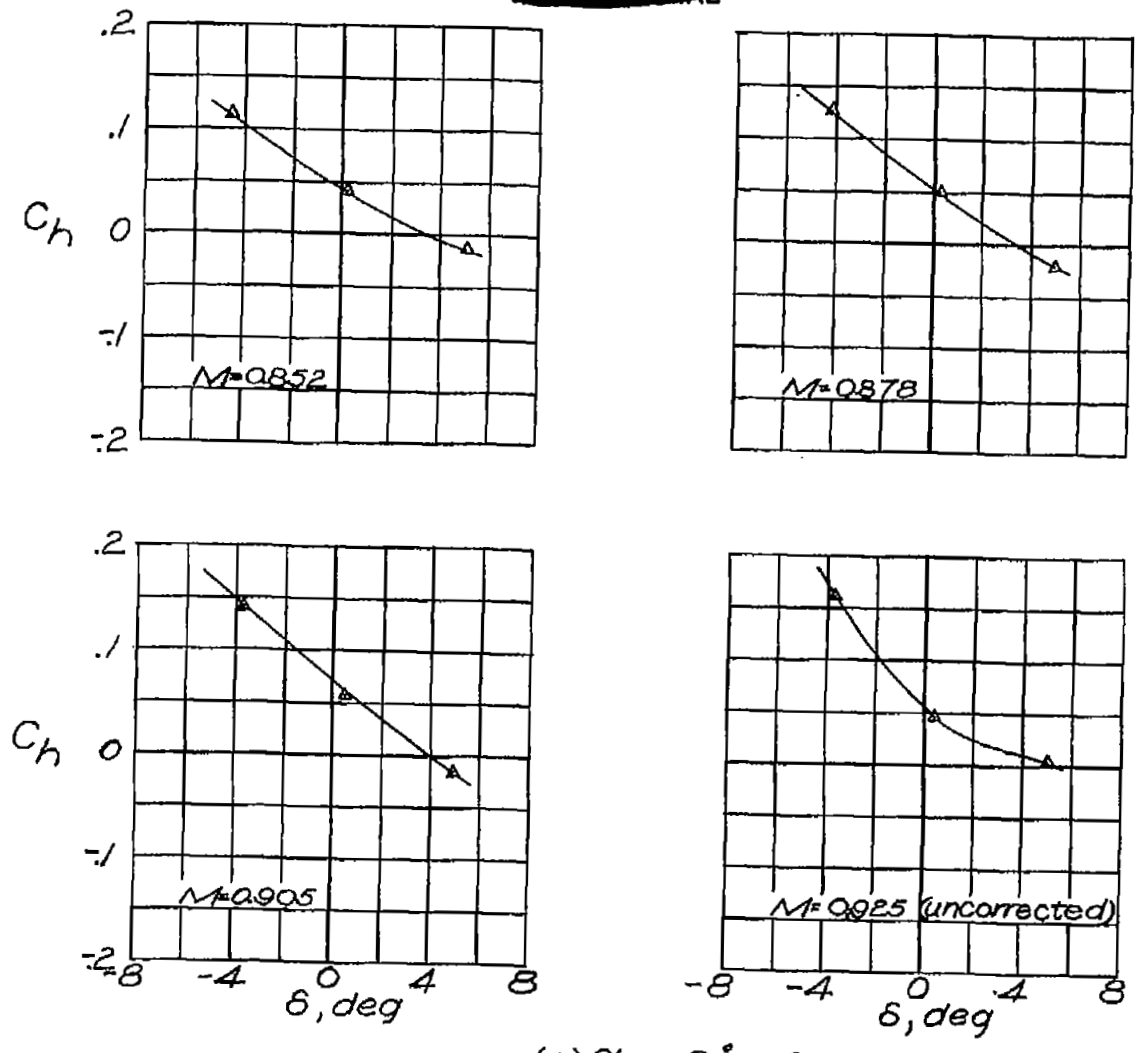

Figure 26.- Continued. (a) $\alpha = -2°$. Concluded.

[redacted]

NATIONAL ADVISORY
COMMITTEE FOR AERONAUTICS

[redacted]

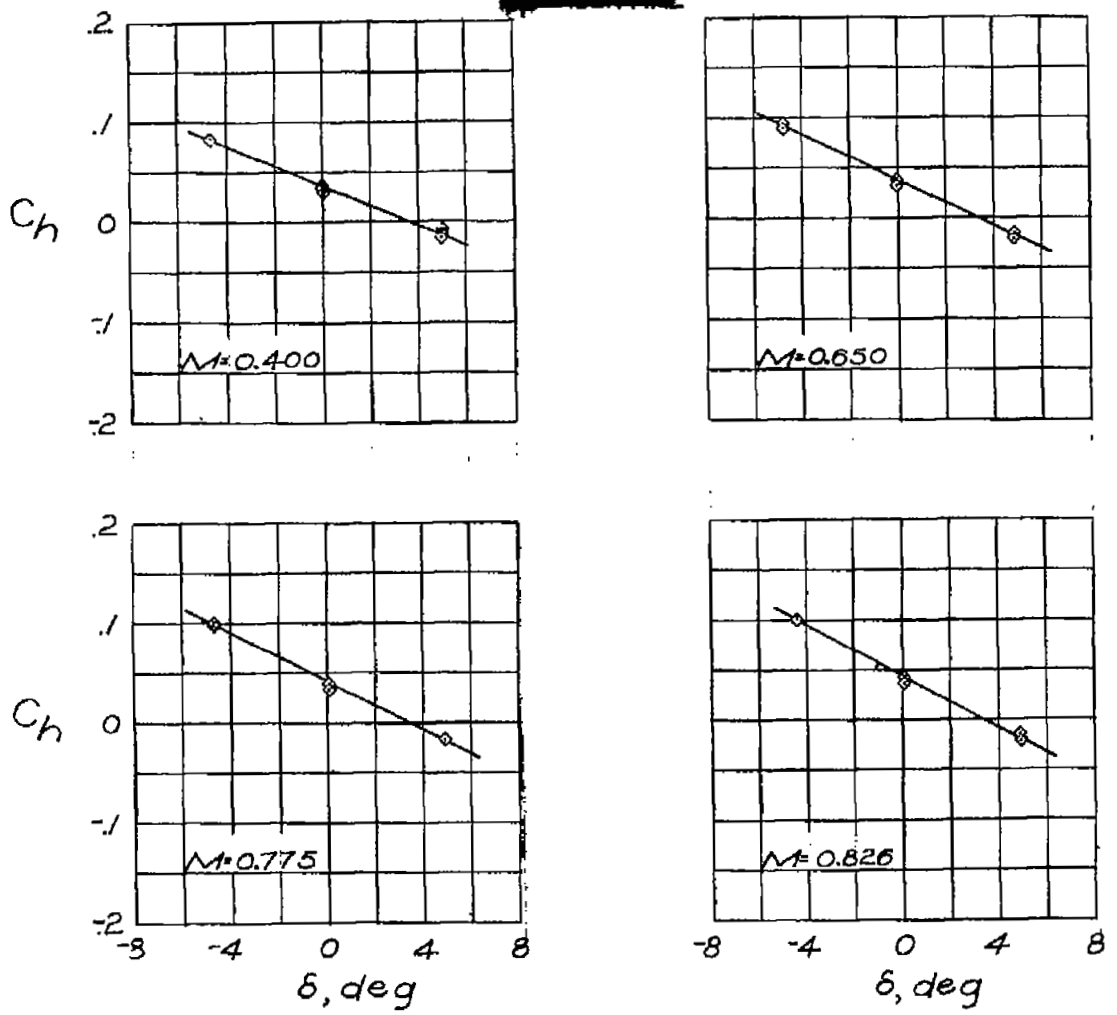

(b) $\alpha = 0°$

NATIONAL ADVISORY COMMITTEE FOR AERONAUTICS

Figure 26.-Continued.

[redacted]

[redacted]

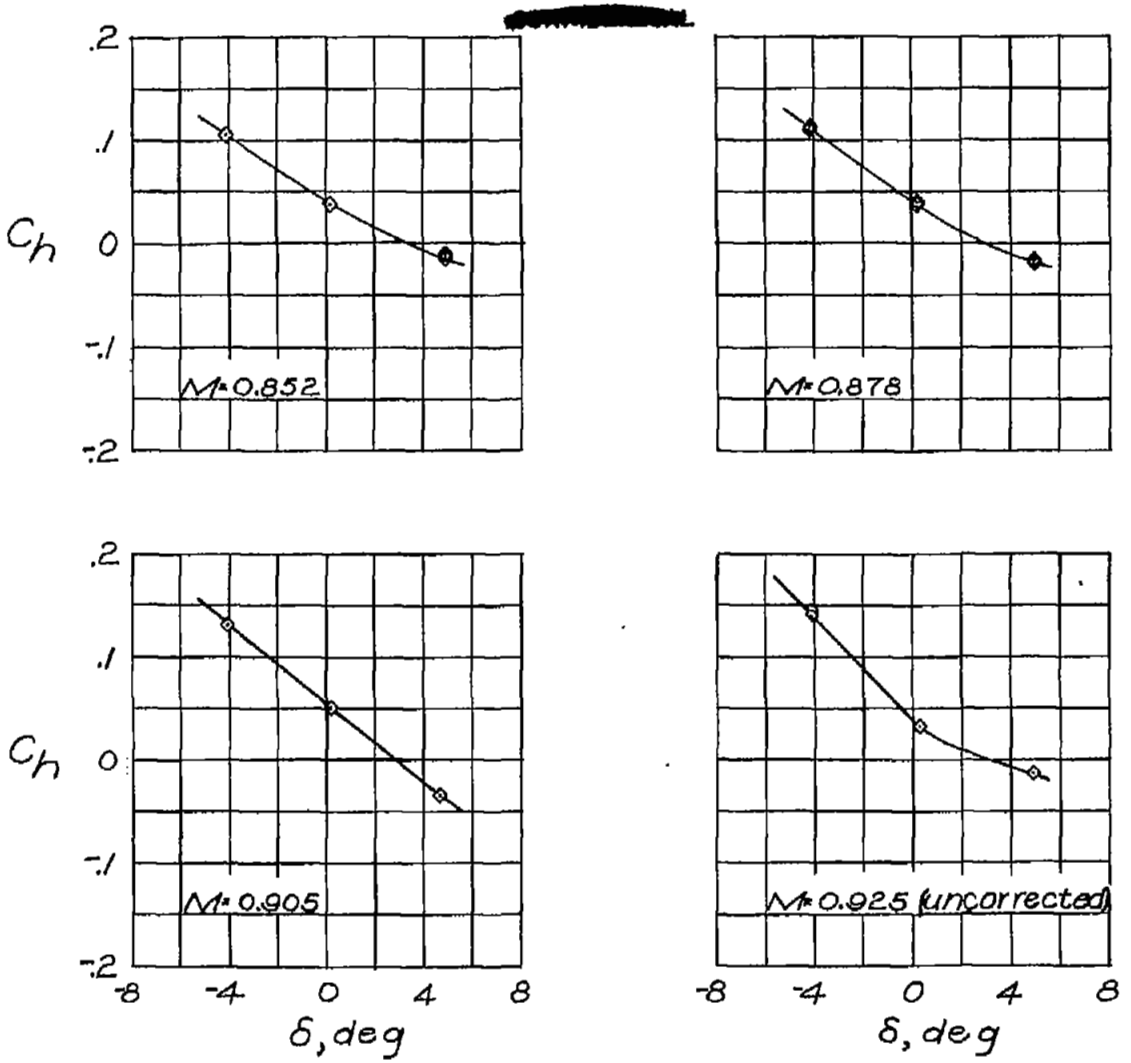

(b) $\alpha = 0°$. Concluded.

Figure 26.- Continued.

[redacted]

NATIONAL ADVISORY COMMITTEE FOR AERONAUTICS

[redacted]

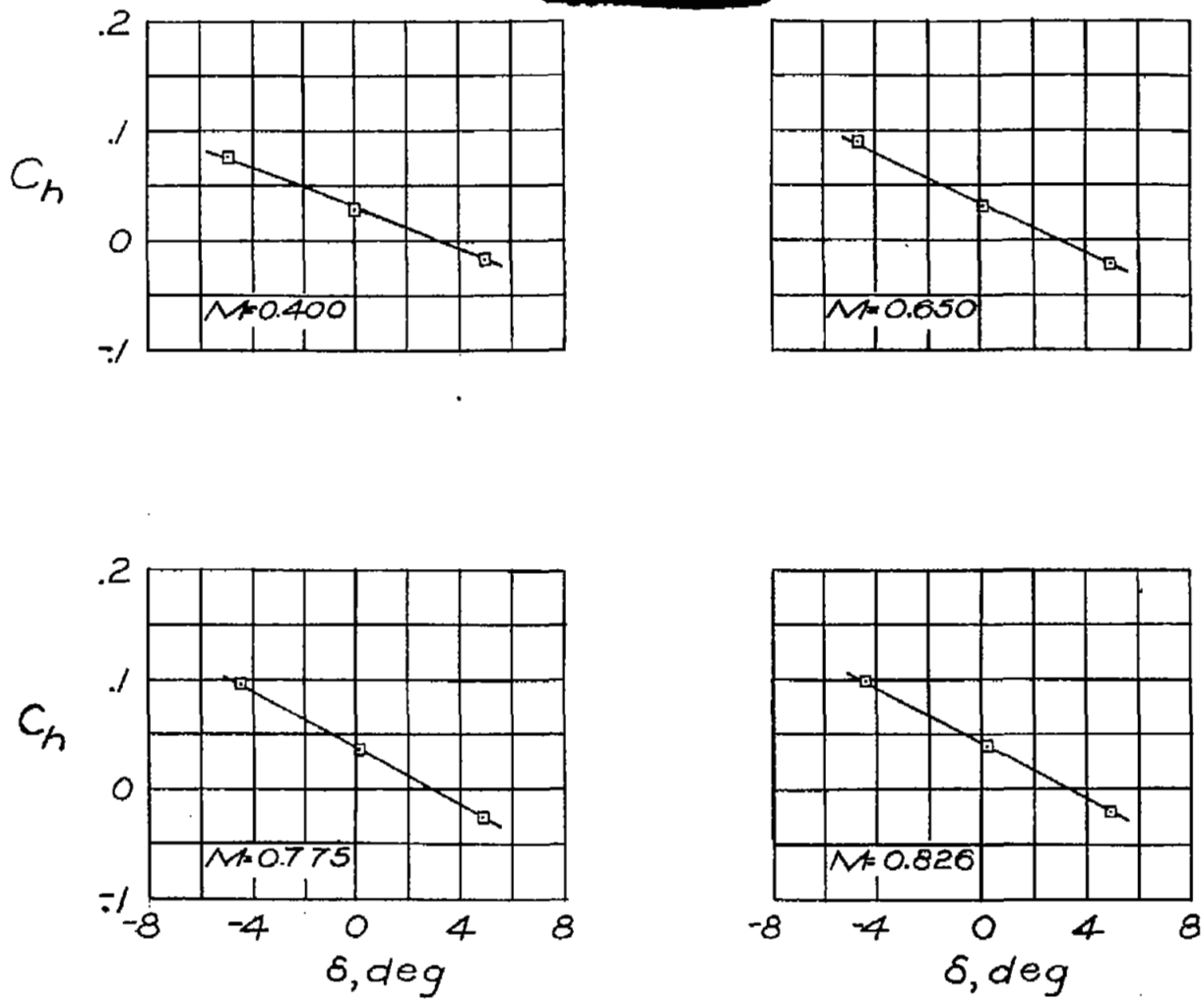

(c) $\alpha = 2°$.

Figure 26.- Continued.

[redacted]

NATIONAL ADVISORY
COMMITTEE FOR AERONAUTICS

[redacted]

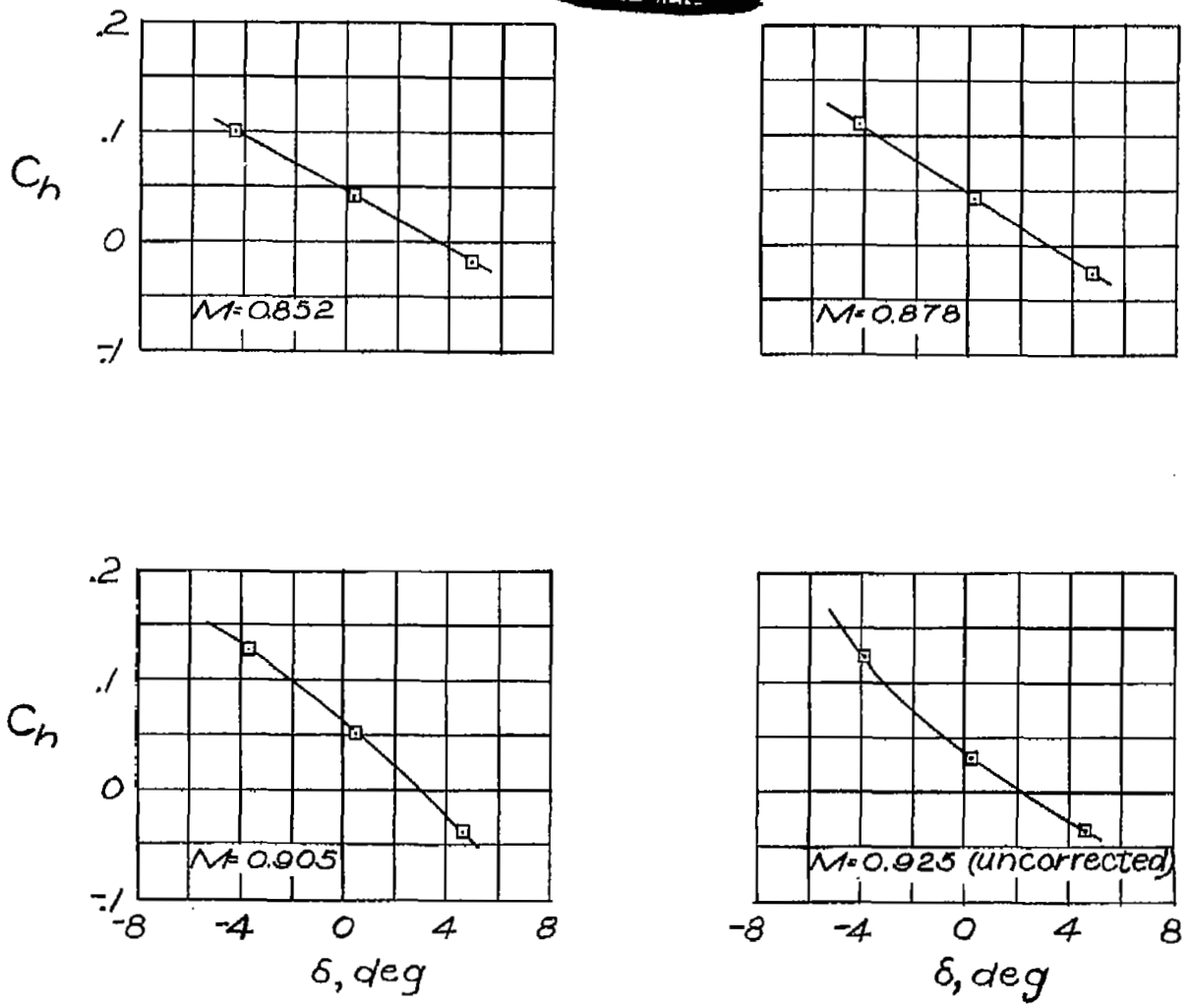

(c) $\alpha = 2°$. Concluded.

Figure 26.-Continued.

[redacted]

NATIONAL ADVISORY
COMMITTEE FOR AERONAUTICS

[redacted]

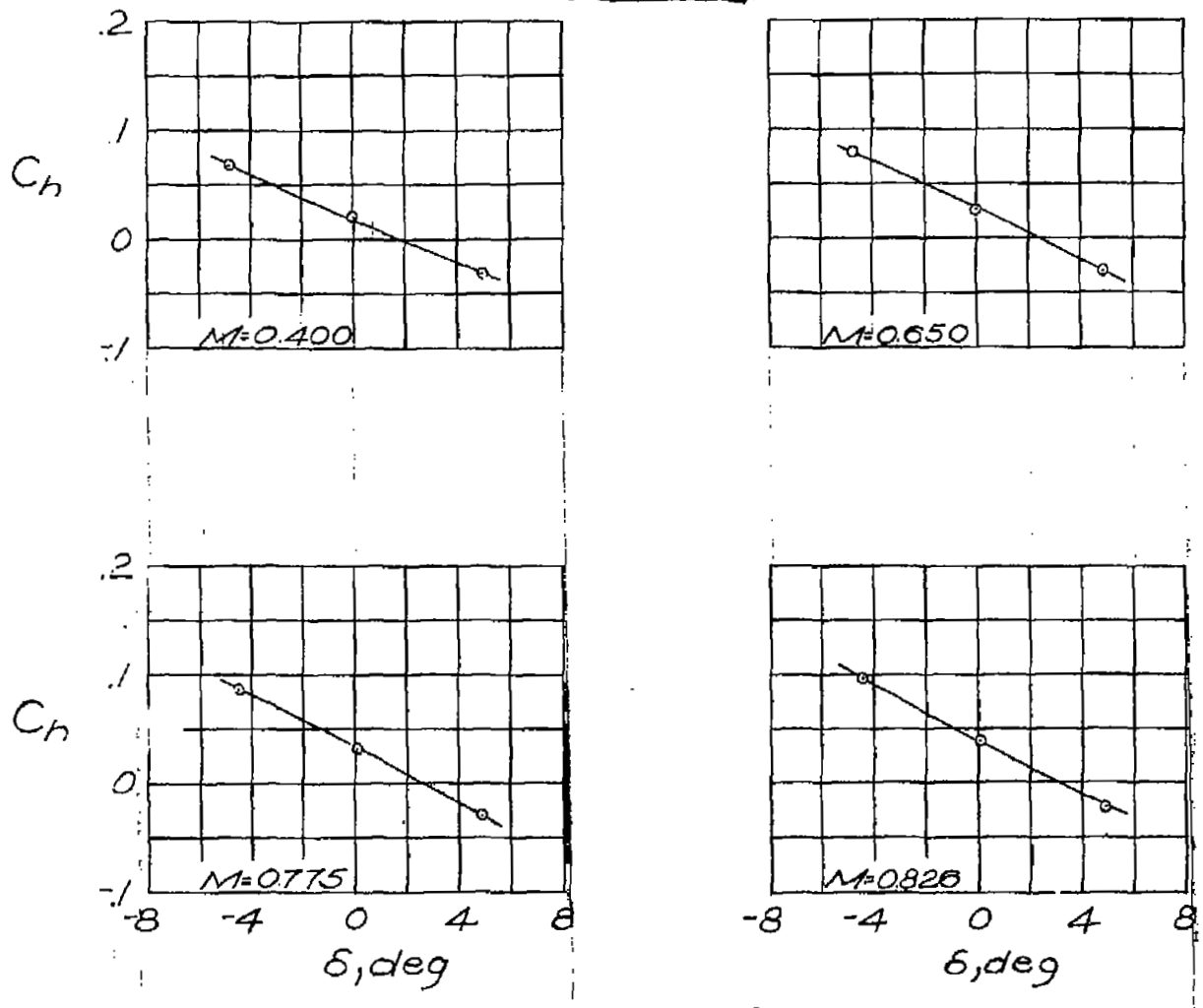

(d) $\alpha = 5°$.

Figure 26.- Continued.

[redacted]

NATIONAL ADVISORY
COMMITTEE FOR AERONAUTICS

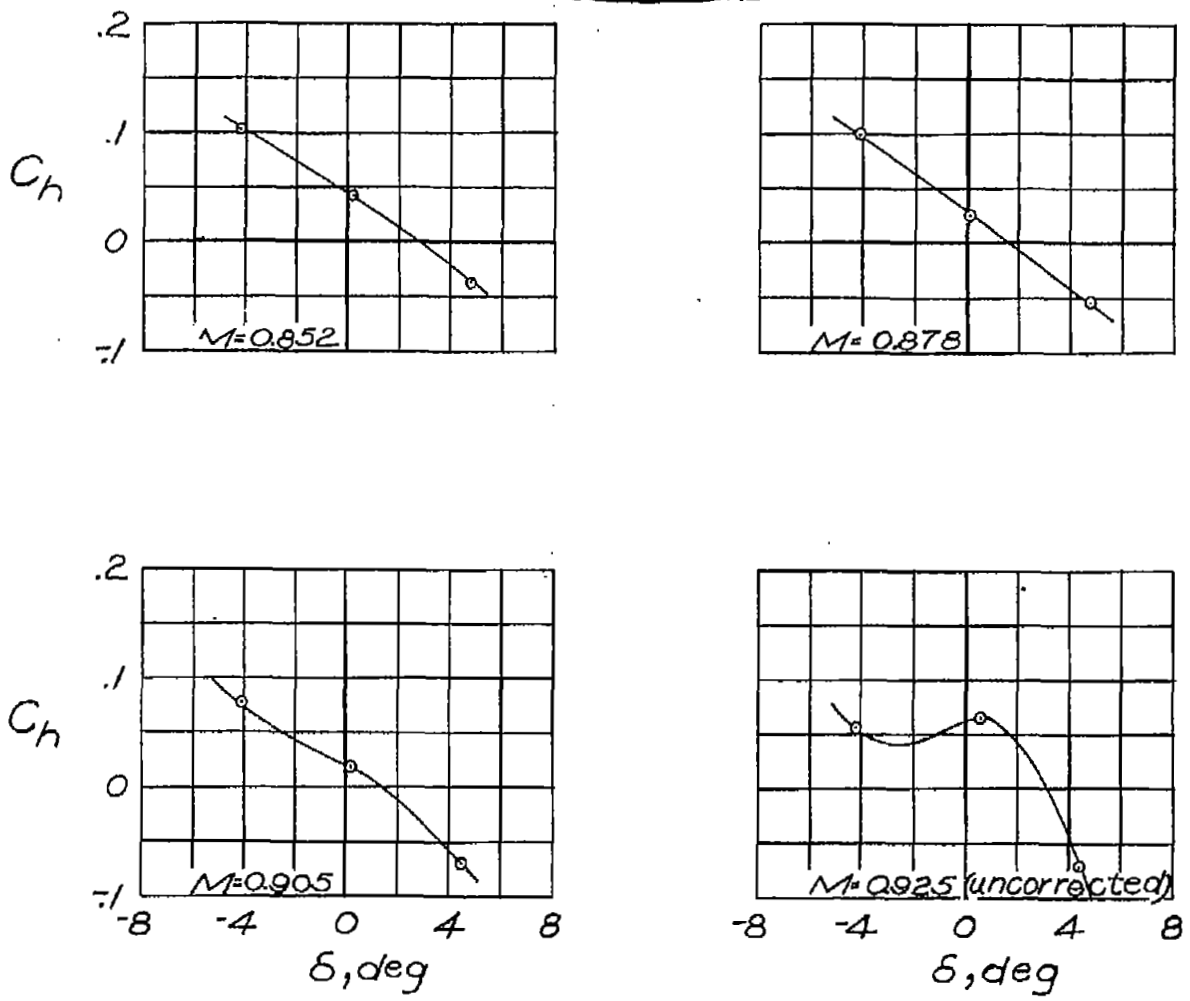

(d) $\alpha = 5^\circ$. Concluded.

Figure 26. – Concluded.

NATIONAL ADVISORY
COMMITTEE FOR AERONAUTICS

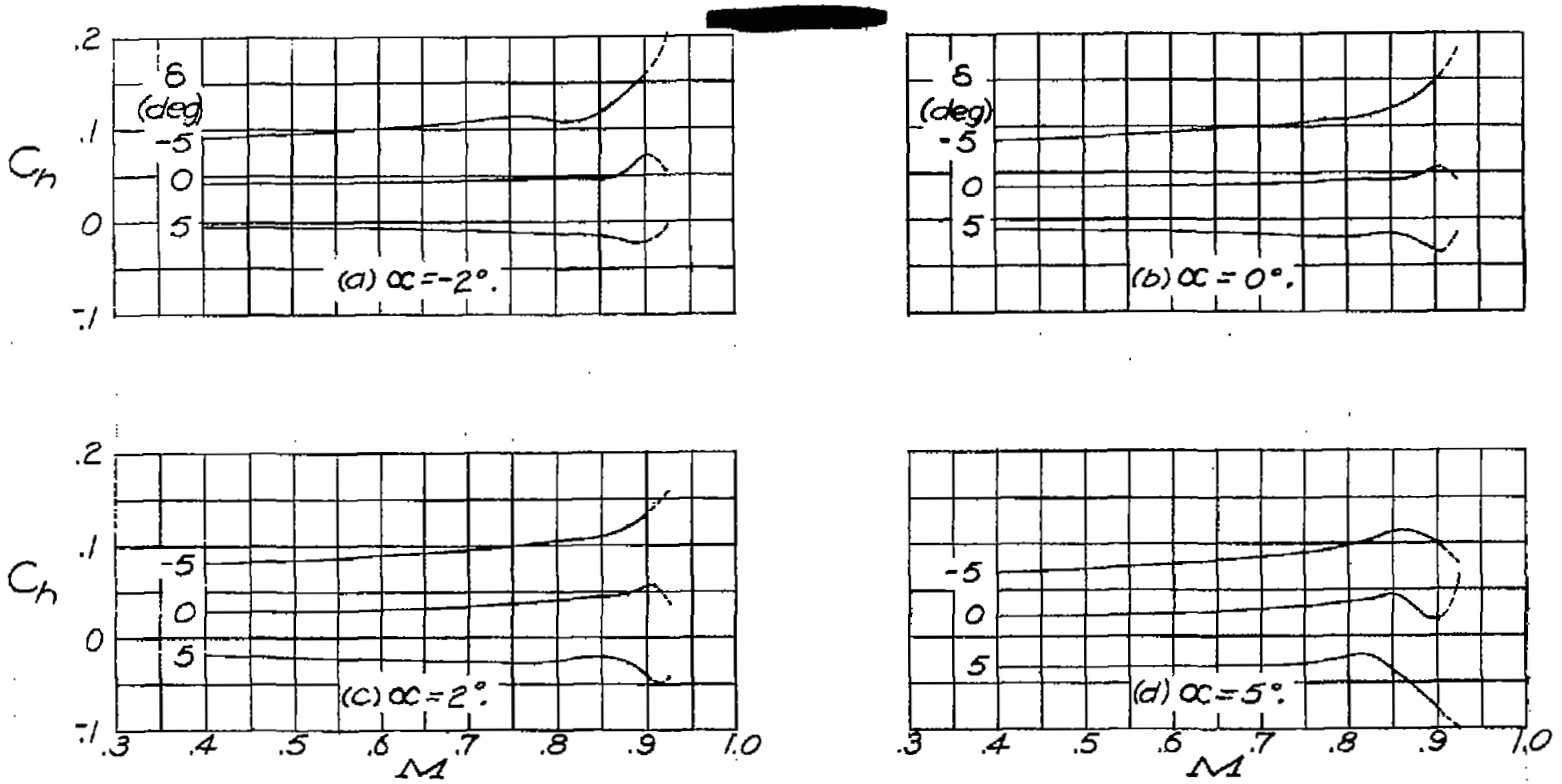

Figure 27.- Elevator hinge-moment-coefficient data. Transition fixed at 10 percent chord; $\delta_t = 0°$.

NATIONAL ADVISORY
COMMITTEE FOR AERONAUTICS

[redacted]

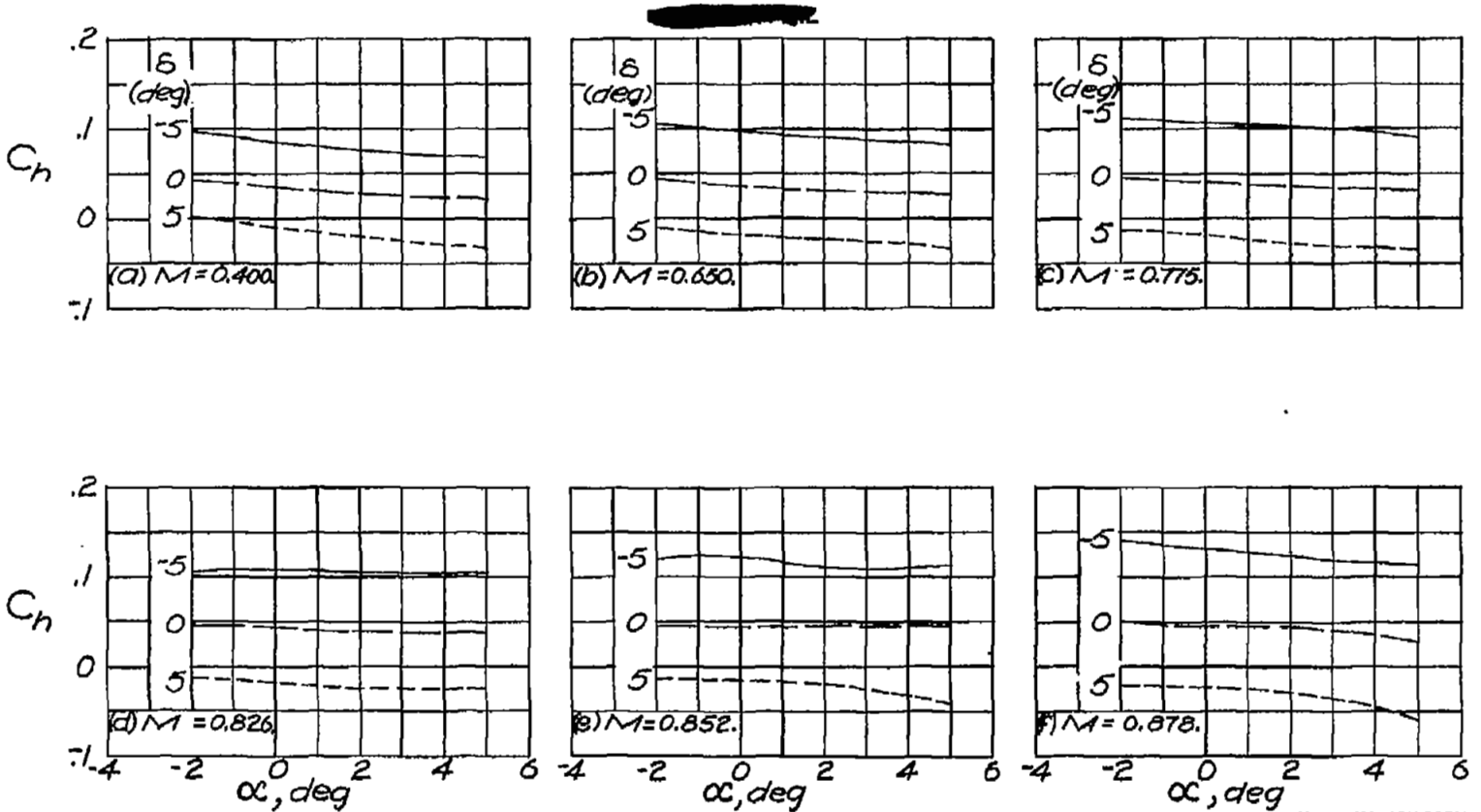

[redacted]

NATIONAL ADVISORY COMMITTEE FOR AERONAUTICS

Figure 28.- Variation of elevator hinge-moment coefficient with angle of attack for various elevator deflections and Mach numbers. Transition fixed at 10 percent chord, $\delta_f = 0°$.

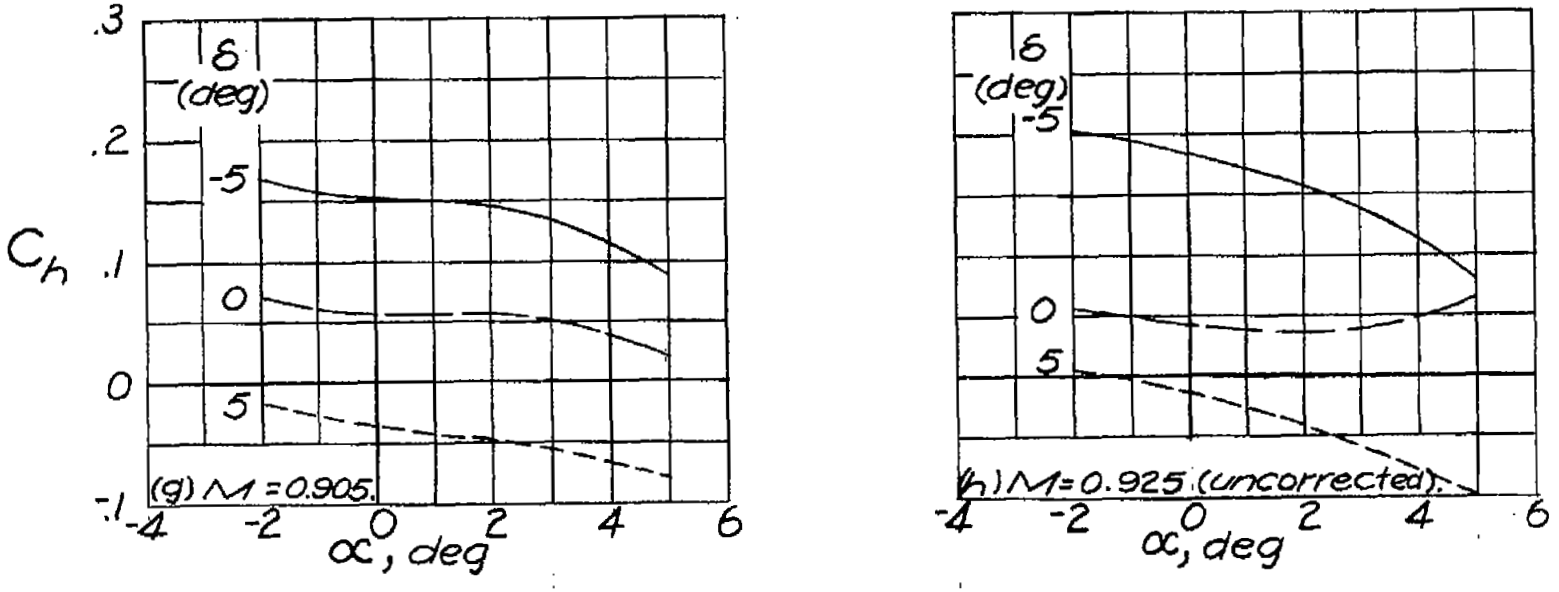

Figure 28.- Concluded.

NATIONAL ADVISORY
COMMITTEE FOR AERONAUTICS

[redacted]

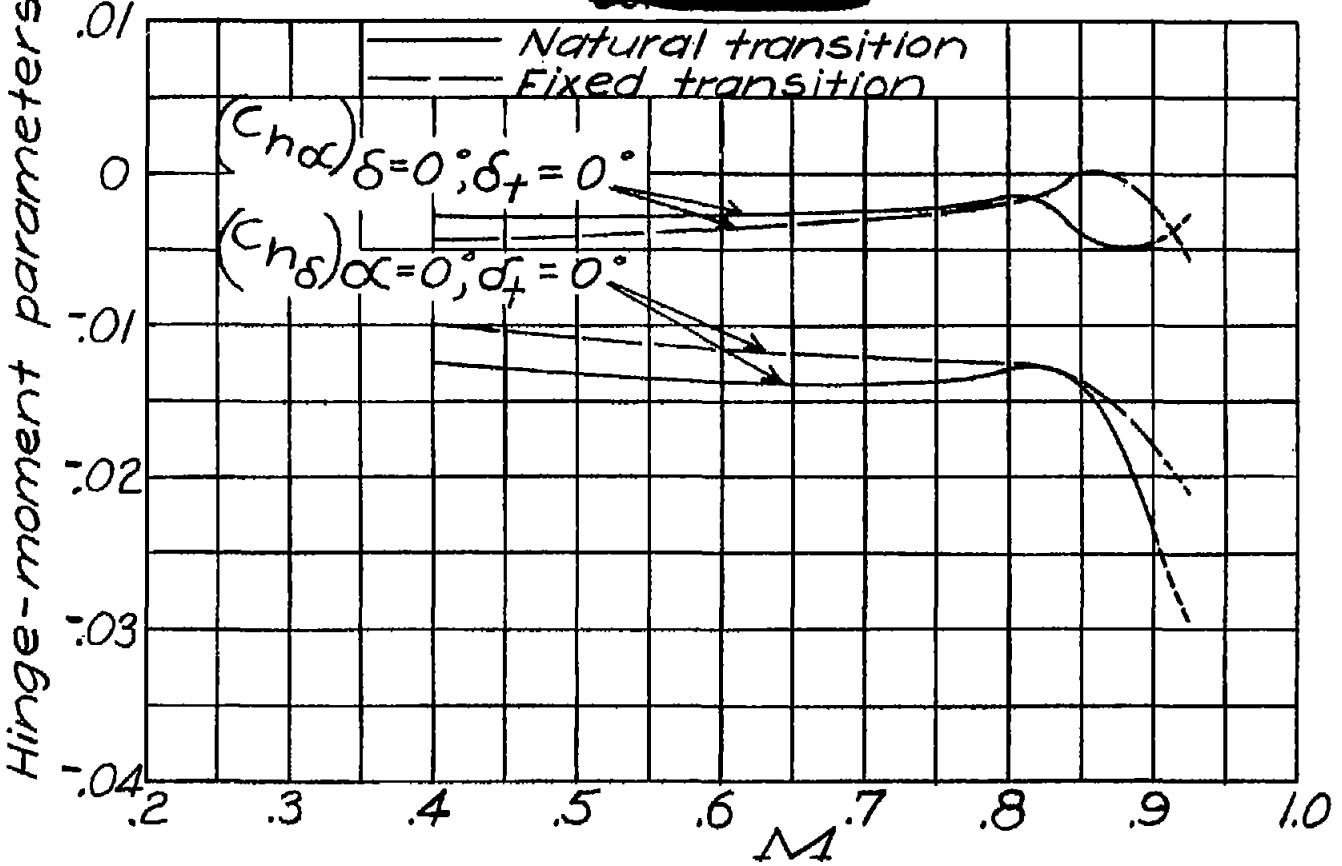

Figure 29.- Variation of hinge-moment parameters with Mach number.

NATIONAL ADVISORY
COMMITTEE FOR AERONAUTICS

[redacted]

[redacted]

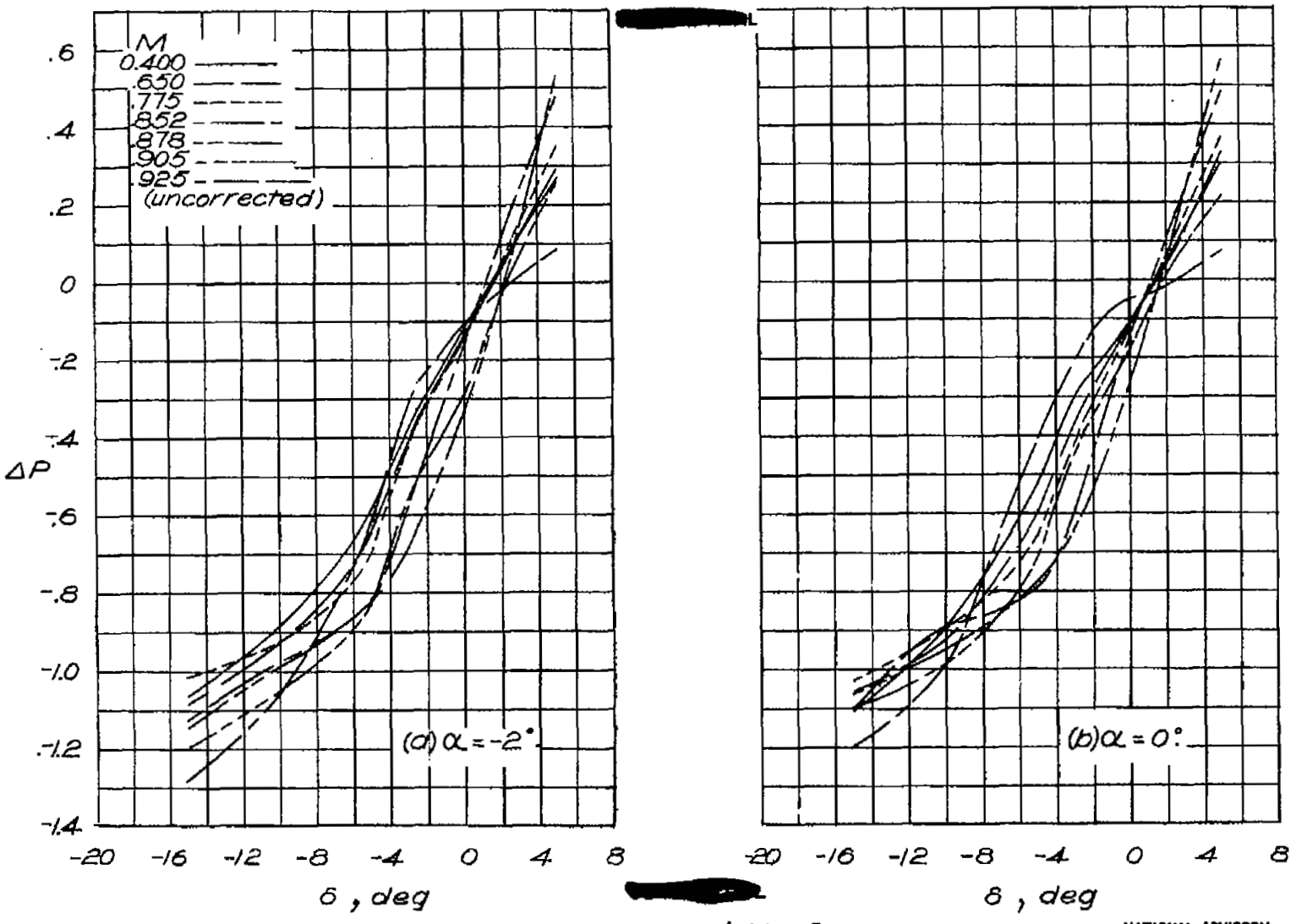

[redacted]

Figure 30.- Resultant pressure coefficient data. $\delta_f = 0°$.

NATIONAL ADVISORY COMMITTEE FOR AERONAUTICS

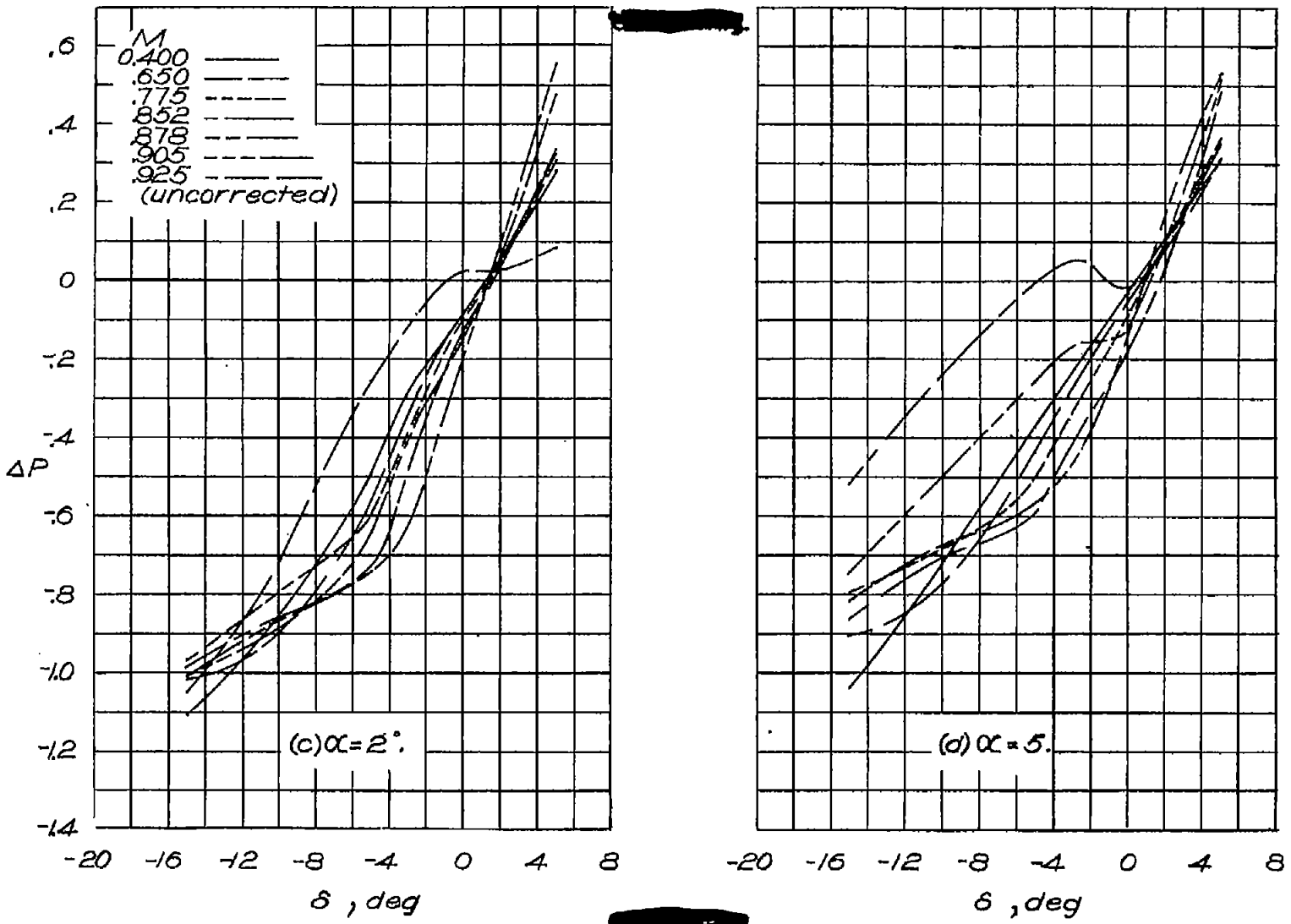

Figure 30. - Concluded.

NATIONAL ADVISORY COMMITTEE FOR AERONAUTICS

[redacted]

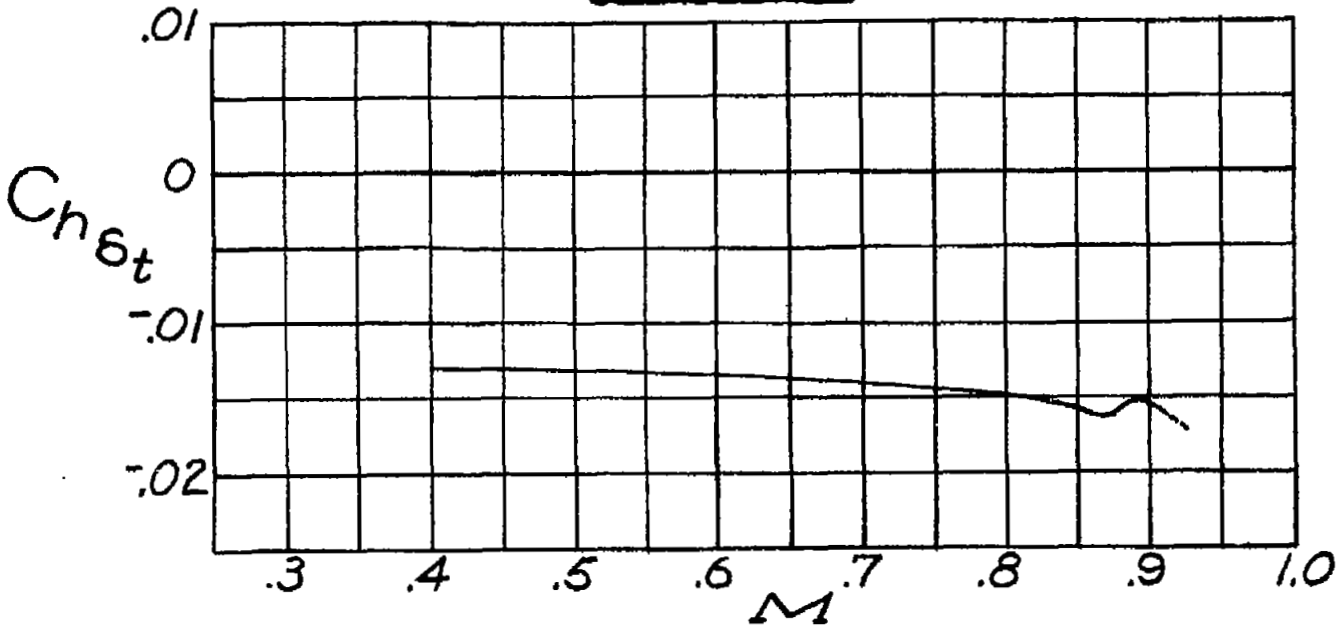

Figure 31 .- Variation of tab effectiveness with Mach number.

NATIONAL ADVISORY COMMITTEE FOR AERONAUTICS

[redacted]

UNCLASSIFIED

[redacted]

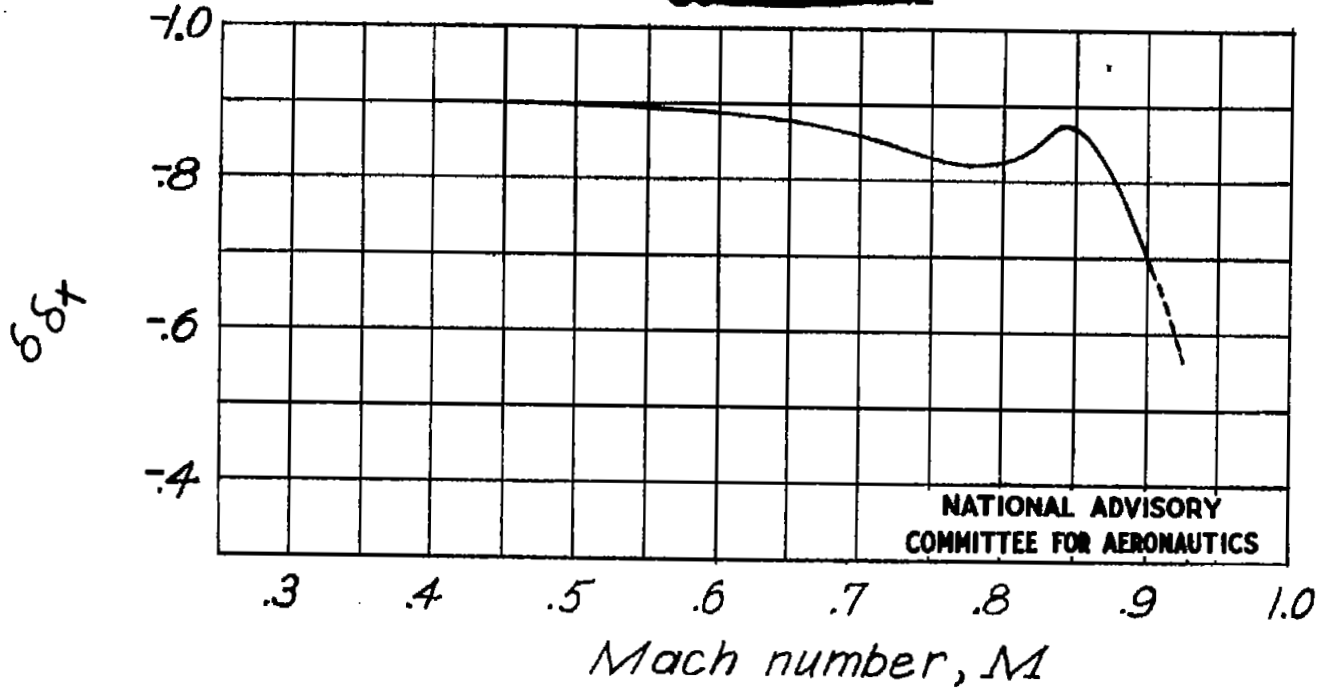

Figure 32.- Variation with Mach number of the rate of change of elevator deflection with tab deflection required to produce zero elevator hinge-moment coefficient.

[redacted]

UNCLASSIFIED

NASA Technical Library
3 1176 01437 0226